UNIVERSITÀ DI PARMA

UNIVERSITA' DEGLI STUDI DI PARMA

DOTTORATO DI RICERCA IN

" Scienze del Farmaco"

CICLO XXXV

Serine metabolism in the human brain: serine racemase regulation and pathological variants of phosphoserine aminotransferase

Coordinatore:
Chiar.mo Prof. Marco Mor

Tutore:
Chiar.mo Prof. Stefano Bruno

Dottoranda: Annalisa Michielon

Anni Accademici 2019/2020 – 2021/2022

Table of contents

Abstract

L-serine and D-serine play crucial roles in the central nervous system (CNS). Indeed, L-serine is a neurotrophic factor and represents the precursor of the neurotransmitters glycine and D-serine, the co-agonists of N-methyl-D-aspartate (NMDA) glutamate receptors. Serine racemase (SR) is the enzyme responsible for converting L-serine into D-serine and eliminating both enantiomers to pyruvate and ammonia. NMDA receptors are involved in the brain's development, plasticity and function. In addition, they are related to Alzheimer's and Parkinson's diseases, ischemia and amyotrophic lateral sclerosis.

In the CNS, the primary route of L-serine biosynthesis is the phosphorylated pathway (PP), which starts from the glycolytic precursor 3-phosphoglycerate. The PP takes place in astrocytes thanks to three sequential enzymatic reactions catalyzed by 3-phosphoglycerate dehydrogenase (3-PHGDH), phosphoserine aminotransferase (PSAT) and phosphoserine phosphatase (PSP). Defects in the genes that encode the PP's enzymes lead to severe CNS diseases, known as serine deficiency disorders (SDDs), characterized by a low concentration of L-serine in the cerebrospinal fluid and plasma. These syndromes exhibit highly variable neurological phenotypes, with retardation, microcephaly, and seizures typical in newborns and progressive polyneuropathy in adults. Early recognition is crucial for their successful treatment with L-serine repletion. In addition, since SDDs can affect all three enzymes of the PP, with overlapping phenotypes, the molecular understanding of their pathogenetic variants is fundamental for diagnosis, prognosis, and therapy.

Chapter 1 of this PhD dissertation offers a general introduction to the state of the art of human brain serine metabolism. In particular, the role and characteristics of the pyridoxal-5'-phosphate-dependent enzymes human phosphoserine

aminotransferase (hPSAT) and human serine racemase (hSR) are described in detail. The following chapters report the experimental activity.

Chapter 2 focuses on the functional and biochemical characterization of hPSAT, especially its pathogenic variants S43R, G79W, A99V, D100A, S179L, C245R, and R342W associated in the literature with SDDs. In addition, the non-pathogenic P87A variant was studied for comparison. All PSAT variants were investigated to understand the loss-of-function mechanisms that can be responsible for SDDs pathogenesis.

Chapters 3 and 4 focus on hSR regulation, especially evaluating the possible biochemical link between serine metabolism and the glycolytic flux in humans. Chapter 3 explores the interaction of hSR with the glycolytic human enzyme glyceraldehyde-3-phosphate dehydrogenase (hGAPDH). Chapter 4 reports the investigation of hSR inhibition by glyceraldehyde 3-phosphate (G3P), the hGAPDH substrate.

Chapter 1. Introduction

1.1 The roles of serine

In nature, the amino acid serine is present in two enantiomeric forms: L-serine and D-serine, which differ in the relative spatial arrangement around the α-carbon (Dai et al., 2019). Both enantiomers are fundamental for human health; their main functions are summarized in Figure 1.

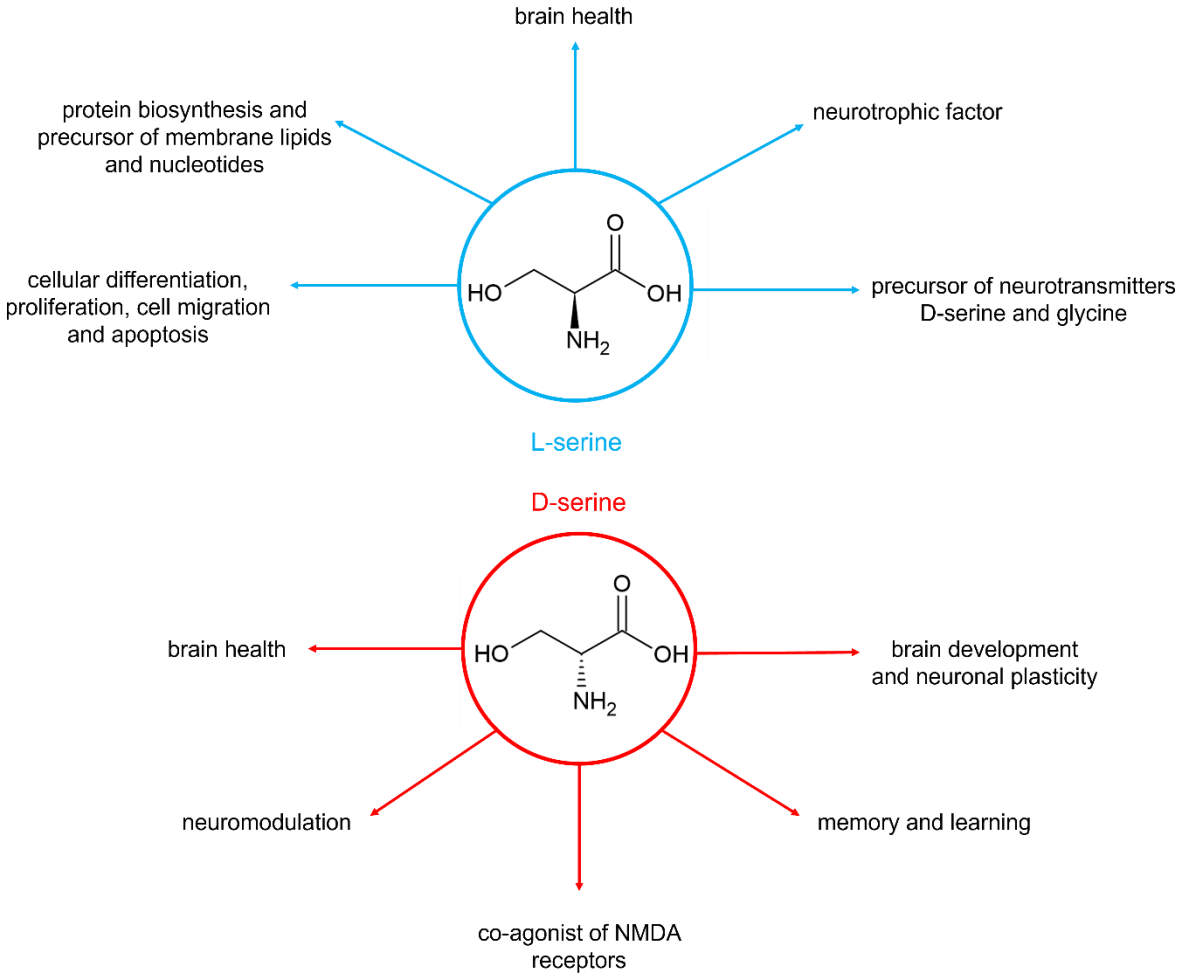

Figure 1. Structures and principal roles of L-serine and D-serine.

L-serine – besides being the proteinogenic enantiomer – plays a key role in intermediate metabolism in eukaryotic cells. Indeed, it is involved in the regulation of important cellular processes such as growth, differentiation, proliferation, cell migration and apoptosis (Kent et al., 1995; Holeček et al., 2022). L-serine also participates in protein biosynthesis, is the main source of monocarbonic cell units, serves as a precursor of membrane lipids such as phosphatidylserine, sphingolipids, i.e., sphingomyelin (Hirabayashi et al., 2008; McCluskey et al., 2022) and cerebrosides, and is necessary for the synthesis of nucleotide precursors as thymidine (Herbig et al., 2002). Moreover, L-serine plays an essential function in the central nervous system (CNS) as a neurotrophic factor (Yoshida et al., 2004; Holeček et al., 2022). It is also the precursor of glycine and D-serine signal molecules, which represent the co-agonists of N-methyl-D-aspartate (NMDA) glutamate receptors. NMDA receptors are involved in the development, plasticity and function of the central nervous system (Furuya et al., 2008; Chen et al., 2023). The important role of L-serine in the brain was evidenced in both *in vitro* and clinical data. L-serine improved, in a dose-dependent manner, the survival of human cultured hippocampal neurons and Purkinje cells (Yoshida et al., 2004). In addition, patients with significantly decreased levels of L-serine and glycine in plasma and cerebrospinal fluid are affected by severe neurological disorders (Tabatabaie et al., 2011; Van der Crabben et al., 2013; Swanson et al., 2022). The other evidence of the strong connection between L-serine and CNS is that the *de novo* synthesis of L-serine is mainly produced in astrocytes through the phosphoglycerate pathways (PP), indicating that it represents an essential amino acid for neurons (Furuya et al., 2000; Yamasaki et al., 2001; Holeček et al., 2022). Also, D-serine is fundamental for the brain. Indeed, abnormalities of D-serine

levels have been related to several neuropathologies and psychiatric disorders caused by hyper or hypo-activation of the NMDA receptors. In physiological conditions, D-serine accounts for 5 to 20 percent of the total serine in the cerebrospinal fluid (Dietzen et al., 2018). In particular, low levels of D-serine are associated with schizophrenia, while a high concentration is linked to Alzheimer's and Parkinson's diseases (Martineau et al., 2008; Lu et al., 2023). The critical role of D-serine in neuromodulation was highlighted by Inoue et al., 2008 thanks to knockout mice for serine racemase (SR-KO mice). SR is the enzyme responsible for D-serine production. SR-KO mice exhibited an altered brain transmission; in particular, they presented hypofunction phenotypes of NMDA receptors which the typical characteristics of schizophrenia, with a lower number of dendrites spines and a diminished of hippocampal volume (Balu et al., 2013). In addition, the animals presented alterations in spatial memory and difficulties in pre-pulse inhibition (Labrie et al., 2009).

1.2 Serine metabolism

In humans, there are several sources of L-serine; it can be absorbed at the intestinal level through the diet or obtained by the turnover of proteins and phospholipids (Herbig et al., 2002; Holeček et al., 2022). However, in the CNS, the primary route of L-serine biosynthesis is the phosphorylated pathway (PP). It takes place in the astrocyte, starting from the glycolytic intermediate 3-phosphoglycerate. Under physiological conditions, the *de novo* synthesis through the PP is essential to supply the L-serine needed by the brain. Indeed, L-serine distribution in CNS is limited due to the reduced permeability to the blood-brain barrier (Yoshida et al., 2004; D'Souza et al., 2023). L-serine produced in astrocytes by the PP is critical for brain

neurotransmission since it is the precursor of D-serine and glycine, two co-agonists of NMDA receptors (Neame et al., 2019). An overview of serine metabolism in the human brain is shown in Figure 2.

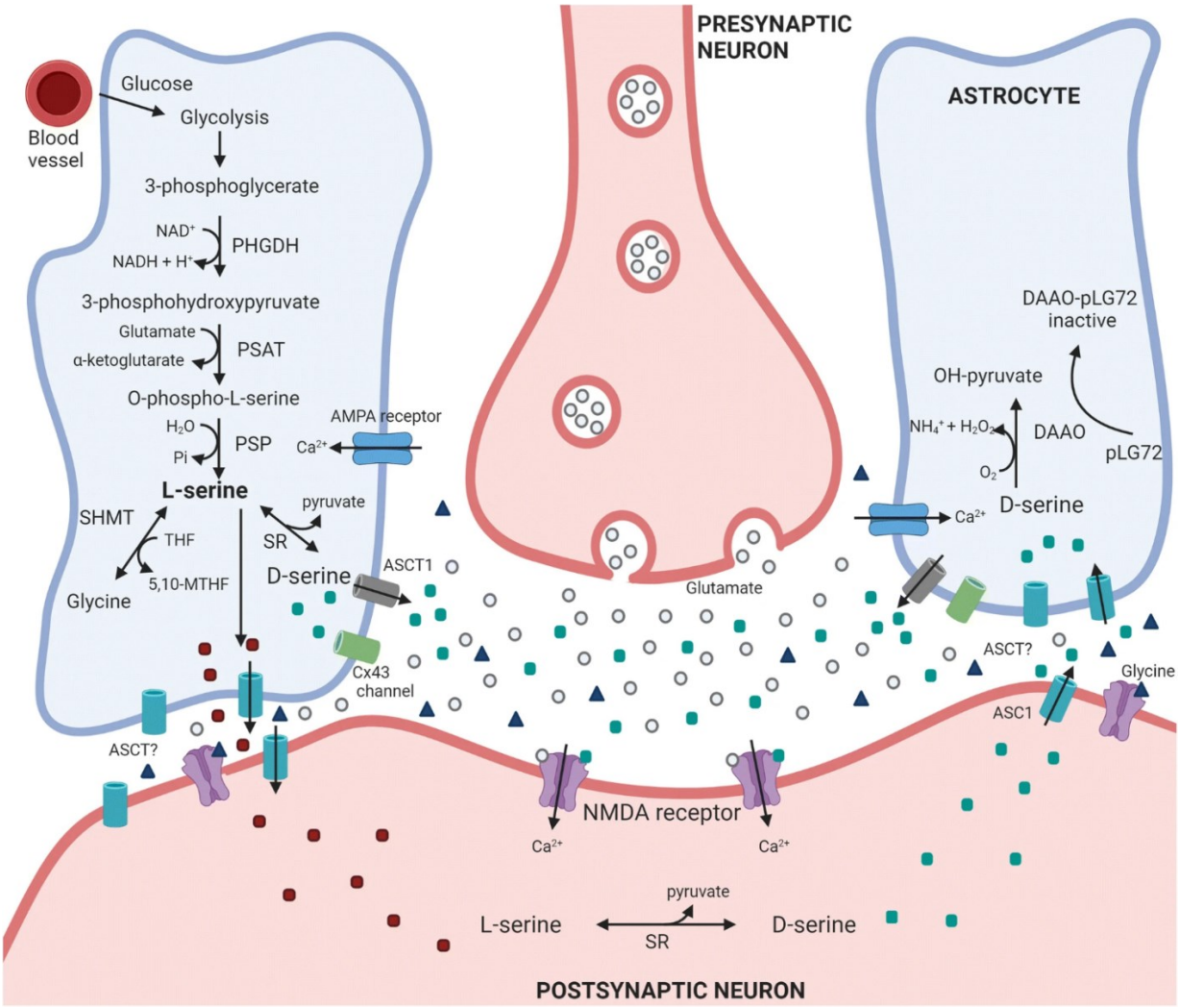

Figure 2. Model of the L-serine/D-serine metabolism in the CNS (Murtas et al., 2020).

The cytosolic PP consists of three sequential enzymatic reactions. The first two reactions are reversible and are catalyzed respectively by 3-phosphoglycerate dehydrogenase (PHGDH, EC 1.1.1.95) and phosphoserine aminotransferase (PSAT, EC 2.6.1.52). PHGDH oxidizes 3-phosphoglycerate to 3-phosphohydroxypyruvate

using NADH as a co-substrate (Figure 3-A), while PSAT converts 3-phosphohydroxypyruvate to 3-phosphoserine (Figure 3-B). The third and last reaction is irreversible and is catalyzed by phosphoserine phosphatase (PSP, EC 3.1.3.3), which catalyzes the dephosphorylation of 3-phosphoserine to L-serine (Figure 3-C) (Wang et al., 2013). PHGDH is abundantly expressed in astrocytes, whereas the cellular levels are barely detectable in neurons. Instead, PSAT and PSP are expressed in both cell types (Furuya et al., 2000).

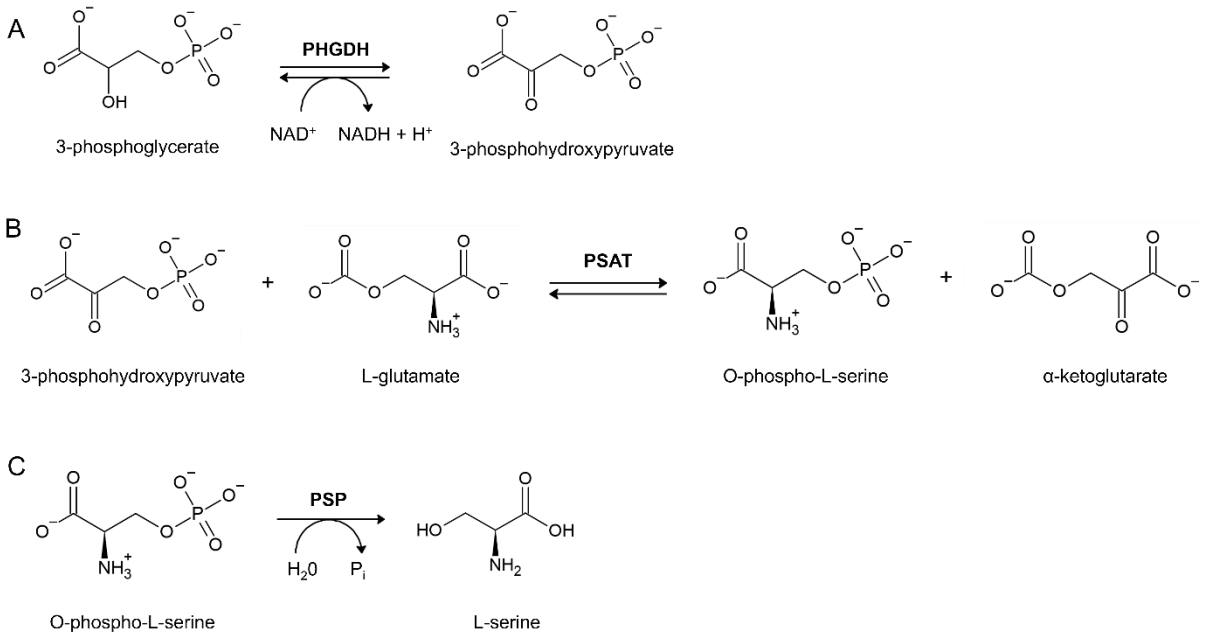

Figure 3. Schematic representation of the three sequential enzymatic reactions in the phosphorylated pathway. **A)** PHGHD enzyme. **B)** PSAT enzyme. **C)** PSP enzyme.

L-serine produced by PP can be converted into the neurotransmitters glycine and D-serine thanks to serine hydroxymethyltransferase and serine racemase enzymes, respectively. The enzyme serine hydroxymethyltransferase (SHMT, EC 2.1.2.1) can catalyze the reversible and simultaneous conversion of L-serine to glycine and of

tetrahydrofolate into 5,10-Methylenetetrahydrofolate (Figure 4) (Verleysdonk et al., 1999; Cappello et al., 2022). There are two isoenzymes of SHMT, mitochondrial and cytosolic forms. Only the mitochondrial isoenzyme is probably present in the CNS.

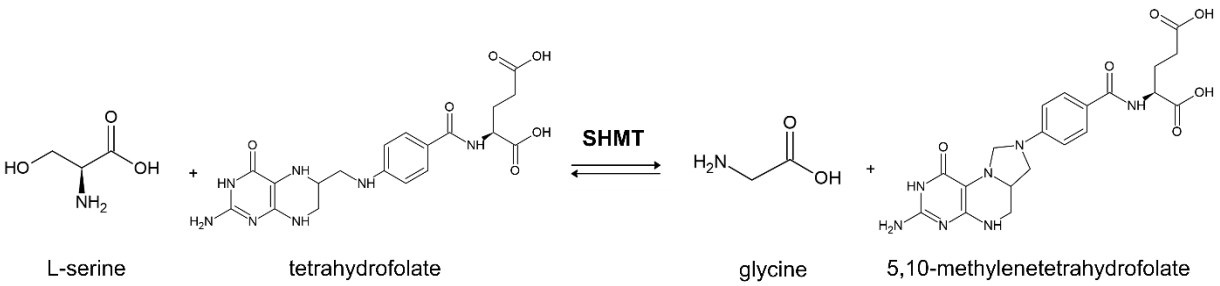

Figure 4. Reactions catalyzed by serine hydroxymethyltransferase.

Serine racemase (SR, EC 5.1.1.18) converts L-serine into D-serine (Figure 5-A). This enzyme also catalyzes the dehydration of both enantiomers to pyruvate and ammonia (Figure 5-B) (Wolosker et al., 1999; Ramos et al., 2023).

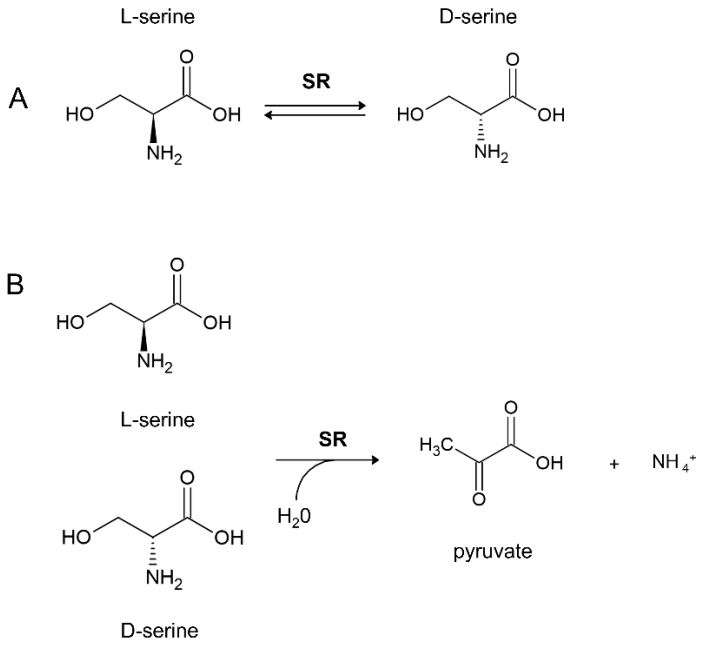

Figure 5. Reactions catalyzed by serine racemase. **A)** Racemization. **B)** Dehydration.

D-serine is then degraded by D-amino acid oxidase (DAAO, EC 1.4.3.3) (Pollegioni et al., 2007). It is notable that L-serine and their precursors are primarily found in astrocytes, while SR is founded mainly in neurons (Wolosker, 2011), suggesting the presence of a transport mechanism of L-serine from astrocytes to neurons. The “shuttle hypothesis” has been proposed in which L-serine produced in astrocytes can be shuttled to neurons, where it is converted to D-serine by SR. Based on this mechanism, neurons release D-serine at the synaptic interface. Then, the neurotransmitter can be re-uptaken by neurons and possibly astrocytes through serine transporters (ASCT-1) (Wolosker et al., 2016). Recent work supported this astrocyte-neuron crosstalk demonstrating that the inhibition of astrocytic PHGDH suppressed the de novo synthesis of L- and D-serine and reduced the NMDA receptor's synaptic potentials (Neame et al., 2019).

1.3 PLP-dependent enzymes in serine metabolism

Both enzymes investigated in this dissertation are pyridoxal-5'-phosphate-(PLP)-dependent enzymes: PSAT and SR. The PLP-dependent enzymes are characteristic for requiring the PLP as a cofactor for their catalytic activity. PLP functions as a cofactor in many enzymatic processes, including decarboxylation, deamination, transamination, racemization, and others (Percudani & Peracchi, 2009; Yoshimura, 2022). PLP represents the most important metabolically active form of vitamin B6. The denomination "vitamin B6" refers to a group of six biologically interconvertible compounds of 3-hydroxy-2-methylpyridine: pyridoxal, pyridoxine, pyridoxamine, and their respective 5'-phosphates (Figure 6) (Percudani & Peracchi, 2009; Saxena et al., 2022). The PLP structure is formed by a pyridine ring

heteroaromatic with four substituents: an aldehyde group on C4, a methyl group on C2, a phosphate ester on C5 and a hydroxide on C3 (John et al., 1995; Yoshimura, 2022)

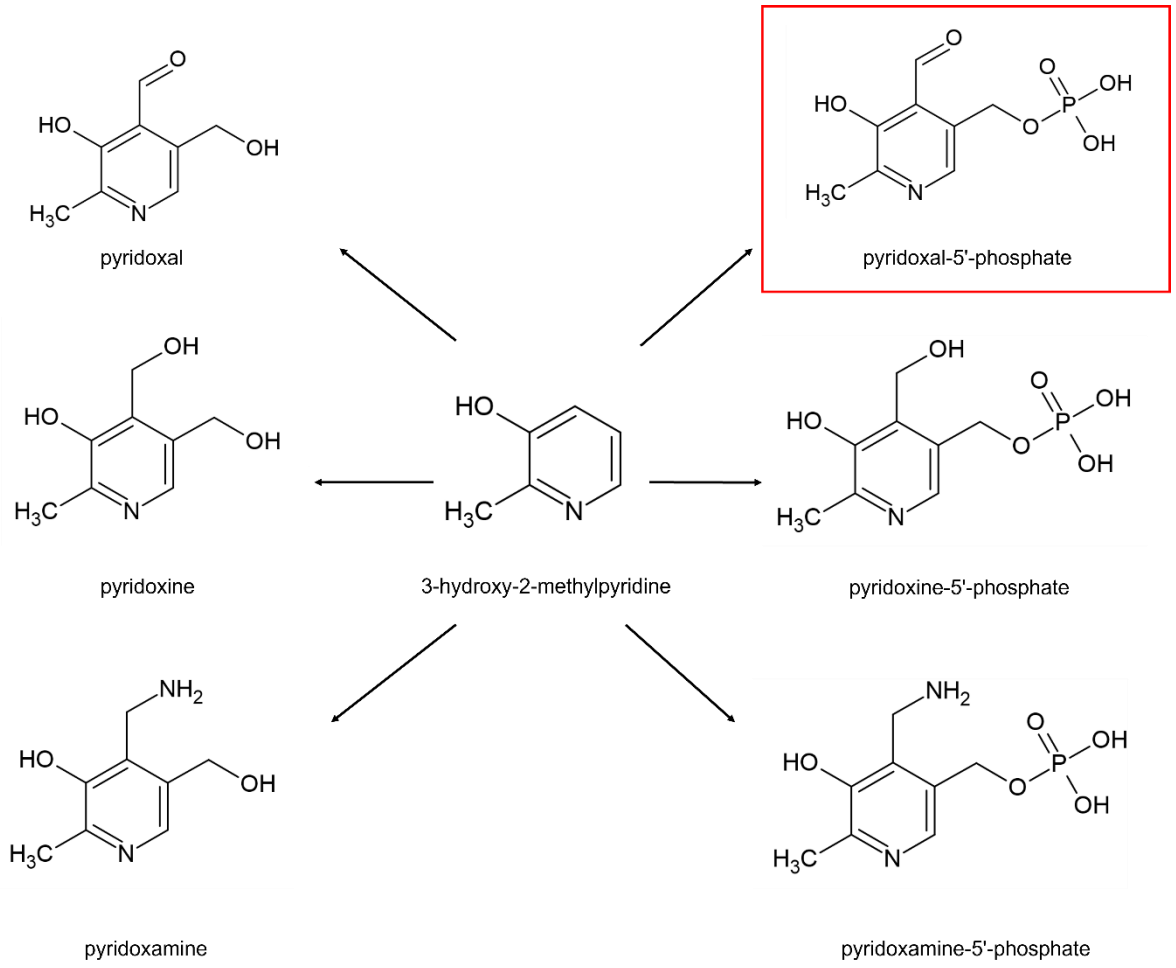

Figure 6. Biologically interconvertible compounds of the vitamin B6. PLP is highlighted with a red square.

Since the principal substrates of PLP-dependent enzymes are amines and amino acids, they are involved in key cellular metabolic pathways in all organisms, such as serine metabolism (Yoshimura, 2022). Consequently, they are frequently related to important metabolic diseases (Nguyen et al., 2022). In the human brain's

serine metabolism, there are three examples of PLP-dependent enzymes: PSAT, the second enzyme in the PP, SR, the enzyme responsible for D-serine regulation, and SHMT, which converts L-serine into glycine.

PLP-dependent enzymes are classified into seven "fold types" based on their structural organization and evolution (Yoshimura, 2022). PSAT is a transaminase and belongs to the fold type group IV of the α-family (Murtas et al., 2020). SR is part of the fold type II, which includes enzymes capable of catalyzing reactions of β-elimination and β-substitution (Raboni et al., 2019). Instead, SHMT is a ubiquitous representative of the largest and best-characterized family of fold type I (Florio et al., 2011; Fauziah Ma'ruf et al., 2021).

1.4 Phosphoserine aminotransferase (PSAT)

1.4.1 Structure

PSAT is the second enzyme of the L-serine phosphorylated pathways (Tabatabaie et al., 2011). The crystal structure of human enzyme complexed with PLP deposited in the protein data bank (PDB) had a resolution of 2.5 Å (PDB entry 3E77, residues L17–L370).

PSAT forms a homodimer characterized by an α/β fold, in which each monomer contains one PLP moiety (Figure 7-A). The interface between the monomers is extensive; around 12% of the protomer surface is buried (Figure 7-B) (Coulibaly et al., 2012; Murtas et al., 2020).

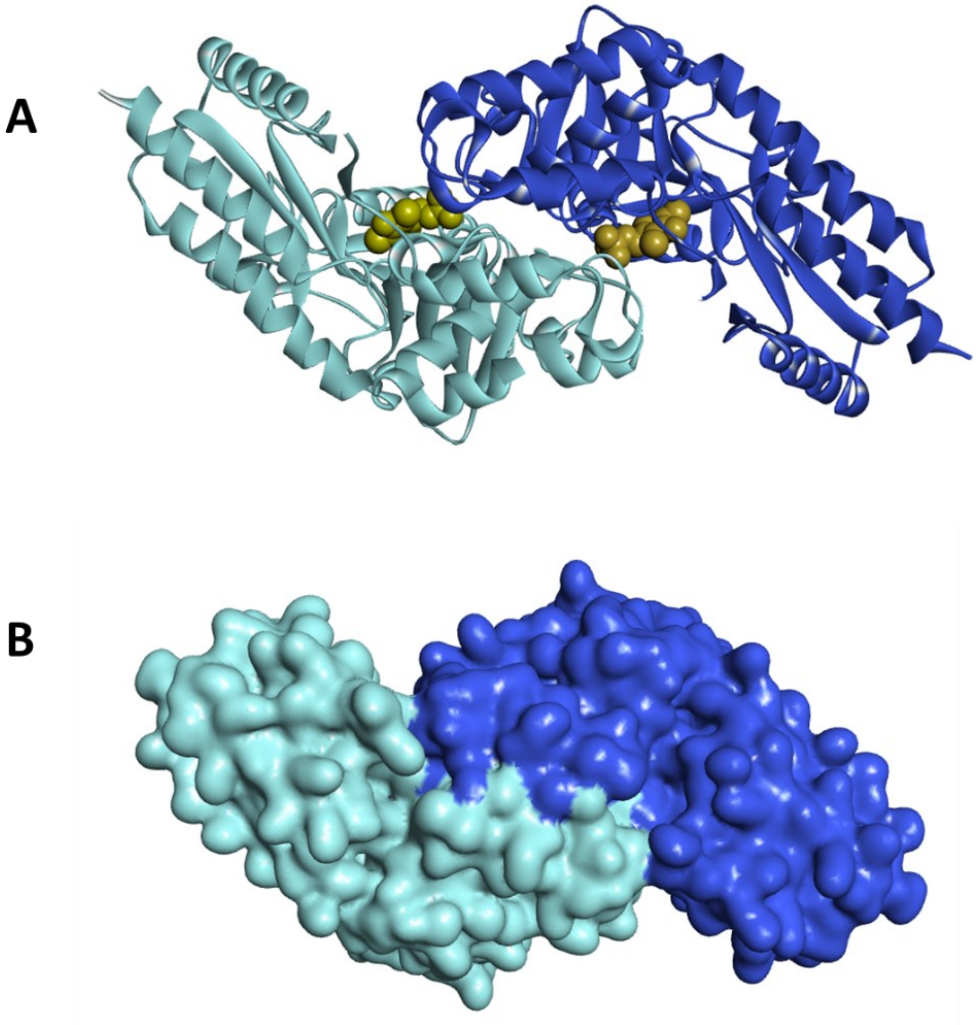

Figure 7. A) Structure of PSAT human enzyme (hPSAT) in complex with the cofactor PLP (PDB 3E77). The PLP is represented in yellow. **B)** Molecular surface of hPSAT dimers. The two subunits are in different shades of blue.

In the human enzyme, each monomer consists of 362 amino acid residues and is formed by a large and a small domain (Figure 8). The large domain includes residues 17-263 and exhibits six α-helixes and seven β-sheets, all parallel except for the second. The small domain consists of residues 3-16 and 264-362 and has a compact structure with three α-helixes and two antiparallel β-sheet.

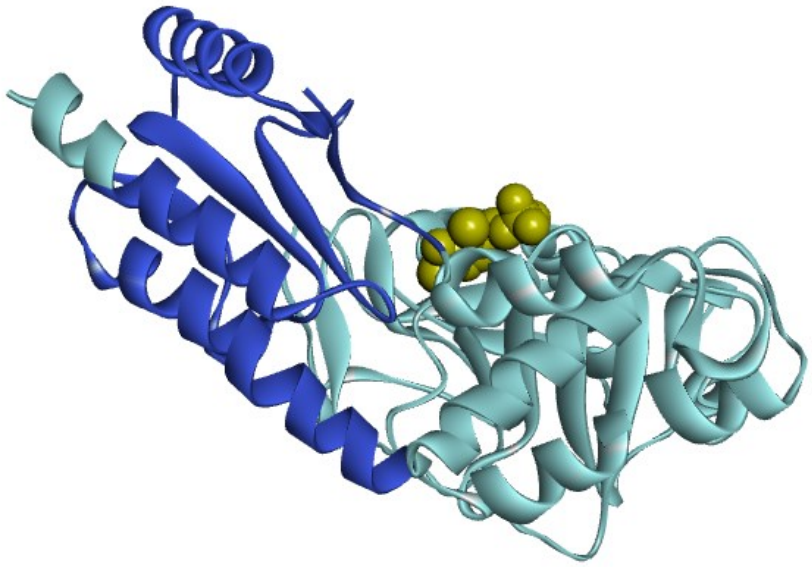

Figure 8. Structure of PSAT monomer (PDB 3E77). The small domain is shown in dark blue, and the large domain is highlighted in cyan. The cofactor PLP is represented in yellow.

Residues from both domains contribute to the active site, which is at the interface between the two monomers. This feature, typical of the PLP-dependent enzymes of the α family, suggests that the dimeric state is fundamental for enzyme activity (Murtas et al., 2020; Singh et al., 2021).

PSAT has been isolated and characterized from bacteria, yeast, plants, rodents and mammals (Tabatabaie et al., 2011). In a recent comparison of PSAT structures of different organisms, it emerged that its architecture is quite similar, except for the length of the two last α-helixes belonging to the small domain. In human PSAT (hPSAT), the loop near the two α-helixes is longer than in other organisms (Singh et al., 2019). Interestingly, this loop is close to the active site. Indeed, both loops are located at the entrance of the active site cleft. The longer loop in hPSAT probably

provides major flexibility and, consequently, better access to the active site influencing the biochemical properties (Singh et al., 2019).

Like other PSATs, the human enzyme exhibits local positive charges around the active site and negative charges distributed over the surface (Basurko et al., 1999; Sekula et al., 2018). The cofactor PLP is bound to Lys200, belonging to the large domain. This bond forms the internal aldimine. The pyridine N atom interacts with the large domain and creates hydrogen bonds with W107, T156, and D176. These connections stabilize the aromatic ring of PLP that assumes a parallel direction with the indole ring of W107, resulting in a more favourable stacking interaction (Figure 9). Thanks to the crystal structure of *Bacillus alcalophilus* PSAT, complex with the substrate L-phosphoserine, it is known that the residues S43, H44, R45, and R335 are located at the hPSAT active site and participate in the substrate binding (Battula et al., 2013).

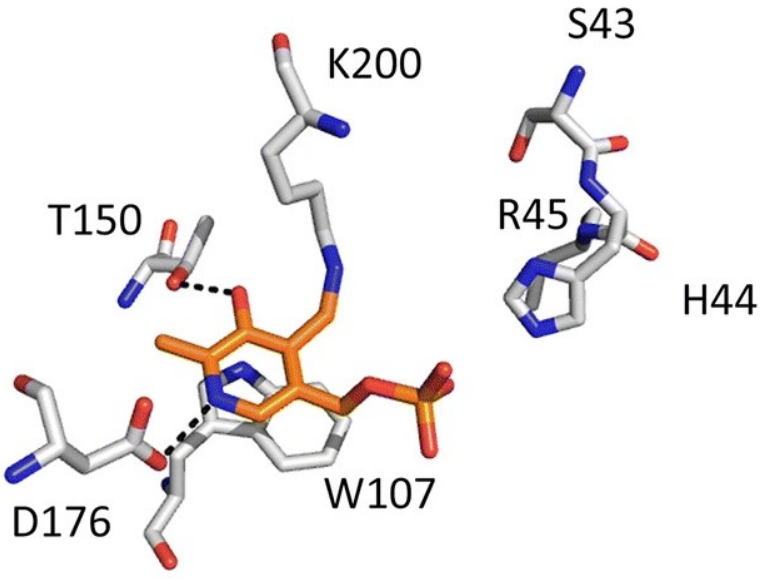

Figure 9. Representation of PLP (orange) covalently bound to Lys200 and amino acid interactions in the active site of hPSAT (adapted from Murtas et al., 2020).

PSAT variants of the protozoan parasite *Entamoeba histolytica* allowed to understand that a small loop between N-terminal residues 1-16 is crucial for enzyme activity. It is buried in the active site with the role of maintaining the active site architecture and limiting the movement of the loop containing the Lys200, stabilizing the internal aldimine formation. Indeed, the PSAT variants in the N-terminal loop show almost complete enzymatic inactivity, demonstrating that it is crucial to enzyme activity (Singh et al., 2019).

Experiments on green alga *Scenedesmus obliquus* PSAT have led to the conclusion that the enzyme active site is optimized to bind L-glutamate, 3-phosphohydroxypyruvate, 2-oxoglutarate and O-phospho-L-serine, which have side chains of equal length (Stolz et al., 1995). Bovine PSAT is able to use the 2-amino-5-valerate, L-homocysteate and 2-amino-4-phosphobutyrate as substrates (Basurko et al., 1999). At the same time, *Escherichia coli* PSAT accepts L-aspartate (Figure 10) (Duncan et al., 1984; Lewendon et al., 1984).

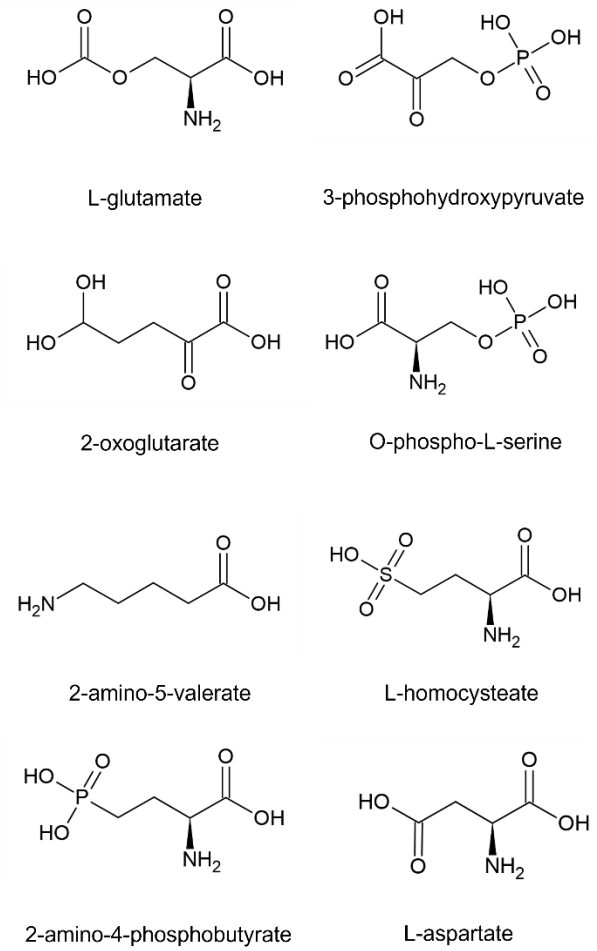

Figure 10. Examples of PSAT substrates.

The crystal structure of *Escherichia coli* PSAT, complexed with α-methyl-l-glutamate (PDB, 1BJO), shows that the arginine residues in the active site may contribute to stabilizing the L-aspartate bond (Hester et al., 1999). However, the substrate preference of hPSAT is still unclear.

1.4.2 Catalysis

PSAT catalyzes the reversible glutamate-dependent transamination of 3-phosphohydroxypyruvate to 3-phosphoserine, releasing 2-oxoglutarate. The cow

PSAT and *Arabidopsis thaliana* PSAT enzymes show a bimolecular ping–pong mechanism (Basurko et al., 1999; Sekula et al., 2018), probably also present in the human enzyme. In this mechanism, the enzyme reacts with the substrate to form a product, dissociating before the second substrate binds to the active site (Lueck et al., 1973). It is a pH-dependent enzymatic reaction that, for PSAT, has an optimum pH between 7.5 and 8.5 (Hester et al., 1999). A schematic representation of hPSAT catalytic mechanism is shown in Figure 11.

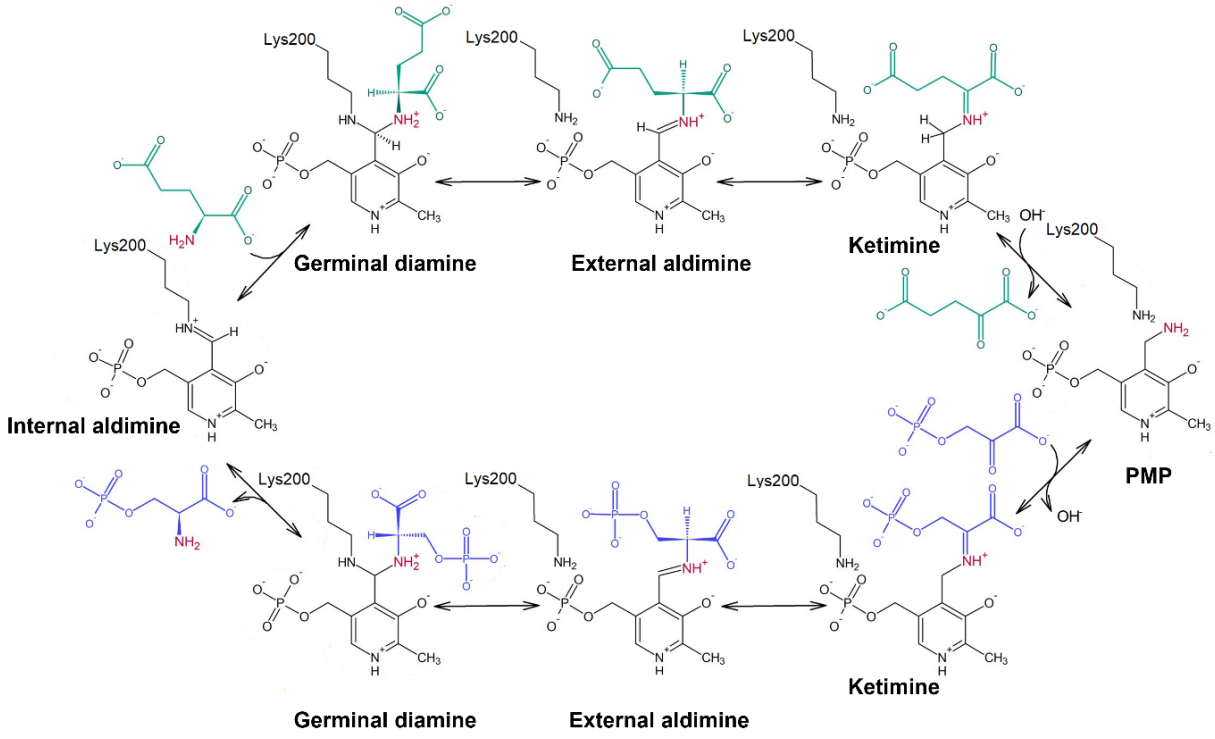

Figure 11. Representation of the hPSAT-catalyzed transamination reaction (modified from Sekula et al., 2018). In the human enzyme, the PLP is bound to Lys200.

Two reversible half-reactions form the transamination reaction (Eliot & Kirsch, 2004). Initially, the PLP aldehyde group covalently binds the ε-amino group of the lysine residue at the enzyme's active site (in hPSAT, the Lys200), forming a Schiff

base defined as internal aldimine. After L-glutamate binding, the internal aldimine breaks up, and the amino group of the substrate makes a nucleophilic attack on the aldehyde group of the PLP, forming a PLP-glutamate *gem*-diamine as an intermediate (Fukui et al., 2008) and then a new Schiff base, termed external aldimine. The exchange of aldimine is known as a transaldimination reaction (Figure 12) (Liang et al., 2019).

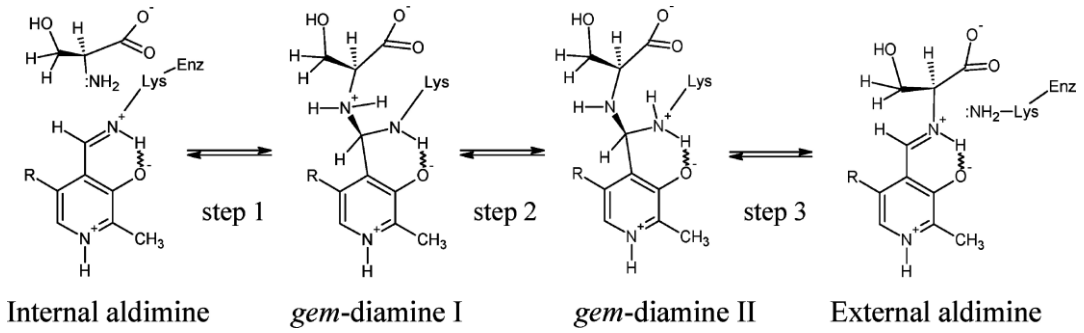

Figure 12. Schematic representation of transaldimination reaction (Vivoli et al., 2009)

Subsequently, the aldehyde group of PLP allows the formation of an imine with a free amino group, while another deprotonated primary amino group can attack the external or internal aldimine making it reversible. This reaction enables the binding of PLP and substrate, the release of the product and the regeneration of the enzyme with the bound PLP in the active site (Liang et al., 2019). After the external aldimine formation, Cα deprotonation leads to a carbanionic or quinonoid intermediate. The subsequent protonation of the PLP in C4, which serves as an "electronic trap", allows the formation of a ketimine intermediate. Then, the hydrolysis of the imine bond enables the release of α-ketoglutarate, and the enzyme binder pyridoxamine-5'-phosphate (PMP) is ready to accept the 3-phosphohydroxypyruvate, which covalently binds PMP. The release of

one molecule of water produces another ketimine and then an external aldimine PLP-3-phosphoserine. At this point, catalytic lysine carries out a nucleophilic attack on the PLP C4 to create an intermediate germinal diamine PLP-3-phosphoserine. The reaction ends when the initial inner aldimine is regenerated, and 3-phosphoserine is released from the active site (Liang et al., 2019; Sekula et al., 2018).

1.4.3 Isoforms

In humans, the primary transcript encoding PSAT can undergo an alternative splicing process, resulting in the production of two mature isoforms: hPSATα and hPSATβ. The hPSATα and hPSATβ have 324 amino acids (35.2 kDa) and 370 amino acids (40.0 kDa), respectively. The two isoforms differ in the presence of 46 residues encoded by exon 8 (138 bp) in the Val290-Ser337 region, which is missing in the shortest isoform (Baek et al., 2003). PSATα is not present in other organisms, then the primary transcript of the gene undergoes alternative splicing only in humans. Experiments in human cell lines showed that hPSATα transcript could be barely detected. In addition, it was not detectable in the healthy tissue. Moreover, there was evidence that it is poorly active (Baek et al., 2003). In contrast, hPSATβ was highly expressed in all cell lines and many human tissues, indicating that, under physiological conditions, this protein isoform is involved in the L-serine biosynthetic pathway (Baek et al., 2003).

1.5 Serine racemase

1.5.1 Structure

Serine racemase belongs to the fold type II family of PLP-dependent enzymes. In solution, SR forms a homodimer with a typical open structure α-β, in which each monomer binds a molecule of PLP (Figure 13).

Until today, more than ten X-ray crystallography structures of SR from various organisms have been deposited in PDB (Raboni et al., 2019). Among these are four human crystal structures; the most recent (PDB, 6SLH) has a resolution of 1.89 Å and represents the hSR holoenzyme, including the PLP cofactor (Koulouris et al., 2020).

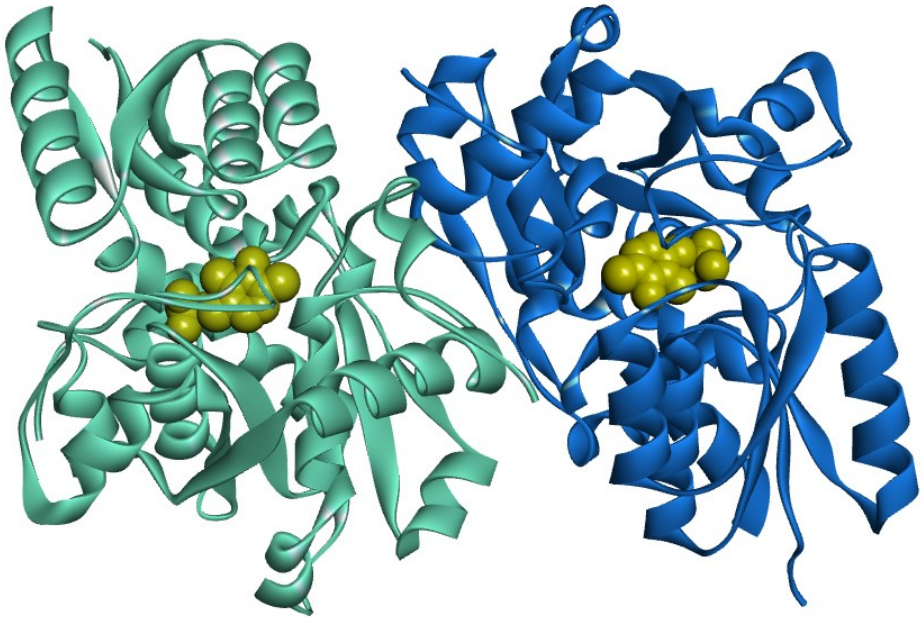

Figure 13. Structure of hSR (PDB, 3L6B). The monomers are shown in cyan and blue, and the PLP is in yellow.

In the human enzyme, each monomer consists of 340 amino acids, formed by a large and a small domain (Figure 14). The large domain is organized into seven β-sheets

(all parallel except the first) surrounded by ten α-helixes, contains the binding site for PLP and is composed of amino acids 1-68 and 157-340. Instead, the small domain has four parallel β-sheets, and three α-helices, arranged in such a way that two (helix 4 and 5) are near the interface between the domains and the third is on the side exposed to the solvent. The small domain includes 78-155 amino acid residues and is connected to the large domain by a flexible region consisting of 69-77 amino acids (Smith et al., 2010; Takahara et al., 2018).

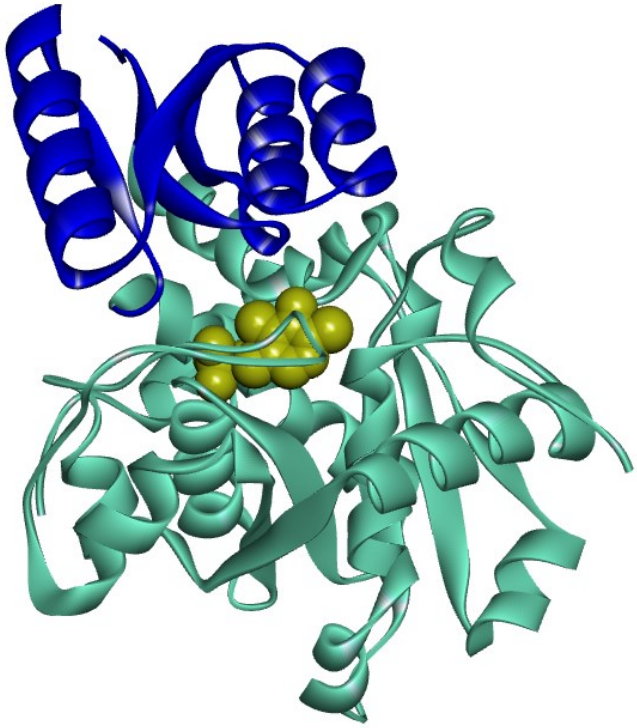

Figure 14. Structure of hSR monomer (PDB, 3L6B). The large domain is shown in cyan, the small domain is represented in dark blue, and the PLP is in yellow.

The cofactor, PLP, is covalently bound as an internal aldimine to Lys56 into the large domain. Other residues interacting with PLP include the Met189 and the

tetraglycine loop (Gly185, Gly186, Gly187 e Gly188) that coordinates the PLP phosphate group with their peptide skeleton nitrogen atoms contributing to the correct positioning of the cofactor for the catalysis reactions (Figure 15). In addition, Ser313 is bound to the pyridine nitrogen, and Asn86 interacts with the 5-OH group (Jiraskova-Vanickova et al., 2011; Campanini et al., 2013; Graham et al., 2019).

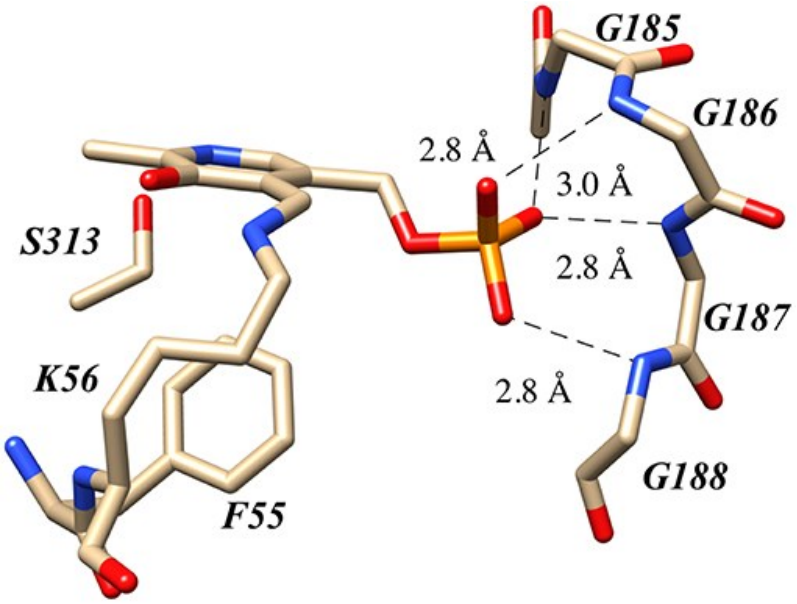

Figure 15. The PLP phosphate binding pocket in hSR (PDB, 3L6B) with the coordination of the tetraglycine loop (Graham et al., 2019).

The PLP binding site residues as tetraglycine loop, 54-9 and 313-316 are conserved between SR orthologues and other dependent PLP enzymes and were demonstrated to be essential for racemase and D-serine dehydratase reactions (Yoshimura & Goto, 2008; Goto et al., 2009; Smith et al., 2010).

The other two binding sites have been crystallographically characterized: one for divalent cations, such as Ca^{2+} and Mg^{2+} and one for nucleotides, such as AMP-PCP, a stable structural analogous of adenosine triphosphate (ATP) (Figure 16).

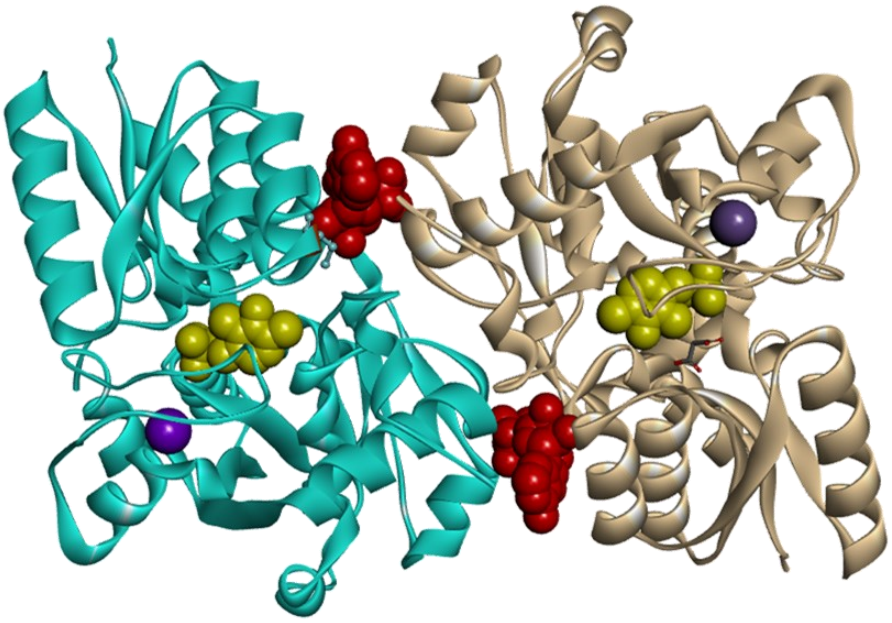

Figure 16. Structure of hSR (PDB, 3L6B). The monomers are shown in cyan and grey, the PLP in yellow, the divalent cation in dark purple and the AMP-PCP in red. The AMP-PCP was placed based on the overlap of the human structure with that of yeast (PDB, 1WTC).

The divalent cations are coordinated with the lateral chains of Glu210 and Asp216, the backbone of Ala214 and three water molecules. They are not directly involved in the catalytic processes of hSR but are necessary for the proper folding and stabilization of the protein structure (Cook et al., 2002; Ito et al., 2012; Bruno et al., 2017).

The organization of the ATP binding site was solved in *Schizosaccharomyces pombe* (SpSR) in complex with AMP-PCP (PDB, 1WTC) by Goto et al., 2009. The nucleotide complexed with Mg^{2+} ions binds into a cleft at the interface between the two monomers. The ATP interacts both with the small and the large domains. The phosphate groups

are positioned at the dimerization interface while the adenine is exposed to the solution. In SpSR the binding site of the ATP is formed by the Ala115 and Tyr119 of the small domain; Asn25, Phe50, Gln51, Lys52, Met53 and Asn311 of the large domain and Ser32, Ser33, Thr34, Arg275, Met276 and Lys277 of the large domain of the other subunit. The adenine ring of AMP-PCP is placed between Ala115 and Arg275. Ribose O3' interacts with the lateral chains of Asn311 and Lys277 of the other subunit. Of these 14 residues interacting with ATP, 11 are conserved in human and rat SR, while Asn25, Thr34 and Met53 are replaced by His, Ile and Thr, respectively. This observation suggested a similar localization of ATP in mammalian (Jirásková-Vanícková et al., 2011).

1.5.2 Dynamics

Human serine racemase shows a complex conformational landscape (Raboni et al., 2019). The conformational change from open to closed forms in the presence of a competitive inhibitor (malonate) was studied in human and rat SR (rSR) by Smith and coworkers. Indeed, rSR and hSR have 90% identical sequences and are structurally indistinguishable. The analysis of rSR buried monomer-monomer surfaces of the open (PDB, 3HMK) and closed (PDB, 3L6C) forms shows that the dimer interface exhibits a high degree of flexibility (Smith et al., 2010). This probably depends on the rearrangement of the interaction between the two monomers upon ligand binding to the active site due to an open-close conformational switch (Raboni et al., 2019). It has been observed that the binding of a physiological substrate (L-serine and D-serine) or an inhibitor (glycine or malonate) causes the rotation of about 20° of the small domain on the large domain to close the active site. In particular, helix 6 and 5

(with the exception of helix 4) move towards the PLP, while the large domain maintains the same orientation in both conformations. This movement leads to the correct positioning of the Ser84 residue with respect to L-serine, allowing the racemization reaction (Yamauchi et al., 2009; Smith et al., 2010). The presence of a conformational change when a ligand is present at the active site was confirmed by the comparison of the hSR bound to malonate (PDB, 3L6R) (Smith et al., 2010) with the more recent structure of hSR without ligand (PDB, 5X2L) (Takahara et al., 2018). The superimposition of the two human structures, open and closed, is shown in Figure 17.

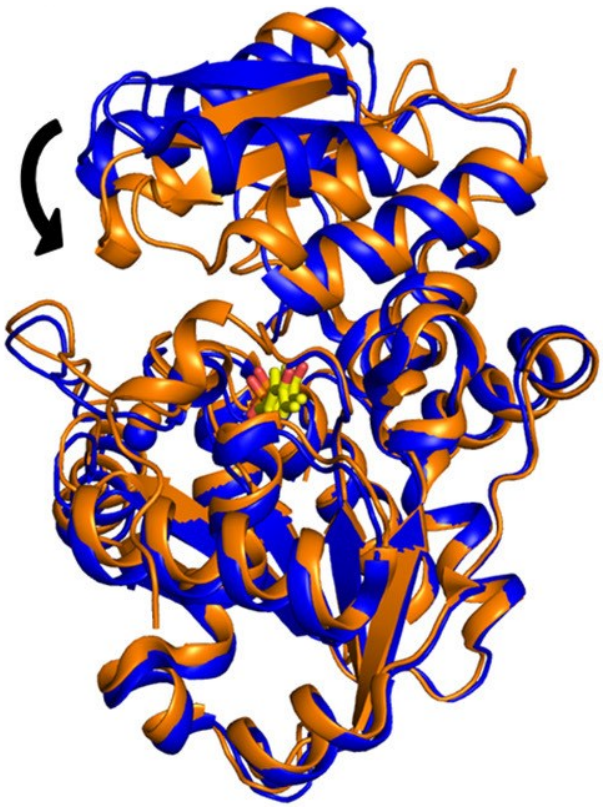

Figure 17. Comparison of the open (PDB 5X2L, blue) and closed (PDB 3L6B, orange) structures of hSR. The PLP is in yellow sticks. The arrow indicates the movement (around 20°) of the small domain toward the large domain after binding with malonate (Raboni et al., 2019).

The SR dynamic in the presence of Mg^{2+}-AMP-PCP was studied in the yeast SR (SpSR) crystal structure (PDB, 1WTC) by Goto and coworkers, 2009. There is a unique structure complex with ATP analogues deposited in the PDB to date. SpSR exhibits 35.1% sequence identity with hSR. It has been observed that the Mg^{2+}-AMP-PCP complex, which binds at the nucleotide site in the open form of the enzyme, does not induce a conformational change. However, when the nucleotide is bound at the dimers interface, the respective orientation between the two domains changes, each revolving around the axis of the adenyl rings of the AMP-PCP, increasing the surface of the posterior groove formed by the two monomers (Figure 18) (Goto et al., 2009).

In addition, it was reported by size exclusion chromatography *in vitro* studies that when ATP is present in solution, the enzyme is present in an equilibrium between dimeric and monomeric form (Bruno et al., 2017). Moreover, fluorescence spectroscopy experiments demonstrated that, in the presence of ATP, SR assumed a conformation like the open state, in which the active site is more closed (Marchetti et al., 2013).

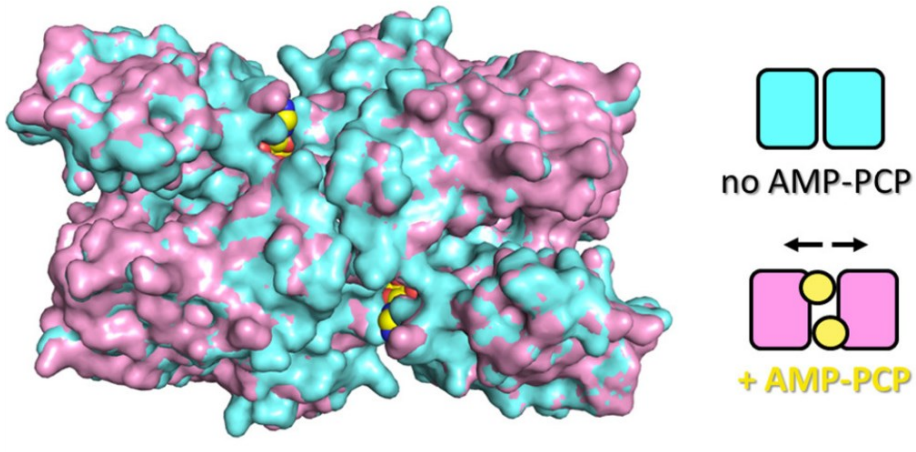

Figure 18. Surface representation of conformational rearrangement of SpSR in the presence (PDB 1WTC, pink) and absence (PDB 1V71, cyan) of AMP-PCP bound at the dimer interface in the two symmetric sites (adapted from Raboni et al., 2019).

1.5.3 Catalysis

Serine racemase has two distinct catalytic activities: it performs the reversible racemization from L-serine into D-serine and their irreversible dehydration to pyruvate and ammonia (Wolosker et al., 1999; Ramos et al., 2023). In addition, it is the only confirmed mammalian enzyme responsible for the isomerization of L-serine to D-serine (Wang et al., 2012). The reactions catalyzed by SR are shown in detail in Figure 19.

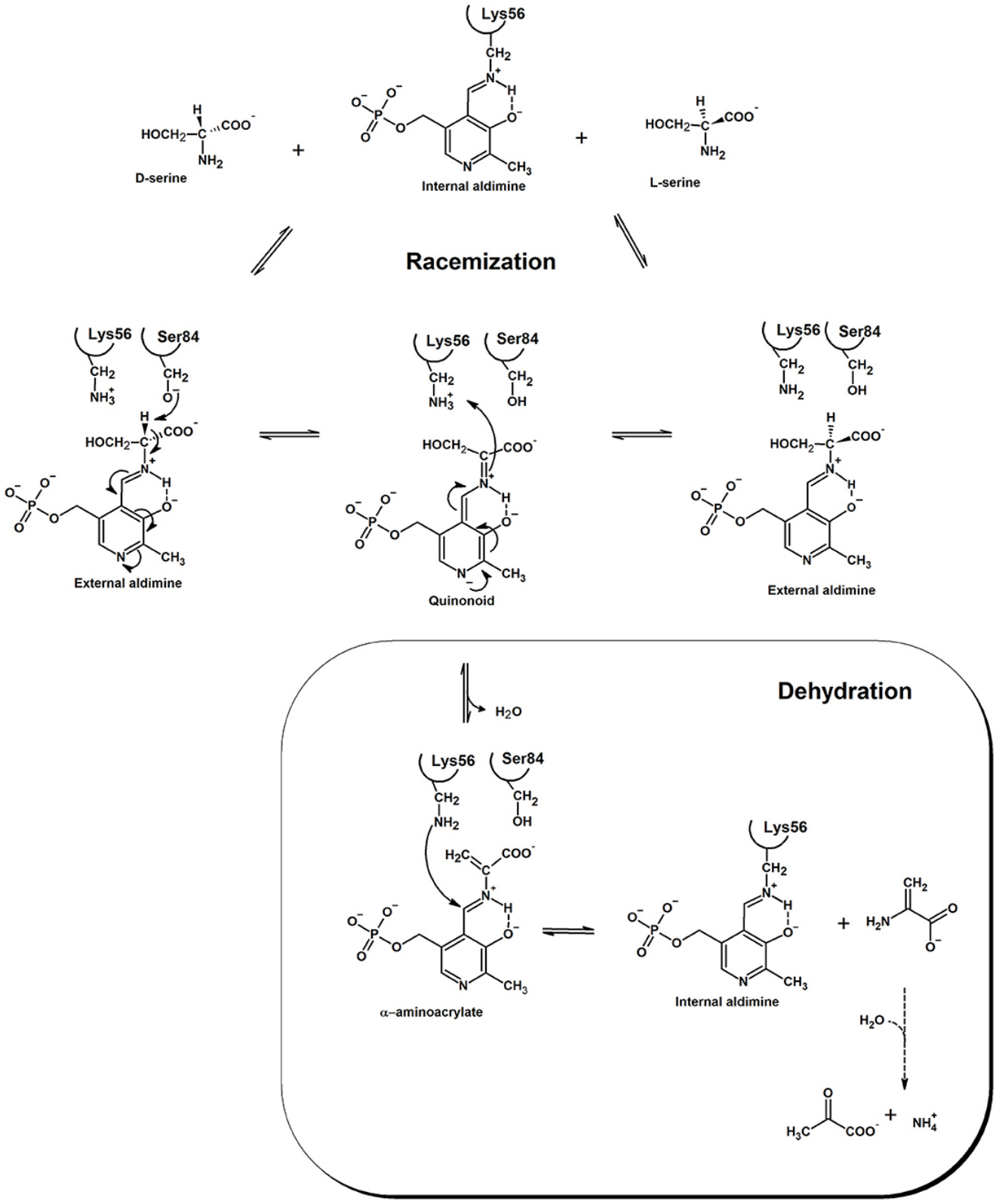

Figure 19. Reactions mechanisms catalyzed by SR: racemization and dehydration (Raboni et al., 2019).

In the absence of substrate, the aldehyde group of PLP is covalently bound to the amino group of Lys56 present in the active site of the enzyme, forming a Schiff base (internal aldimine). The bond with the amino acid substrate allows the PLP to form an external aldimine. Indeed, the α-amino deprotonate group of lysine attacks the C4 of the internal aldimine allowing the release of Lys56 and the reorientation of Ser84, essential for the catalytic activity of the enzyme. If the starting amino acid substrate is L-serine, the α carbon of aldimine gives a proton to Ser84. Instead, when the substrate is D-serine, Lys56 is protonated. Both reactions lead to the formation of a quinonoid intermediate, a planar carbanion that is stabilized by resonance from PLP by delocalizing negative charges on pyridine (Foltyn et al., 2005). After the first two steps, common for both enzymatic reactions, starting from the quinonoid intermediate, the two pathways are separated. In the racemization reaction occurs, the α re-protonation of the carbanion (by Ser84/Lys56) that leads to the regeneration of the external aldimine with L/D-serine as an intermediate, the amino acid substrate is then divided by a transimination with Lys56, thus regenerates the free enzyme. In the dehydration reaction, instead, the hydroxyl of the carbanion in β is protonated, and the amino acid intermediate generated after dehydration is very unstable. It is rapidly hydrolyzed to pyruvate and ammonia. The final quantity of the products of the two reactions is not equivalent. Indeed, the racemization and dehydration reactions occur simultaneously but with different catalytic efficiency. In particular, the performance of dehydration of L-serine is more outstanding than D-serine, and both are more effective than racemization (Marchetti et al., 2013).

1.5.4 Protein interactors

Human serine racemase has a complex interactome fine-tuned at different levels by small ligands, post-translational modifications and proteins (Raboni et al., 2019). Many proteins have been proposed to interact with the hSR, particularly those associated with glutamatergic neurotransmission and the glutamatergic receptors AMPA (α-amino-3-hydroxy-5-methylisoxazole-4-propionic acid) and NMDA. The C-terminal portion of hSR appears to be most relevant for protein partner interactions. Indeed, in this region, there is a well-characterized consensus sequence (Ser-Val-Ser-Val) that is able to recognize PDZ domains (Baumgart et al., 2007). The PDZ domain consists of 80-90 amino acids and is involved in protein-protein interactions (Kim et al., 2004; Stevens et al., 2022). It is known that PICK1 (protein interacting with C-kinase) and GRIP (glutamate receptor interacting protein) bind SR through the PDZ domain (Figure 20) (Jiraskova-Vanickova et al., 2011; Baumgart et al., 2007).

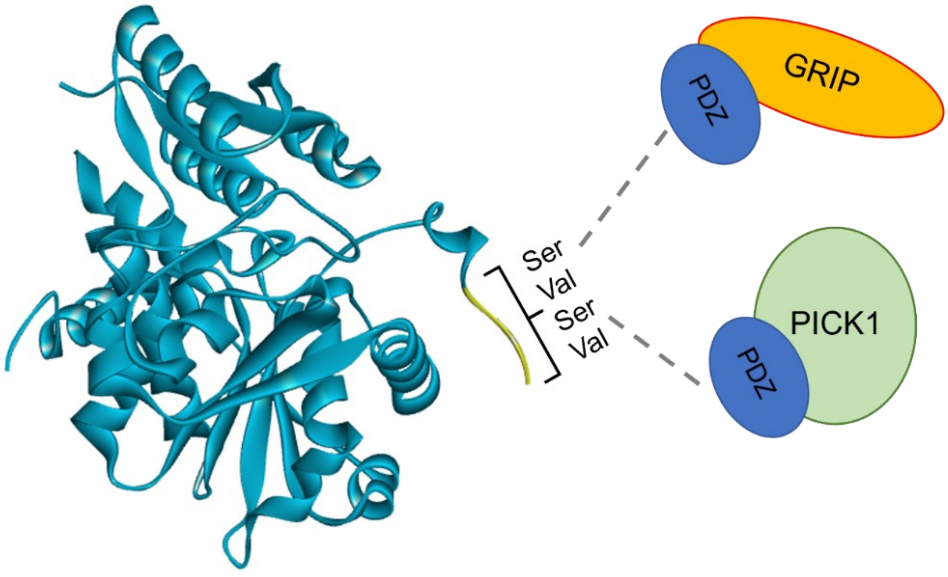

Figure 20. Model of hSR protein-protein interactions. In yellow is shown the consensus sequence (Ser-Val-Ser-Val) of hSR, which is able to recognize the PDZ domains (blue circle) of GRIP (orange) or PICK1 (green) proteins.

Furthermore, it is reported that PICK1 enhances D-serine release from the glia and increases hSR activity (Jiraskova-Vanickova et al., 2011). However, it is still unclear how PICK1 and GRIP interact to regulate the SR, but both depend on the AMPA receptor's phosphorylation state (Wolosker et al., 1999; Fujii et al., 2005; Kim et al., 2005; Matthews et al., 2021). Moreover, SR degradation via the ubiquitin-proteasome system is mediated by GOLGA3 (golgin subfamily A member 3 or GCP70 or golgin-160) and DISC1 (disrupted-in-schizophrenia-1). GOLGA3 stabilizes SR levels through the inhibition of its ubiquitination. Indeed, GOLGA3 interferes with the binding of ubiquitin E3, reducing the levels of ubiquitination and degradation in vivo (Wolosker et al., 1999; Fujii et al., 2005; Dumin et al., 2006; Canu et al., 2014; Ito et al., 2020). A similar action is performed by DISC1, which is an interesting drug target for schizophrenia and other psychiatric disorders. DISC1 mutant studies have clarified its role in binding and stabilizing SR, preventing its degradation through ubiquitination (Ma et al., 2013).

In addition, the interaction between SR and glyceraldehyde 3-phosphate dehydrogenase (GAPDH) has been studied in murine orthologues by Suzuki et al., 2015. The authors reported that murine SR interacts directly with murine GAPDH in the presence of glyceraldehyde-3-phosphate (G3P), the GAPDH substrate, resulting in SR inhibition. Since GAPDH catalyzes the sixth step of glycolysis, SR-GAPDH interaction may be a biochemical link between glycolysis and D-serine metabolism (Suzuki et al., 2015). This topic is a part of my PhD research work and will be discussed in detail in chapters 3 and 4.

1.6 Serine metabolism disorders

Anomalies in the L-serine and D-serine metabolism are related to different pathologies. The main diseases are summarized in Table 1.

L-SERINE	❖ SDDs	• PHGHD deficiency • PSAT deficiency • PSP deficiency • NLS • NLS2
	❖ Cancer	
D-SERINE	❖ NMDA receptors hyperactivation	• Alzheimer's disease • Parkinson's disease • Ischemia • Amyotrophic lateral sclerosis
	❖ NMDA receptors hypoactivation	• Schizophrenia • Neuronal damage

Table 1. Overview of the main L-serine and D-serine metabolism pathologies.

Serine deficiency disorders (SDDs) are a heterogeneous clinically and genetically group of rare autosomal recessive pathologies caused by pathogenetic alterations in genes coding for phosphorylated pathway enzymes, namely PHGDH, PSAT and PSP. These neurometabolic disorders are characterized by neurodevelopmental defects, epilepsy, microcephaly and low plasma and cerebrospinal fluid serum levels (Acuna-Hidalgo et al., 2014; Brassier et al., 2016; Ni et al., 2019; Abdelfattah et al., 2020).

The first described disruption of L-serine biosynthesis was reported by Jaeken et al., 1996, on the *PHGDH* gene. Most cases of SDDs are still associated with pathogenic variants of 3-PHGDH (Yoshida et al., 2004; Tabatabaie et al., 2010; Van

der Crabben et al., 2013; Benke et al., 2017), but recently there have been an increasing number of cases related the mutations in the gene *PSAT1* encoding for PSAT. SDDs associated with the genetic impairment of *PSAT1* are known as PSAT deficiency (PSATD, OMIM # 610992). The first two cases of PSATD were observed in the year 2007 in two siblings heterozygous that had a frameshift and a missense mutation of the *PSAT1* code for the D100A variant. Both siblings exhibited typical intractable seizures, microcephaly, psychomotor retardation, and hypertonia. Unlike other L-Ser disorders, they were not symptomatic at birth, suggesting the possibility of post-natal treatment (Hart et al., 2007). More recently, PSATD was associated with a case of S43R PSAT variant (Brassier et al., 2016) and with the cases of T156M and A15P PSAT variants (Debs et al., 2021). Noteworthy that the A15P PSAT variant was reported as the first case of successful therapy with administration post-birth of L-serine (Debs et al., 2021). Thanks to early diagnosis, the integration of serine in the mother and newborn could reduce and, in some cases, even prevent the onset of symptoms (Jaeken et al., 1999; Brassier et al., 2016; Debs et al., 2021). However, accurate assessment of serine levels requires measurement of cerebrospinal fluid concentration and accurate comparison with control levels of the same age. For this reason, early diagnosis depends on personal family history and genotypic information. Therefore, this is a disease in which knowledge of the functional significance of genetic variants can dramatically alter patient clinical outcomes (De Koning et al., 2004; Moat et al., 2010; Brassier et al., 2016; Sirr et al., 2020).

Neu–Laxova syndrome (NLS) is the most severe disease in the spectrum of SDDs the first description was in 1971 (Neu et al., 1971), is a rare lethal multiple-malformation disorder with less than 100 cases reported to date (Manning et al., 2004;

Coto-Puckett et al., 2010; Acuna-Hidalgo et al., 2014; Shaheen et al., 2014; Mattos et al., 2015; El-Hattab et al., 2016; Ni et al., 2019; Bourque et al., 2019; Cavole et al., 2020). The distinctive clinical features of NLS consist of intrauterine growth restriction (IUGR) and typical craniofacial abnormalities. CNS abnormalities such as microcephaly and cerebellar hypoplasia, skin alterations such as ichthyosis and joint contractures are also frequent. Other congenital malformations such as the lip and cleft palate, spina bifida or genitourinary tract abnormalities have also been reported occasionally. Although NLS causes pre-perinatal death, some cases of survival have been observed for weeks or months (Abdelfattah et al., 2020; Sirr et al., 2020). When associated with homozygous or compound heterozygous mutations of *PSAT1*, NLS is known as Neu-Laxova syndrome-2 (NLS2, OMIM # 616038) (Abdelfattah et al., 2020). NLS was initially associated with variants of *PHGDH* (Shaheen et al., 2014). However, pathogenic variants of PSAT have been recently identified (Acuna-Hidalgo et al., 2014; Abdelfattah et al., 2020). The PSAT variants A99V and S179L were associated with NLS2 (Acuna-Hidalgo et al., 2014; Abdelfattah et al., 2020). In addition, the Y70N and R342W variants were identified in Chinese families (Ni et al., 2019), and a screening of 15 families with NLS2 led to the identification of the G79W, C245R, E155Q and R61W PSAT variants (Abdelfattah et al., 2020). The same study confirmed the association of NLS2 with the A99V and S179L variants (Abdelfattah et al., 2020). The PSAT pathogenic variants are a part of my PhD research work, and their functional and biochemical characterization will be discussed in detail in chapter 2.

In addition to SDDs, recent studies have highlighted the role of the phosphorylated pathway in cancer, suggesting that the hyperactivation of serine biosynthesis may drive oncogenesis (Amelio et al., 2014; Singh et al., 2021). Indeed,

high levels of L-serine increase the carbon units and building blocks for the production of amino acids, nucleotides and lipids used by cancer cells for proliferation. Moreover, in cancer cells, a part (around 10%) of 3-phosphoglycerate obtained from glycolysis is converted to 3-phosphohydroxypyruvate. PSAT uses this molecule to convert glutamate to α-ketoglutarate, which supports cancer cell metabolism through the Krebs cycle (Possemato et al., 2011; De Berardinis et al., 2011). In addition, it is known that PSAT overexpression is linked to a less efficacy response to treating breast cancer (Martens et al., 2005; Zhu et al., 2022), and it is associated with most colorectal cancer (Friederichs et al., 2005; Van de Gucht et al., 2022) and adenocarcinoma (Ojala et al., 2002; Zhao et al., 2022). Moreover, recently, L-serine metabolism could be related to the development of diabetes (Holm et al., 2019).

Also the anomalies in D-serine metabolism are related to severe pathologies. Indeed, the correct levels of D-serine in the CNS are fundamental to regulating the activity of NMDA receptors and, consequently, to brain health (Furuya et al., 2008; Ni et al., 2022). In physiological conditions, D-serine levels were in the range of 5-20 percent of the total serine in the cerebrospinal fluid (Dietzen et al., 2018). Altered levels of D-serine represent a trigger for glutamatergic transmission dysregulation (Conti et al., 2011; Chen et al., 2022), resulting in many pathologies. In particular, an increase in neurotransmission is associated with Alzheimer's and Parkinson's diseases (Martineau et al., 2008; Lu et al., 2023), ischemia and amyotrophic lateral sclerosis (Sasabe et al., 2007; Kapil & Sharma, 2020). A decrease is related to schizophrenia and neuronal damage (Bennett et al., 2009; Wu et al., 2022).

Aim of the work

L-Serine metabolism is critical in the human brain. Indeed, it plays an essential role in the development and functioning of the central nervous system. Defects in the genes that encode for the enzymes in the phosphorylated pathway are related to a different spectrum of CNS diseases, from serine deficiency disorders to Neu-Laxova syndrome. The first aim of this PhD thesis was to carry out a structural and biophysical characterization of some relevant pathogenic variants of human phosphoserine aminotransferase (PSAT) to clarify their loss of function mechanism. Since all three enzymes of the PP can affect SDDs producing overlapping phenotypes, the molecular understanding of their pathogenetic variants is relevant for the affected individuals' diagnosis, prognosis, and therapy. Therefore, eight PSAT variants and wild-type PSAT were selected from the literature, expressed, and purified. The PSAT variants were biochemically characterized by various techniques: spectroscopy of absorbance, activity assay, circular dichroism, size exclusion chromatography and dynamic light scattering.

In addition, L-serine is the precursor to D-serine, a natural co-agonist of the NMDA glutamate receptors involved in brain development and plasticity and strength related to Alzheimer's and Parkinson's diseases, amyotrophic lateral sclerosis and ischemia. Since serine racemase (SR) is the enzyme responsible for D-serine regulation in the human brain, it is a possible drug target. Therefore, the second aim of this PhD work was to better explore the hSR interactome and to expand existing knowledge on enzyme regulation. In particular, I focused my scientific effort on studying the possible interaction/inhibition between human serine racemase and human glyceraldehyde dehydrogenase. This was important to clarify the presence of a biochemical link between glycolysis and serine metabolism. Therefore, the

expression and purification of both enzymes were carried out. In addition, the possible protein interaction was studied by size exclusion chromatography and cross-linking techniques, while hSR inhibition was characterized by spectroscopic techniques. Understanding the mechanisms that control the function and dynamics of the human serine racemase enzyme could have interesting consequences from a pharmaceutical point of view and allow to design of molecules that can indirectly modulate the NMDA receptor's activity.

Chapter 2. Functional characterization of pathogenic variants of human phosphoserine aminotransferase

2.1 Introduction

As mentioned in chapter 1, L-serine is a vital molecule for protein synthesis, a precursor of phospholipids and glutamatergic neurotransmitters such as D-serine and glycine. L-serine is mainly synthesized in astrocytes through the phosphorylated pathway (PP), which starts from the glycolytic precursor 3-phosphoglycerate. The PP takes place thanks to three sequential enzymatic reactions catalyzed by 3-phosphoglycerate dehydrogenase (3-PHGDH), phosphoserine aminotransferase (PSAT) and phosphoserine phosphatase (PSP).

Mutations in the genes that encode for the three enzymes are associated with a group of neurometabolic autosomal recessive disorders known as serine deficiency disorders (SDDs), characterized by low concentrations of L-serine in cerebrospinal fluid and plasma (Tabatabaie et al., 2010; Van der Crabben et al., 2013). Although most cases of SDD are associated with pathogenic variants of 3-PHGDH (Tabatabaie et al., 2010; Van der Crabben et al., 2013; Benke et al., 2017; Yoshida et al., 2004), a small but increasing number of cases were shown to involve mutations in the gene *PSAT1* encoding for PSAT.

PSAT is a homodimeric pyridoxal 5'-phosphate PLP-dependent enzyme that catalyzes the second step in PP, the transamination of 3-phosphohydroxypyruvate and L-glutamate to 3-phosphoserine and α-ketoglutarate. SDDs associated with the genetic impairment of PSAT are known as PSAT deficiency (PSATD), clinically characterized by neurodevelopmental defects, epilepsy, microcephaly and low plasma and cerebrospinal fluid serum levels. PSATD was first reported in two siblings heterozygous for a frameshift and a missense mutation of *PSAT1*, the latter encoding for the D100A variant. Unlike other L-serine disorders, there were no symptoms at

birth, suggesting the possibility of postnatal treatment (Hart et al., 2007). More recently, a case exhibiting the S43R PSAT variant was reported and classified as PSATD (Brassier et al., 2016).

Neu–Laxova syndrome (NLS) is the most severe disease in the spectrum of SDDs. When associated with homozygous or compound heterozygous mutations of *PSAT1*, NLS is known as Neu-Laxova syndrome-2 (NLS2) (Abdelfattah et al., 2020). The syndrome exhibits a wide range of phenotypes, including lethality, severe neurologic symptoms, seizures, and intellectual disability. Acuna-Hidalgo et al., 2014 reported a study of a cohort of 12 unrelated families affected by NLS2 with two missense *PSAT1* mutations, coding for variants A99V and S179L. The R342W variants were identified in Chinese families (Ni et al., 2019). Other PSAT pathogenic variants, G79W and C245R, were found by screening 15 families with NLS2 (Abdelfattah et al., 2020).

In this work, after careful bibliographical research, we selected the PSAT variants that were more interesting from a biochemical and medical perspective associated in the literature with either PSATD or NLS2. We produced the human recombinant protein of S43R, G79W, A99V, D100A, S179L, C245R, and R342W with the aim of identifying the specific loss-of-function mechanisms that can be responsible for SDDs pathogenesis. For comparison, we also characterized P87A PSAT, the only non-disease-associated Uniprot-reviewed natural variant. We have excluded pathogenic variants resulting in early (i.e., before the catalytic Lys200 binding PLP) truncation of PSAT. We used a wide range of experimental techniques for the biochemical characterization: absorption spectroscopy, activity assay, dynamic light scattering, circular dichroism and size exclusion chromatography.

2.2 Materials and Methods

2.2.1 Materials

If not otherwise specified, all reagents were purchased from Sigma Aldrich (St. Louis, MO, USA) at the best commercial quality available and used as received. Tris (2-carboxyethyl) phosphine (TCEP) was obtained from Apollo Scientific (Stockport, UK).

2.2.2 Expression system for human PSAT variants

Human phosphoserine aminotransferase WT and variants were expressed in recombinant form as a fusion protein with a six-histidine tag encoded in the expression vector pET28CpoI. The characteristics of PSAT WT expression vector were described in detail by Donini et al., 2009. The expression vectors for PSAT variants were produced by Genscript Industry (Rijswijk, Netherlands) based on the same vector. The sequence of the expressed WT PSAT protein is shown in Figure 21.

```
        10         20         30         40         50         60
MGSSHHHHHH SSGLVPRGSH IGPMDAPRQV VNFGPGPAKL PHSVLLEIQK ELLDYKGVGI

        70         80         90        100        110        120
SVLEMSHRSS DFAKIINNTE NLVRELLAVP DNYKVIFLQG GGCGQFSAVP LNLIGLKAGR

       130        140        150        160        170        180
CADYVVTGAW SAKAAEEAKK FGTINIVHPK LGSYTKIPDP STWNLNPDAS YVYYCANETV

       190        200        210        220        230        240
HGVEFDFIPD VKGAVLVCDM SSNFLSKPVD VSKFGVIFAG AQKNVGSAGV TVVIVRDDLL

       250        260        270        280        290        300
GFALRECPSV LEYKVQAGNS SLYNTPPCFS IYVMGLVLEW IKNNGGAAAM EKLSSIKSQT

       310        320        330        340        350        360
IYEIIDNSQG FYVCPVEPQN RSKMNIPFRI GNAKGDDALE KRFLDKALEL NMLSLKGHRS

       370        380        390
VGGIRASLYN AVTIEDVQKL AAFMKKFLEM HQL
```

Figure 21. FASTA sequence of recombinant hPSAT-WT (isoform-β). The number of amino acids is 393, molecular weight is 42.875 kDa, and theoretical pI is 8.07. Analysis carried out via online software: *https://web.expasy.org/compute_pi/*.

The hPSAT variants selected for this research work were: S43R, G79W, P87A, A99V, D100A, S179L, C245R, and R342W. For all variants, the lyophilized plasmid DNA (4 µg) was accurately resuspended with 40 µL of water for injection and centrifugated at 13.000 g for 3 minutes at 4 °C. The stock DNA concentration was around 100 ng/µL, then diluted at the final concentration of 10 ng/µL for storage at -20 °C and at 2 ng/µL for the transformation protocol. The expression plasmids containing the mutation were electroporated in *Escherichia coli* TUNER™ BL21(DE3) (Merck Millipore, Darmstadt, Germany) cells for protein expression and purification.

2.2.3 Protein expression

The transformed cells were plated in Luria Bertani (LB) agar solid medium (tryptone 10 g/L, NaCl 10 g/L, yeast extract 5 g/L and agar 15 g/L) with 50 µg/mL

kanamycin at 37 °C overnight. Then, a single-cell colony for each PSAT variant was picked up from the plate and was incubated in 10 mL of LB (tryptone 10 g/L, NaCl 10 g/L and yeast extract 5 g/L) with 50 µg/mL kanamycin at 37 °C overnight with soft shaking. The overnight culture was diluted 1:100 in LB medium with 50 µg/mL kanamycin. Bacterial growth was followed by measuring optical density (OD) at 600 nm. When cells reached about 0.7-0.8 OD, the culture was transferred at 4 °C for 20 minutes. Subsequently, a concentration of 0.2 mM Isopropyl-β-D-1-thiogalactopyranoside (IPTG) was added to induce the human PSAT expression. Bacterial growth continued at 20 °C for the next 16 hours with a shake of 110 rpm. Subsequently, the cells were collected by centrifugation at 7200 g for 10 minutes at 4 °C. Finally, three washes in phosphate buffer and NaCl (PBS) were carried out, and the pellets were frozen at the temperature of -80 °C.

2.2.4 Protein purification

The purification protocol was identical for WT and all PSAT variants. Cell frozen at -80 °C were resuspended with a vortex in 30 mL of lysis buffer (25 mM Tris HCl and 300 mM NaCl, pH 8.00 a 6 °C) in the presence of protease inhibitors 0.2 mM phenylmethylsulfonyl fluoride at pH 8.0 (PMSF), 0.2 mM benzamidine and 1.5 µM pepstatin A. The final concentrations of 1 mM TCEP, 50 µM PLP and 0.2% Tween20 were added. Then, the suspension was left for 50 minutes in the dark and in agitation at 4 °C in the presence of lysozyme (1 mg/mL) to promote the breaking of the cell wall. Cell lysis was completed by sonication. The suspension was divided into two parts, about 15 mL each, to facilitate the operation. Then approximately 5 cycles lasting 20 seconds with a "macro tip" probe were performed. Next, a 45-minute centrifugation

was carried out at 4 °C at 18000 g to separate the soluble and insoluble components. The supernatant, carefully collected to avoid the particle aggregates, was incubated with 5 mL of TALON® resin (Clontech, Mountain View, CA, USA) for 1 hour at 4 °C in agitation. Previously the resin was preequilibrated with 60 mL of 25 mM Tris HCl e 300 mM NaCl, pH 8.00 a 6 °C and with 25 mM Tris HCl, 300 mM NaCl, 1 mM TCEP, 50 µM PLP and 0.2% Tween20, pH 8.00 a 6 °C. After loading the sample, the resin was washed with 250 mL of washing buffer (25 mM Tris HCl, 300 mM NaCl and 20 mM imidazole, pH 8.00 a 6 °C). Then the protein was recovered by suspending the resin in 8 mL of elution buffer (25 mM Tris HCl, 300 mM NaCl and 250 mM imidazole, pH 8.00 a 6 °C). The protein eluted was dialyzed against 1 L of dialysis buffer (25 mM Tris HCl and 300 mM NaCl, pH 8.00 a 6 °C) in the presence of 1 mM TCEP and 4 µM PLP. The process took place in the dark at 6 °C. After 3 hours, 1 L of fresh dialysis buffer was changed, and the buffer exchange continued overnight to eliminate any trace of imidazole. Finally, the protein was concentrated in Amicon® (Merck/Millipore, Burlington, MA, USA) and stored in aliquots of 200 µL at -80 °C. Purity was analyzed by SDS-PAGE electrophoresis and densitometric analysis carried out by ChemiDoc Image System™ (Bio-Rad, Hercules, CA, USA).

2.2.5 Absorption spectra

Protein UV-visible absorption spectra were acquired using a CARY4000 UV-Vis spectrophotometer (Agilent Technologies, Santa Clara, CA, USA) with a temperature-controlled cell-holder Hellma™. Far UV Quartz Cuvettes (1 cm pathlength) were used for all experiments. For the WT and S43R, P87A, A99V, D100A, S179L, C245R variants, the extinction coefficient ε(280 nm) was 35870 M^{-1} cm^{-1}. While G79W and

R342W had an extinction coefficient ε(280 nm) of 41370 M^{-1} cm^{-1}. We used the molecular weight of 42853 g/mol for all proteins.

- **Spectra after purification**

Spectra of hPSAT variants were collected after purification in the 600-240 nm range at 20 °C, with 1-minute thermal equilibration in a cell holder. The proteins were diluted with 25 mM Tris and 300 mM NaCl at 36 µM concentration for all variants. The baselines were performed using the dialysis buffer corresponding to each variant to obtain a better background correction and evaluate the PLP saturation without external interference. All spectra were acquired in duplicate.

- **PSAT pure forms**

For WT PSAT and all variants, we produced pure catalytic intermediates, exploiting the natural PSAT transamination reaction. To obtain the internal aldimine ketoenamine form (PLP) and pyridoxamine 5'-phosphate (PMP) pure forms, we added to each protein 0.11 mM 3-phosphohydroxypyruvate and 20 mM L-glutamate, respectively. The reaction was spectroscopically followed in the region between 300-500 nm to verify the change in PLP maximum absorption: 408 nm for the internal protonated aldimine and 340 nm for the PMP. Immediately after the transamination reaction, the samples were dialyzed against 20 mM potassium phosphate buffer at pH 7, then aliquoted and stored at -80 °C.

- **Spectra of PLP saturation levels**

The spectra of PSAT-PLP pure forms were acquired in the range of 240-500 nm at the concentration of 40 µM for all proteins. The experiments were carried out in a solution containing 50 mM HEPES, 50 mM Bicine, and 100 mM NaCl pH 5.9 to stabilize the internal aldimine protonated forms with absorbance at 408 nm. To evaluate the PLP saturation levels, the spectra were acquired in the absence and the presence of 1 µM and 5 µM of free PLP in the solution mix. Each sample was thermostated at the temperature of 20 °C in the cell holder for 3 minutes before the recording. All spectra were corrected for the specific buffer contribution and acquired in duplicate. To calculate the PLP saturation levels, we divided the absorbance value at 408 nm for the absorbance at 280 nm. All data were normalized for the WT PSAT absorption ratio and expressed in percentage.

2.2.6 Enzyme activity

To measure the PSAT catalytic reaction, we used a Cary 4000 UV-Vis spectrophotometer (Agilent Technologies, Santa Clara, CA, USA) with a temperature-controlled cell-holder Hellma™. PSAT catalyzes the transamination of 3-phosphohydroxypyruvate (3-PHP) to O-phospho-L-serine with glutamate as an amino donor and concomitantly produces α-ketoglutarate. We performed an in-solution coupled assay with glutamate dehydrogenase (GDH). Indeed, the α-ketoglutarate produced by PSAT is a substrate for GDH, which uses nicotinamide adenine dinucleotide (NADH) to convert α-ketoglutarate to L-glutamate. The NADH has a characteristic absorption peak at 340 nm, whereas its oxidized shape does not absorb

at this wavelength. Therefore, it was possible to follow the PSAT α-ketoglutarate formation by NADH oxidation at 340 nm (Figure 22).

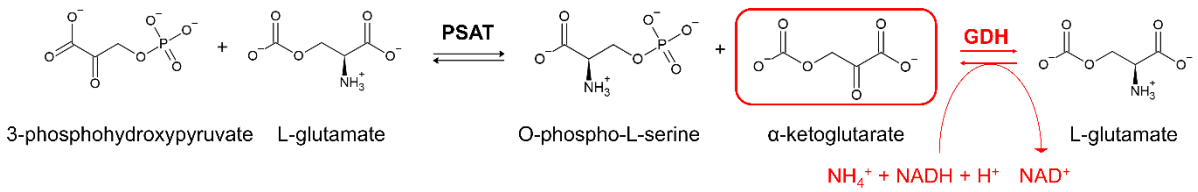

Figure 22. Schematic representation of PSAT enzymatic coupled assay with GDH.

The enzyme assays were performed at 37 °C in a reaction mixture containing 50 mM HEPES pH 7, 100 mM KCl, 1 mM DTT, 32 mM NH_4Cl, 0.1 mM NADH, 0.1 mM 3-PHP and 20 mM L-glutamate. For the assays in the presence of PLP, a concentration of 170 µM or 500 µM was added to the solution mix. The final volume of the assay solution was 150 µL, and the protein concentration was 80.8 nM in a quartz cuvette with 1 cm of path length. The solution with protein was thermostatic for 2 minutes in a cell holder in the presence of protein and NADH, and then a trace of 1 minute was acquired. The eventual slope of this trace reflected the contribution of NADH oxidation. The addition of L-glutamate trigged the reaction. The signal was recorded for a total of 10 minutes. The slope was read immediately after the addition of protein. The initial rate value was calculated on a 1-minute track. The slope (ΔOD / min) was divided for the NADH molar coefficient (6200 M-1 cm-1) after subtracting the rate of the pre-incubation phase. All data were acquired in triplicate.

2.2.7 Circular dichroism

The circular dichroism (CD) experiments were performed with a Jasco J-1500 spectropolarimeter equipped with a Peltier thermostatic unit. The software was JASCO Spectra Manager II. For all analyses, 0.1 mm quartz cells were used.

- **Protein stability**

For all PSAT variants, the CD spectra were collected in the spectral scans of 250 and 180 nm in a solution containing 20 mM potassium phosphate buffer at pH 7, with 2 minutes of thermostatation in the cell holder. Since the protein storage solution was rich in NaCl (25 mM TRIS, 300 mM NaCl), to avoid the absorbance interferences due to salt, all proteins were dialyzed against a solution containing 20 mM potassium phosphate buffer at pH 7 before the experiment. For all spectra, the protein concentration was 5 µM, and the temperature was set at 20 °C. To improve the signal-to-noise ratio, the data pitch was set at 0.5 nm, DIT at 8 seconds, bandwidth at 2 nm, and the scan speed was 50 nm/min. For all proteins, we collected 3 independent measurements, each resulting from 3 averaged accumulations. All CD spectra were corrected for buffer background. Secondary structure estimation was performed through the Dichroweb algorithm using the analysis program CONTIN and the reference set optimized for 185-240 nm.

- **Thermal stability**

For all PSAT variants, the far-UV CD signal changes at 220 nm were monitored as a function of increasing temperature in a range of 20-80 °C, with steps of 5 °C and an equilibration time of 1 s at each temperature before recording a reading. In each

experiment, the protein concentration was 5 μM in a solution containing 20 mM potassium phosphate buffer at pH 7. The measures were collected in triplicate. The general thermal stability was analyzed with SigmaPlot software, considering two-state transitions regarding the unfolding process. The unfolding data were elaborated with the equation:

$$\theta = \theta_0 + f/ (1 + e^{\wedge} ((T - Tm)/k))$$

where θ is the ellipticity at 222 nm, θ_0 is an offset, f is the amplitude of the thermal transition, T is the temperature (°C), Tm is the melting temperature, and k is the slope of the phase. For PSAT variants that exhibited a biphasic curve with a three-state thermal unfolding, to estimate the melting temperatures of the two transitions, we used the double Boltzmann equation:

$$\theta = \theta_0 + A [f/ (1 + e^{\wedge} ((T - Tm_1)/k_1)) + (1 - f)/ (1 + e^{\wedge} ((T - Tm_2)/k_2))]$$

where θ is the ellipticity at 222 nm, θ_0 is an offset, A is the amplitude, f is the fractional abundance of the first phase, T is the temperature in °C, Tm_1 and Tm_2 are the melting temperatures of the two phases and k_1, and k_2 are the slope of the two phases.

2.2.8 Dynamic light scattering (DLS)

The DLS experiments were carried out with a Zetasizer Nano (Malvern Panalytical Instruments, UK) coupled with a 633 nm laser, using NIBS detection (173° backscatter). The temperature control was set at 25 °C, each sample was equilibrated at the temperature for 60 seconds before recording the analysis. Three independently

prepared samples of each protein were analysed, and, for each, three experimental accumulations were collected immediately after preparation (time 0) and after 1 h. The proteins were extensively centrifugated for 45 minutes at 16000 g and then diluted at 23 μM final concentration in a solution containing 50 mM NaH_2PO_4 and 300 mM NaCl, pH 7. To avoid interference with light scattering, the experimental buffer was filtered with a filter membrane of 0.22 μm. The diameter conversion in MW was performed by Zetasizer Software v7.11 (Malvern Panalytical Instruments, UK). The standard proteins myoglobin and conalbumin were used as calibrants.

2.2.9 Size exclusion chromatography (SEC)

Gel filtration analyses were performed by the Prominence HPLC system (Shimadzu, Kyoto, Japan) coupled with an SPD-20A Model UV detector (Shimadzu, Kyoto, Japan) and LabSolutions software (Shimadzu Kyoto, Japan). Chromatographic separation was performed on a Phenomenex BioSep-2000 (300 mm x 7.5 mm) column (Phenomenex, CA, USA) pre-packed with silica beads of 5 μm. The column separation range molecular weights were between 1 and 300 kDa, and the pH range was 2.5-7.5. To ensure the best performance from the column, it was pre-equilibrated for 2 hours at the flow rate of 0.8 mL/min with a solution containing 50 mM NaH_2PO_4 and 300 mM NaCl pH 7 at room temperature. The pumps were set on isocratic elution mode. The manual injection volume was 50 μL at 23 μM protein concentration, and the samples were diluted in 50 mM NaH_2PO_4 and 300 mM NaCl pH 7. All analyses were acquired in triplicate. The total chromatographic run period was 15 min, with a flow rate of 1 mL/min. Detection was performed at 280 nm. The column was calibrated with the

standard: myoglobin (17 kDa), ovalbumin (44 kDa), Immunoglobin G (150 kDa), Immunoglobin A (300 kDa), and bovine thyroglobulin (670 kDa).

2.3 Results and discussion

2.3.1 Structural predictions

In the literature, the single nucleotide polymorphisms (SNPs) on the gene *PSAT1* were consistently associated with disorders in the biosynthesis of serine (SDDs), hallmarked by a low concentration of L-serine in the cerebrospinal fluid and plasma (Tabatabaie et al., 2010; Van der Crabben et al., 2013). In particular, SDDs associated with the genetic impairment of PSAT are known as PSAT deficiency (PSATD). Microcephaly, neurodevelopmental defects, and epilepsy characterize PSATD. In addition, in the most severe cases, we speak about Neu–Laxova syndrome (NLS), which exhibits severe neurologic symptoms, including lethality and intellectual disability. When NLS is associated with homozygous or compound heterozygous mutations of PSAT1, it is known as Neu-Laxova syndrome-2 (NLS2) (Abdelfattah et al., 2020). In this research work, we selected for characterization the PSAT variants that were more interesting from a medical and biochemical perspective (Table 2). The evaluation of the functional impact, based on the evolutionary conservation of the affected residues, was predicted with the Mutation Assessor and the PolyPhen-2 algorithms (Adzhubei et al., 2010; Reva et al., 2011). In addition, also in Table 2, were reported the published prediction about the associated structural perturbations based on the analysis of the PDB model 3E77 (Abdelfattah et al., 2020).

Variant	Associated Pathology	Location	Functional Impact prediction - Mutation assessor	Functional Impact prediction - PolyPhen-2	Predictions based on structural analysis PDB 3E77
S43R	PSATD [1, 2, 6]	PLP domain	High	Possibly damaging	Dimer instability
G79W	NLS2 [1, 2]	PLP domain	High	Probably damaging	Reduced PLP binding
P87A	Non-pathogenic (Uniprot)	PLP domain	Medium	Probably damaging	-
A99V	NLS2 [3,1]	PLP domain	Medium	Probably damaging	Protein instability
D100A	PSATD [5, 2]	PLP domain	Low	Probably damaging	-
S179L	NLS2 [3, 2]	PLP domain	High	Probably damaging	-
C245R	NLS2 [1]	PLP domain	Medium	Probably damaging	Dimer instability
R342W	NLS2 [4]	C- terminus	High	Probably damaging	-

Table 2. PSAT variants, associated pathologies [1] Abdelfattah et al., 2020, [2] Sirr et al., 2020, [3] Acuna-Hidalgo et al., 2014, [4] Ni et al., 2019, [5] Hart et al., 2007, [6] Brassier et al., 2016. Predicted functional alteration based on the Mutation assessor algorithm (Reva et al., 2011), PolyPhen-2 algorithm (Adzhubei et al., 2010) and on structural analysis PDB 3E77 (Abdelfattah et al., 2020).

The visual exploration of the structure of O-phosphoserine-bound human PSAT (PDB 8A5W) helped us to speculate about the connection between structural base changes and pathology (Figure 23).

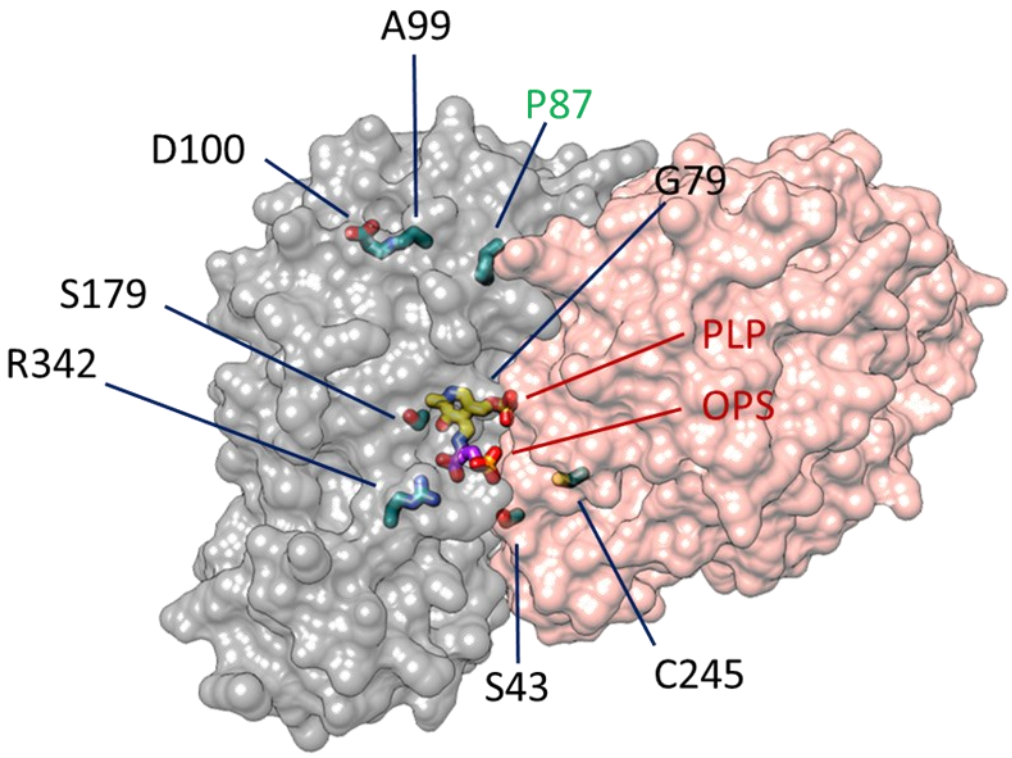

Figure 23. Crystal structure of human PSAT WT in complex with O-phosphoserine (PDB 8A5W).

We observed that S43 is located at the active site, near (5.8 Å) to the phosphate group of the PSAT substrate, suggesting a possible steric clash and, consequently, a probable lower affinity for the substrate in the S43R variant. Residue S43 is highly conserved among the PSAT orthologues; the crystal structures of *Bacillus alcalophilus* PSAT complex with L-serine showed that S43 is directly involved in substrate binding (Battula et al., 2013). Moreover, since S43 is also part of the interdimeric interface, its substitution was also predicted to destabilize the dimer (Abdelfattah et al., 2020). The residue R342 is localized in the C-terminal domain, and it is adjacent to the substrate's binding site forming an ionic bond with its carboxylate group. In the variant, the amino acid arginine, with a positively charged side chain, is replaced by bulky and non-charged tryptophane. Therefore, the amino acid substitution can alter the substrate

binding affinity, and also it can result in a structural change (Ni et al., 2019). Residue G79 is close to the phosphate group of PLP in its binding site. In the G79W variant, glycine is replaced by tryptophan, an amino acid with a larger hydrophobic side chain, which may cause steric clash and prevent or reduce the PLP binding as already predicted (Abdelfattah et al., 2020). S179 and C245 are also close to the PLP moiety, and lower PLP affinity can be hypothesized. In addition, for C245, the amino acid substitution with bulky arginine may alter the dimer stability (Abdelfattah et al., 2020). The residues A99 and D100 are located away from the active site, they are highly conserved within PSAT orthologues. For these reasons, the pathogenic mechanism for the variants A99V and D100A is more challenging to interpret. However, their variants were predicted to cause protein instability and have been associated with serine deficiency disorders in multiple publications (Hart et al., 2007; Abdelfattah et al., 2020). In the case of D100A-PSAT, the hydrophobic alanine residues are solvent-exposed, likely to cause protein aggregation. The residue P87 is located near A99 and D100, far from both PLP and O-phosphoserine. However, its amino acid substitution with alanine is not associated with pathology currently.

2.3.2 Protein expression and purification

All PSAT variants and WT were expressed and purified with the same protocol (see Materials and Methods 2.2.3 and 2.2.4) to obtain the pure enzymes. During the expression step, all variants showed a behaviour like WT PSAT, except S179L. Indeed, S179L exhibited slower growth both in the solid plate and in LB medium at 37 °C and reached the logarithmic phase at 0.7-0.8 OD at almost twice the time of WT

PSAT and all other variants. The variant S179L also had a lower amount of 80% of expressed protein than WT (Figure 24).

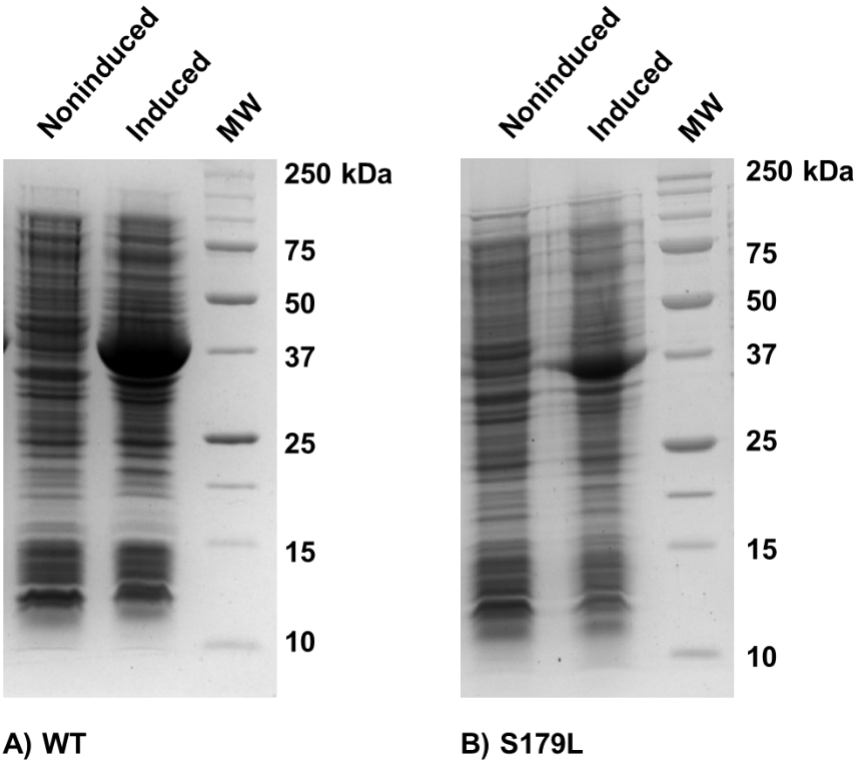

Figure 24. SDS-PAGE of **(A)** WT PSAT and (**B)** S179L PSAT. All samples, noninduced and induced, were normalized to each other.

The purification yields for all variants were in a range of 50-90 mg per litre of culture, except for S179L and A99V. For S179L, we obtained 5-fold lower yields than WT PSAT, probably due to multiple factors, including a possible protein instability. Instead, A99V produced around half the yields compared to WT PSAT, since 50% of the protein was in *E. coli* inclusion bodies (insoluble fraction), indicating a possible folding problem. In literature, Hart et., al 2007 reported that the recombinant D100A variant

was expressed in *E. coli* with a 10-fold lower yield than WT PSAT. However, under our expression system conditions, we observed only a slight drop in yield (Table 3).

	Yield (mg/L)
WT	85 mg/L
S43R	90 mg/L
C245R	90 mg/L
P87A	75 mg/L
R342W	60 mg/L
G79W	50 mg/L
S179L	13 mg/L
A99V	36 mg/L
D100A	70 mg/L

Table 3. Purification yield (mg/L) purity for WT PSAT and all variants PSAT.

To evaluate the WT and PSAT variant's purity and to verify the MWs compared to the predicted based on the protein sequences, we performed an SDS-PAGE experiment. For all PSAT variants, the purity was in the range between 90% - 98% compared to WT PSAT. Moreover, all proteins, except D100A, showed the same electrophoretic mobility according to WT PSAT MW of 42.83 kDa. (Figure 25). The D100A sequence was confirmed by mass spectrometry analysis (data not shown).

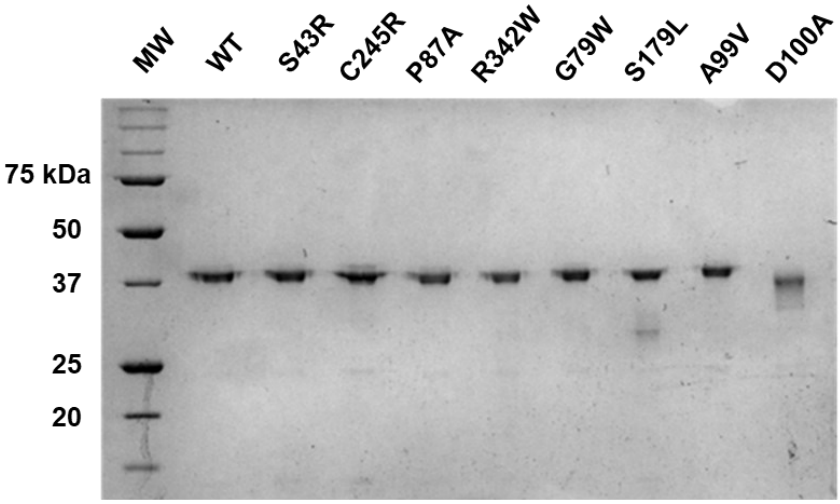

Figure 25. SDS-PAGE of WT PSAT and PSAT variants after IMAC purification. The protein purity (%) was calculated with Image Lab™ software (Bio-Rad, Hercules, CA, USA).

2.3.3 Spectroscopy

We collected the UV-vis absorption spectra of WT PSAT and all variants immediately after purification in the solution 25 mM TRIS, 300 mM NaCl, pH 8 at 25 °C. Since PSAT is a PLP-dependent enzyme, it was possible to assess the spectroscopy difference in the PLP absorbance region (300-500 nm) between the PSAT variants compared to WT. We observed that variants spectra changed significantly, with different relative contributions of the bands at 408 nm and 340 nm. These absorbances were attributed to the different catalytic intermediates of PLP during the transamination reaction of PSAT, which exhibited different absorption spectra (Figure 26). In the PSAT enzyme, the cofactor PLP is covalently linked with Lys200, forming an internal aldimine fraction (Murtas et al., 2020). The protonated

internal aldimine exhibited an absorption maximum of 408 nm, while the absorption at 340 nm was related to pyridoxamine 5'-phosphate (PMP).

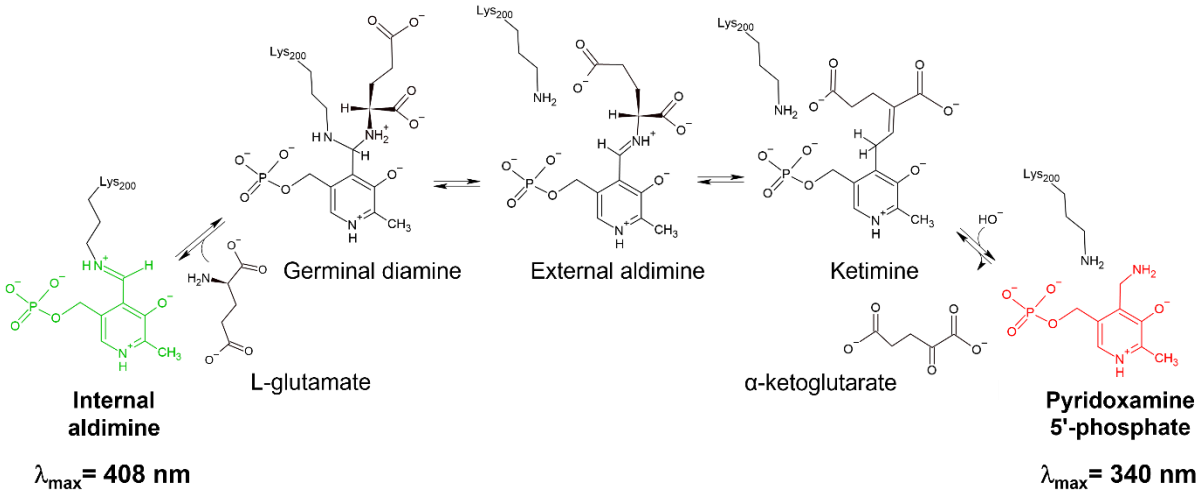

Figure 26. PSAT catalytic intermediate's reaction and relative spectroscopic absorbance.

Variants A99V, S43R, D100A, and P87A exhibited a prevalence of PMP similar to WT PSAT. The absorption spectra of R342W and C345R PSAT indicated a mixture of PLP and PMP forms suggesting a different catalytic reactivity than WT PSAT. The spectra of variants S179L and G79W exhibited very low intensity in the 300-500 nm range compared to absorption at 280 nm, indicating a limited saturation with PLP (Figure 27).

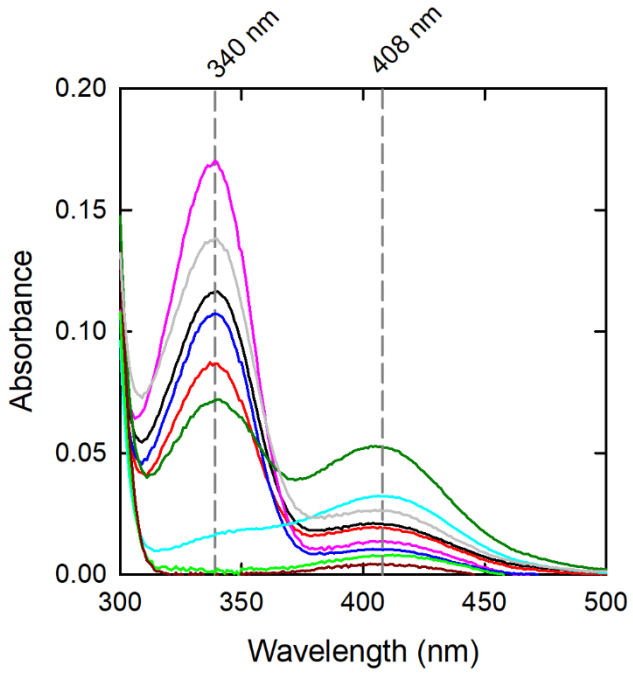

Figure 27. Absorption spectra of 35 μM PSAT immediately after purification, in the region of PLP absorption, in a buffer containing 25 mM TRIS, 300 mM NaCl, pH 8 at 20 °C. The spectra were normalized at 280 nm, with the correction factor for the tryptophane for G79W and R342W variants. WT (black line), S43R (red line), G79W (dark red line), P87A (blue line), A99V (purple line), D100A (grey line), S179L (light green line), C245R (cyan line), and R342W (dark green line).

Pyridoxal 5′-phosphate is a key coenzyme for many enzymes involved in essential biochemical pathways for human health (Clayton et al., 2006). Therefore, it could be possible that differences in PLP saturation levels between PSAT variants were responsible for the pathology. Therefore, to compare the PSAT variants spectra, avoiding mixing of PLP and PMP forms, and to assess in detail the PLP saturation levels for each variant, we produced the pure forms for all proteins: the pure internal aldimine forms and the PMP forms. These pure catalytic intermediates were obtained, using the natural transamination reaction of PSAT, by adding 0.11 mM 3-phosphohydroxypyruvate and 20 mM L-glutamate to aliquots of each protein solution, respectively (Figure 28). The internal aldimine is present in the equilibrium of

protonated and deprotonated forms, with absorption at 408 nm ad 345 nm, respectively.

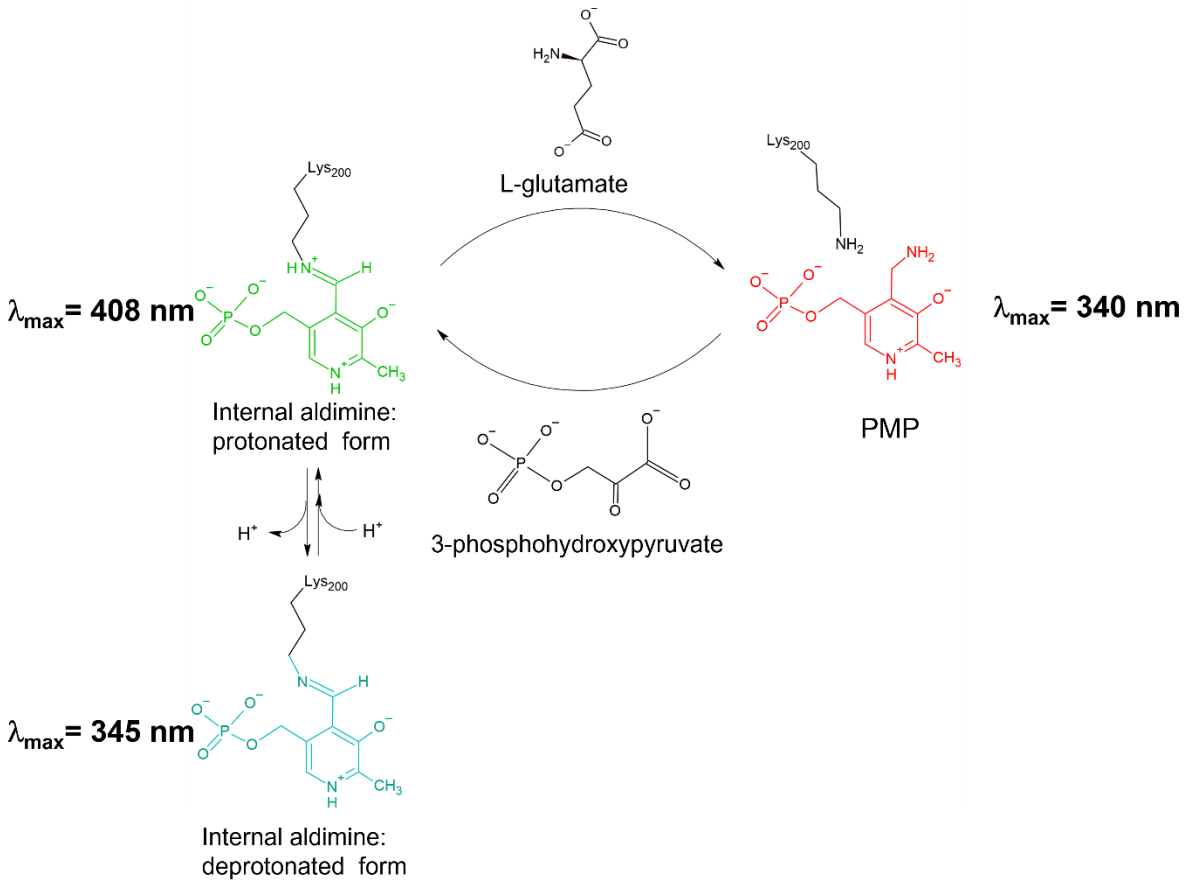

Figure 28. Schematic representation of PSAT catalytic intermediates pure forms and UV-vis absorption maxima.

Since the internal aldimine equilibrium between protonated and deprotonated form is influenced by pH, to evaluate the PLP saturation of internal aldimine, the spectra were acquired in a solution containing 50 mM MES, 50 mM HEPES, 50 mM Bicine, and 100 mM NaCl at pH 5.9 (Figure 29-A). Indeed, this experimental condition permitted the stabilization of only the PLP protonated ketoenamine form with absorption at 408 nm.

The level of PLP saturation was calculated for each variant by the ratio of the band at 280 nm and 408 nm. Variants C245R, S179L, and G79W were 50%, 10%, and 5% saturated compared to WT PSAT. Variants A99V and D100A exhibited a higher A_{408} nm/A_{280} nm ratio than WT PSAT, indicating either a higher saturation or a slightly different extinction coefficient of the PLP moiety at 408 nm (Figure 29-B).

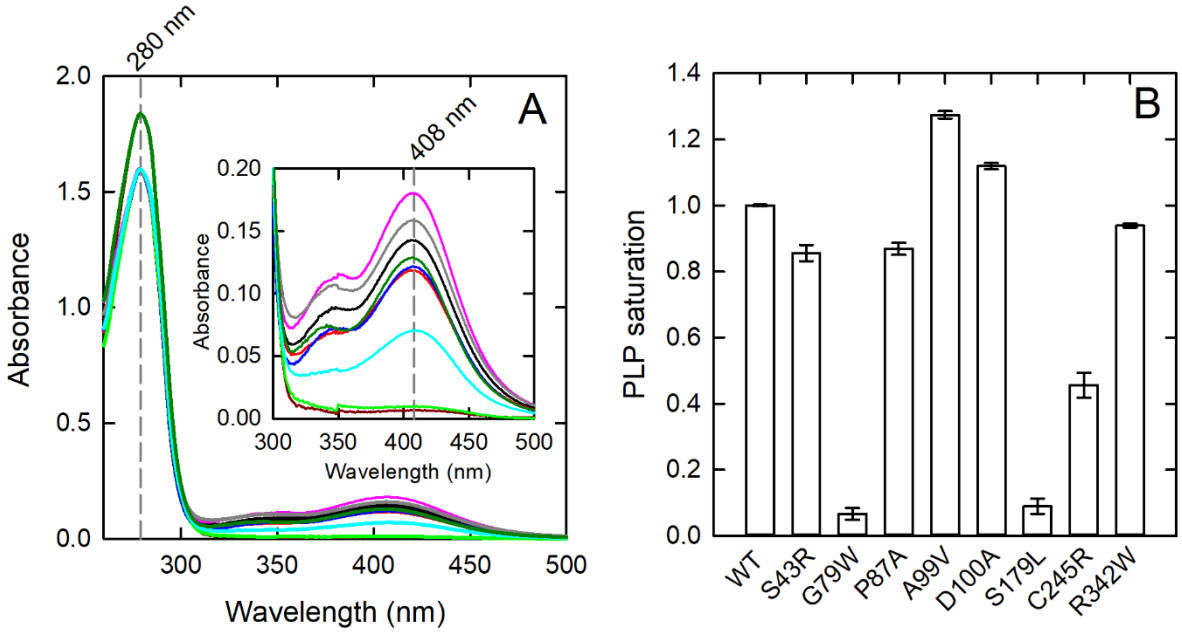

Figure 29. (A) PLP absorption spectra of 40 µM PSAT-PLP form in a buffer containing 50 mM MES, 50 mM HEPES, 50 mM Bicine, and 100 mM NaCl pH 5.9 at 20 °C. Inset: region of PLP absorption. WT (black), S43R (red), G79W (dark red), P87A (blue), A99V (purple), D100A (grey), S179L (light green), C245R (cyan), and R342W (dark green). **(B)** Saturation levels of PLP in PSATs, the absorption ratio was calculated between 408 nm and 280 nm. All absorption ratios were normalized for WT PSAT value.

Since some variants were particularly depleted of PLP, we wondered if it could depend on alterations due to amino acid substitutions or if it depended on the folding process and whether they were able to saturate in the presence of free PLP in the solution. Therefore, we collected the UV-vis spectra of all proteins after extensive incubation in the presence of 1 µM and 5 µM free PLP in solution and calculated the ratio of the

band at 408 to 280 nm (Figure 30). We observed that the PLP saturation for all variants did not increase by a high concentration of free PLP in the solution, suggesting that they could not bind PLP.

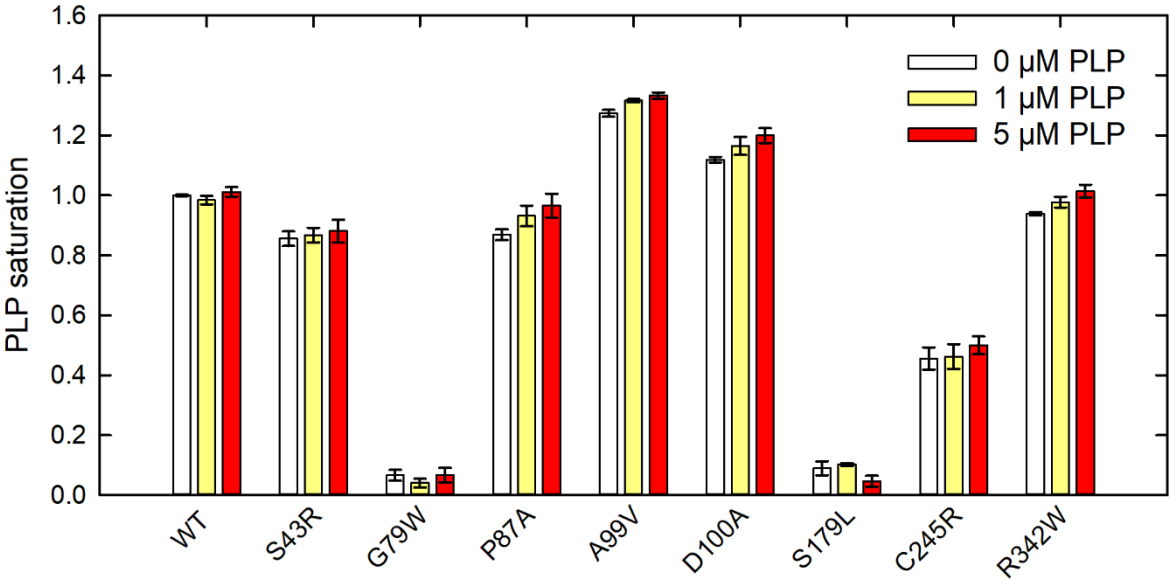

Figure 30. Absorption ratio between 408 nm and 280 nm for all PSAT variants in a solution containing 50 mM MES, 50 mM HEPES, 50 mM Bicine, and 100 mM NaCl at pH 5.9 at 20 °C. In the absence and presence of 1 µM and 5 µM PLP free PLP in the solution mix. All absorption ratios were normalized for WT PSAT value.

In addition, to exclude the possibility of a PLP incorporation that requires long incubation times, we acquired the spectra of protein G79W, the variant with the lower PLP saturation level, compared to WT PSAT in the presence of 5 µM PLP for 16 hours at 25 °C. After 90 minutes, the spectra of the G79W variant showed scattering, probably due to protein precipitation. For both proteins, no significant incorporation of PLP over time was observed (Figure 31).

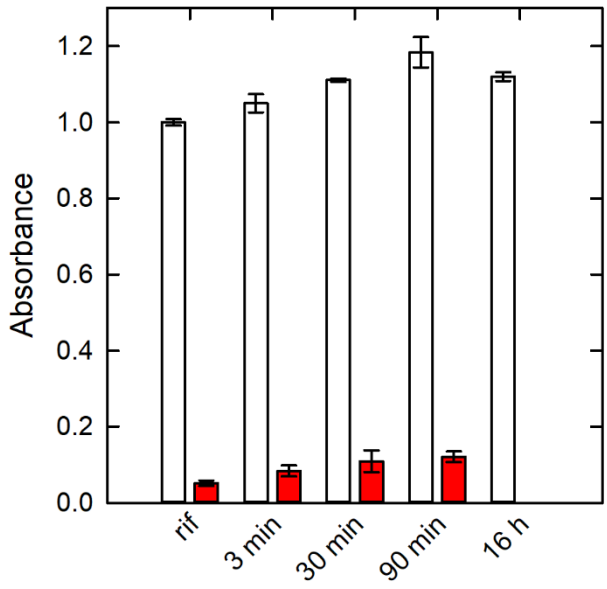

Figure 31. Absorption ratio between 408 nm and 280 nm for WT (white) and variant G79W (red) in a solution containing 50 mM MES, 50 mM HEPES, 50 mM Bicine, and 100 mM NaCl at pH 5.9 at 20 °C. In the presence of 5 μM PLP in the solution mix for 16 hours. The G79W absorption ratios were normalized for WT PSAT value.

2.3.4 Enzyme activity

PSAT catalyzes the transamination of 3-phosphohydroxypyruvate to 3-phosphoserine with glutamate as an amino donor and concomitantly produces α-ketoglutarate (Murtas et al., 2020). We evaluated the catalytic activity of PSAT variants in solution with enzymatic continuous assay coupled to enzyme glutamate dehydrogenase (GDH). Indeed, the alpha-ketoglutarate, produced by PSAT, is the substrate of GDH. The coupled enzyme uses the nicotinamide adenine dinucleotide (NADH) to convert alpha-ketoglutarate to L-glutamate. So, we can detect the PSAT alpha-ketoglutarate production through the NADH oxidation in absorption spectroscopy at 340 nm. We worked in the WT PSAT saturating condition: 20 mM of L-glutamate and 0.1 mM 3-phosphohydroxypyruvate. The activity assays were

performed in a solution containing 50 mM HEPES and 100 mM KCl, in the presence of 170 µM PLP. We observed that P87A, A99V, and D100A variants exhibited an activity assay similar to WT PSAT. The variant S43R showed an intermedia activity of around 60%, while the variant C245R showed only 10% activity compared to WT PSAT. Instead, the variants G79W, S179L and R342W were virtually inactive (Figure 32), suggesting that the amino acid substitution can be responsible for the reduced production of serine that causes the diseases.

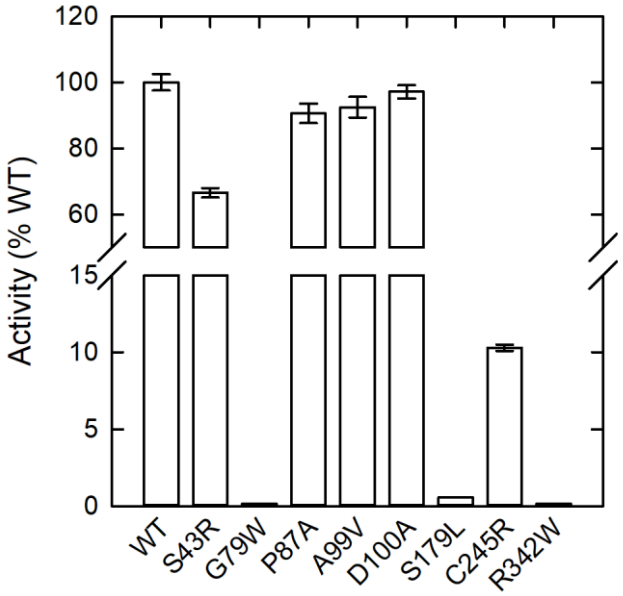

Figure 32. Enzymatic activity of 80.8 nM PSAT variants in a solution containing 50 mM HEPES, 100 mM KCl, 100 µM 3-PHP, 130 µM NADH, 170 µM PLP, 20 mM L-glutamate, 32 mM NH_4Cl and 1.5 mM DTT, pH 7 at 37 °C. All data were acquired in triplicate and normalized for the percentage of WT PSAT activity.

Observing the previously described enzyme activity, we noted that the variants P87A, A99V, and D100A, which exhibited a behaviour similar to WT PSAT, also had high PLP saturation. In contrast, the variants G79W, and S179L, without PLP bound, were inactive. The unique exception was R342W which was inactive despite being almost

entirely PLP-saturated. Therefore, we correlated the PLP saturation levels with enzymatic activity (Figure 33). There was good correspondence, suggesting that the primary molecular mechanism for the loss of function in PSAT pathogenic variants is a reduced affinity for PLP.

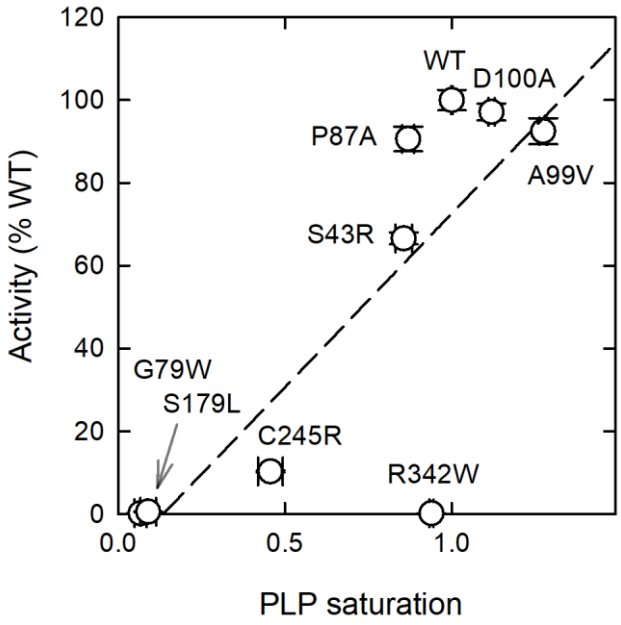

Figure 33. Correlation between the enzymatic activity (%) and the PLP saturation level of PSAT variants.

To rule out definitely that PSAT variants could not bind free PLP in the solution, it was necessary to test the proteins at saturating concentration of PLP. Since in the absorbance experiments, the maximum possible concentration of PLP tested was 5 μM, due to the PLP absorption contribution, we used the activity assays to evaluate the behaviour of the PSAT variants in the presence of a saturating concentration of PLP. Therefore, to estimate PLP affinity, the same enzyme assays described above were performed in the absence and presence of 500 μM PLP in the reaction mixture

and compared to the enzyme activity recorded with 170 µM PLP for each PSAT variant (Figure 34). In the presence of a saturating concentration of PLP, we expected recovery of activities for variants that showed low PLP saturation levels. However, for all variants, we were not able to observe a significant increase in activity, suggesting that the active site is not accessible to PLP after protein folding. The other explanation, only for the non-saturated forms, is that the PLP dissociation constant is significantly greater. However, the concentration of free PLP in cells is in the low micromolar range (Footitt et al., 2011), indicating that PLP's low affinities would result in apo forms in vivo.

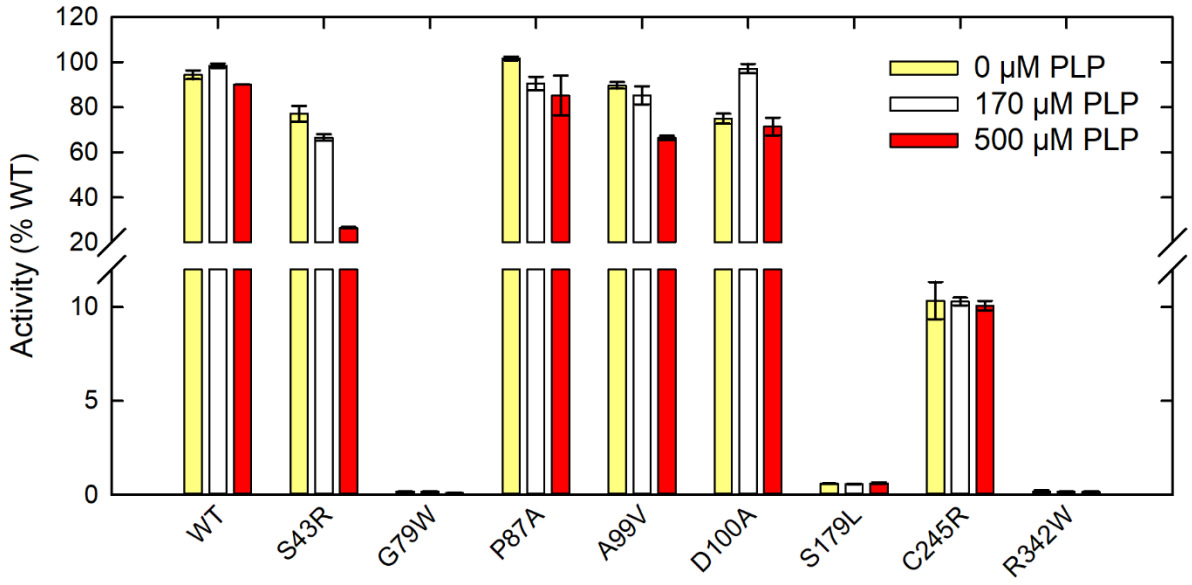

Figure 34. Enzyme activity of 80.8 nM PSAT variants at different PLP concentrations: 0 µM, 170 µM and 500 µM. The solution containing 50 mM HEPES, 100 mM KCl, 100 µM 3-PHP, 130 µM NADH, 20 mM L-glutamate, 32 mM NH_4Cl and 1.5 mM DTT, pH 7.

2.3.5 Secondary structure

Structure and function of proteins are closely linked. Indeed, a reduced secondary structure could be responsible for the lower activity or, the lower affinity for cofactors or substrates (Zeeshan et al., 2019). Therefore, to evaluate the effect of the aminoacidic substitution on the secondary structure in the PSAT pathological variants, in search of the possible pathological mechanism and to try to explain the reduced PLP saturation ad the lower activity for some variants, we carried out circular dichroism experiments. Circular dichroism (CD) spectroscopy is an optical spectroscopic method that, in the region of far UV (180-250 nm), exploits the differential absorption of left- and right-circularly polarised light by peptide backbone chain to obtain protein structure information. The spectra of WT and all PSAT variants for PLP forms were collected (Figure 35) in the 185-250 nm range at 20 °C in 20 mM potassium phosphate solution without salt presence to improve the signal noise ratio (Kelly et al., 2005; Miles et al., 2021). For all proteins, the spectra were acquired in three independent measures. Observing the spectra, we noticed that S179L and C245R variants showed different levels of absorption both in the region of alpha-helix (around 190 nm) and beta sheets (around 220 nm), compared to WT PSAT. In the complex, the others PSAT variants showed absorption spectra similar to WT PSAT.

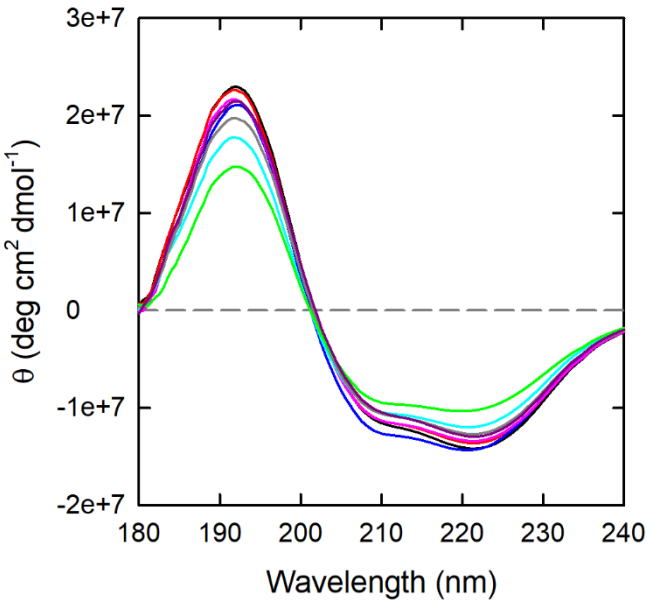

Figure 35. CD spectra of 5 µM PSATs PLP pure form in 20 mM potassium phosphate buffer at 20 °C. All spectra were acquired in triplicate and correct for buffer background. WT (black), S43R (gray), G79W (blue), P87A (dark purple), A99V (dark green), D100A (red), S179L (light green), C245R (cyan) and R342W (purple).

For a more precise analysis, all spectra were elaborated with the DichroWeb algorithm to determine the del percent of secondary structures (Miles et al., 2022). The values are reported in Table 4. Overall, we observed no significant changes in the secondary structure of PLP forms compared to the WT PSAT, except for S179L and C245R variants. Indeed, these variants showed a lower proportion of alpha helix, 26% and 28%, respectively, against 33.2% of WT PSAT. Also, the same variants exhibited a higher share of beta sheets, 23% and 21% for S179L and C245R, respectively, concerning 18% for WT. The G79W variant showed a slight decrease of beta sheets of around 2% compared to WT. For all variants, the percentage of turns was unchanged, except S179L, which exhibited a slightly higher proportion of 20.6% than

18.8% for WT. The DichroWeb algorithm did not recognize a significantly different percentage of unordered structures among variants.

	Alpha helix (%)	Beta sheet (%)	Turns (%)	Unordered (%)
WT	33.2±0.9	18.0±2.0	18.8±0.6	30.2±0.1
S43R	31.9±0.2	19.3±0.5	18.9±0.6	29.9±0.1
G79W	33.9±1.0	16.0±1.0	19.4±0.4	31.0±0.2
P87A	31.0±3.0	19.0±2.0	19.6±0.3	30.3±0.1
A99V	31.0±3.0	18.0±2.0	19.9±0.3	30.4±0.1
D100A	32.2±0.7	18.7±0.2	18.8±0.8	30.3±0.1
S179L	25.9±0.3	23.0±0.3	20.6±0.3	30.4±0.3
C245R	28.0±2.0	21.0±2.0	19.9±0.3	30.7±0.1
R342W	31.9±0.3	19.0±1.0	19.3±0.9	30.0±0.2

Table 4. Secondary structure analysis of 5 μM PSAT-PLP CD spectrum. The percentages of structures were calculated with DichroWeb software.

After assessing the effect of the mutations on the secondary structure for the PLP forms, since the S179L and C245R variants that showed a change in the secondary structure had also reduced PLP saturation levels (50% and 10% respectively), we wondered what impact PLP had on the secondary structure. We explored whether the change in secondary structure for S179L and C245R depended on PLP-reduced saturation or amino acid substitution. We, therefore, investigated the PMP pure forms to assess whether the secondary structure was reduced. We collected the CD spectra of PMP pure forms in the 185-250 nm range at 20 °C in 20 mM potassium phosphate

solution (Figure 36). We observed that in the complex all PSAT variants showed similar spectra to WT PSAT, except for S179L and C245R variants. These variants, as noticed for PLP forms, exhibited different levels of absorption at 190 nm e 220 nm, compared to WT PSAT. In particular, S179L variant showed the most different spectra.

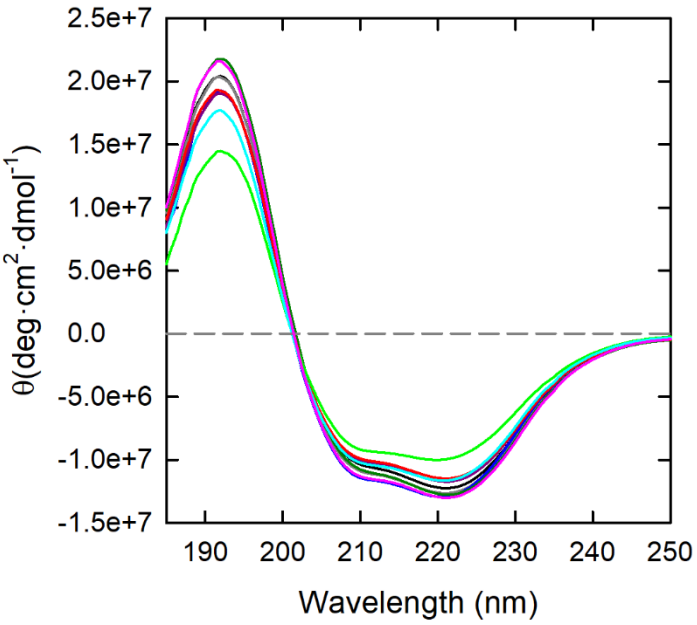

Figure 36. CD spectra of 5 µM PSATs PMP pure form in 20 mM potassium phosphate buffer at 20 °C. All spectra were acquired in triplicate and correct for buffer background. WT (black), S43R (gray), G79W (blue), P87A (dark purple), A99V (dark green), D100A (red), S179L (light green), C245R (cyan) and R342W (purple).

We analyzed the secondary structure components using by DichroWeb algorithm as done for PLP forms. We observed a pattern similar to PLP forms, in which S179L and C245R variants exhibited a decrease in the percentage of alpha helix and an increase in beta sheets compared to WT PSAT. The other variants were like WT (Table 5). These data suggest that the state of PLP did not significantly change the secondary

structure. The structural disruption of S179L PSAT in both PLP and PMP forms was consistent with its lower yields of purification, which suggest decreased stability. In addition, it is necessary to underline that, as well as S179L PSAT and C245R PSAT, the other poorly saturated variant G79W, did not appear to show a significant perturbed secondary structure. This indicates a specific effect of the S179L and C245R substitutions rather than a secondary effect of PLP loss in the virtually apo forms.

	Alpha helix (%)	Beta sheet (%)	Turns (%)	Unordered (%)
WT	33.0±1.0	18.5±1.0	18.7±0.5	29.7±0.1
S43R	30.0±3.1	20.0±2.0	19.6±0.4	29.7±0.2
G79W	30.4±0.4	19.0±1.0	19.9±0.2	31.0±0.5
P87A	29.0±1.0	21.0±1.3	20.1±0.1	30.2±0.1
A99V	33.6±0.3	17.0±1.0	19.3±0.2	29.8±0.6
D100A	30.5±0.2	20.2±0.3	19.8±0.2	29.8±0.3
S179L	24.5±0.7	23.7±0.9	21.4±0.1	30.6±0.1
C245R	28.4±0.9	20.0±1.0	20.7±0.1	30.9±0.1
R342W	31.8±2.0	19.5±1.8	19.3±0.1	29.5±0.1

Table 5. Secondary structure analysis of 5 μM PSAT-PMP CD spectrum. The percentages of structures were calculated with DichroWeb software.

2.3.6 Thermal stability

In the literature, Abdelfattah et al., 2020 proposed the reduced stability of PSAT pathological variants as a pathogenetic mechanism for serine deficiency disorders. Environmental conditions, such as temperature, can be used to assess protein stability (Timr et al., 2020). In the previous experiment, we evaluated the secondary structure content at the constant temperature of 20 °C. Therefore, to investigate the stability of PSAT pathological variants, we performed thermal denaturation experiments between 20-80 °C. We monitored the changes in the secondary structure as a function of temperature by circular dichroism at 222 nm. Experiments were carried out for the PLP-bound, although the poorly PLP-saturated variants (G79W, S179L, C245R) should be essentially regarded as apo-forms. For the variants bound PLP forms, we observed a temperature of melting (T_m) between 46 to 70 °C, compared to 63 °C recorded for WT-PLP PSAT. The variants S43R, D100A and R342W showed thermal stability similar to WT with the T_ms of 56 °C, 64 °C and 59 °C, respectively. Instead, the variants G79W and C245R exhibited lower thermal stability with a T_m of 49 °C and 47 °C. Also in this case, the S179L variant is the most dissimilar to the WT PSAT, with the lowest melting temperature of 56 °C. Unexpectedly, A99V, which had been predicted to be unstable (Acuna-Hidalgo et al., 2014; Abdelfattah et al., 2020), exhibited a T_m of 70 °C with 7 °C higher than WT PSAT (Figure 37).

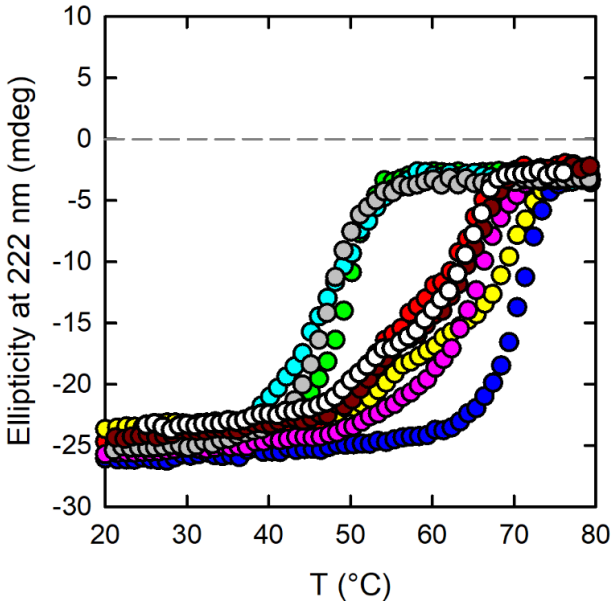

Figure 37. Thermal stability in a range of 20-80 °C of 5 µM PSAT variants: WT (white), S43R (red), G79W (green), P87A (yellow), A99V (blue), D100A (pink), S179L (cyan), C245R (grey), R342W (dark red) in 20 mM potassium phosphate, pH 7.

We observed that the variants G79W, S179L and C245R that showed lower T_ms also had reduced PLP saturation levels, while D100A and S43R, which had the same PLP saturation level as WT, also showed similar thermal stability. Therefore, we correlated the PLP saturation with thermal stability (Figure 38). The correlation was good, indicating that PLP binding stabilizes PSAT by about 10 °C. Thermal instability is, therefore, a possible mechanism of pathogenesis, although it is difficult to dissect this effect from other consequences of low PLP saturation in vivo.

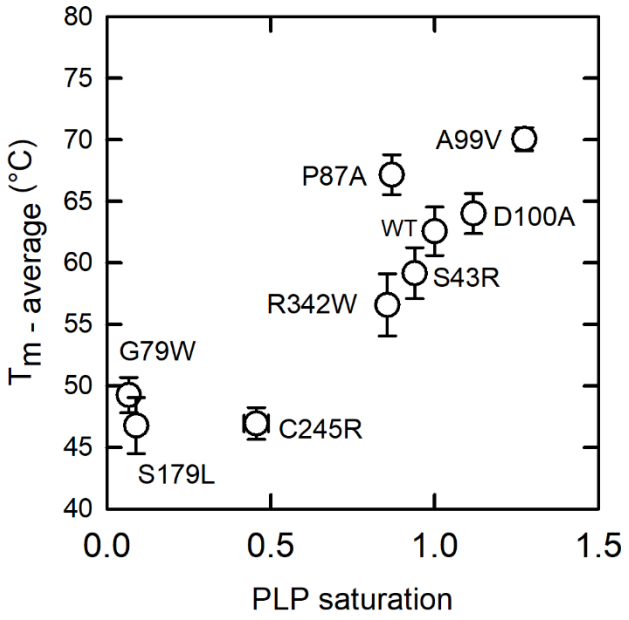

Figure 38. Linear correlation between the melting temperatures estimated considering a single unfolding transition and the PLP saturation level of PSAT variants.

Trying to explain better the pathological mechanism that could be related to thermal stability, we evaluated the stability in the absence of PLP using the PMP-bound forms. The experimental conditions were the same as described above. The PMP WT PSAT exhibited a T_m of 57 °C, 6 °C lower than PLP forms. However, the pathological variants did not show differences in thermal stability between PLP and PMP forms. The T_ms pattern was in the range of 47-69 °C, very similar to PLP. Indeed, we recorded only 1-2 degrees change in T_ms between the pure forms (Table 6). Therefore, it was concluded that the covalent binding of PLP to Lys200 does not confer additional stability in general.

	T_m^{PLP} (±S.E.M.)	T_m^{PMP} (±S.E.M.)
WT	63±2	57±3
S43R	56±2	59±1
G79W	49±1	51±0
P87A	67±2	65±1
A99V	70±1	69±0
D100A	64±2	61±1
S179L	46±2	47±0
C245R	47±1	49±1
R342W	59±2	58±0

Table 6. Value of thermal stability for PSATs PLP and PMP pure forms. The data were analyzed with SigmaPlot software.

Subsequently, observing in detail the unfolding curves for PLP-bound PSAT WT and the PLP-bound variants (S43R, P87A, D100A, R342W), we noticed that the curves were biphasic with a two-step unfolding. On the contrary, the apo-forms G79W and S179L exhibited monophasic unfolding curves, as well as C245R, which was poorly saturated with PLP (Figure 39). Since the biphasic state was present only in variants with PLP bound, we hypothesized that the PLP cofactor was a key to the biphasic unfolding transition, instead of stabilizing the protein in general. Interestingly, the only variant PLP-saturated that showed a monophasic curve was A99V.

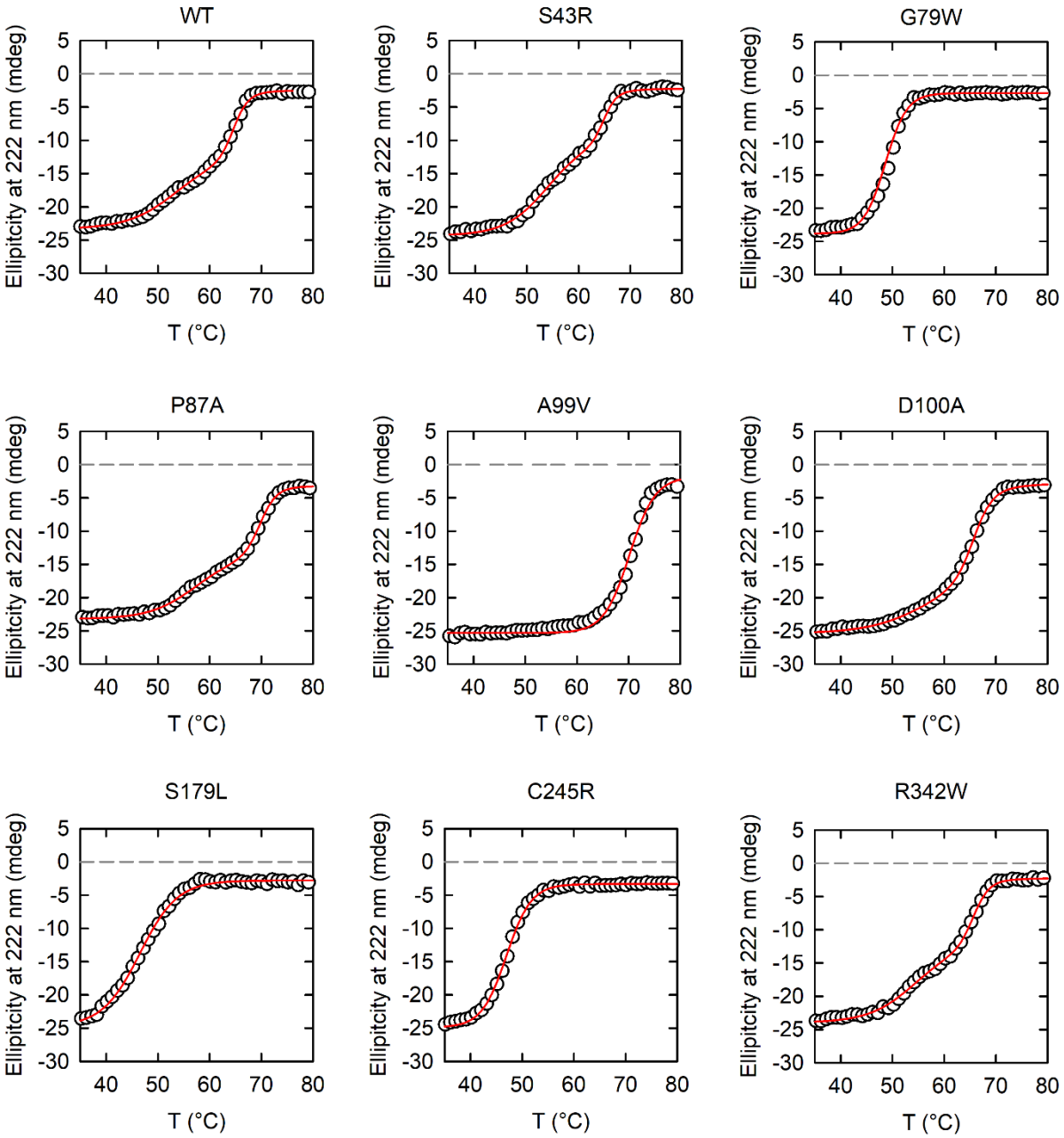

Figure 39. Thermal stability of 5 µM PSAT variants in a range of 30-80 °C in 20mM potassium phosphate buffer. The data were fitting with a double Boltzmann equation.

The biphasic curves were composed of two unfolding intermediates, one at low and the other at high temperatures. To estimate the T_ms of each phase, we analyzed the PLP unfolding curves with the Boltzmann double equation. We observed that, for WT and PLP-bound variants, except A99V, the first phase of unfolding was around 55 °C.

Since the low-temperature unfolding intermedia in PLP-bound corresponded with the unique phase of poorly PLP-bound forms, we proposed that it was independent of PLP. On the contrary, the second denaturation step had a T_m of around 65 °C. It was visible only in PLP-bound forms (Figure 40). Therefore, it was probably stabilized by PLP. We also observed that the transition temperatures were unchanged among variants indicating that amino acid substitutions do not impact protein stability significantly. The variant A99V represented a particular case. Indeed, despite being saturated with PLP, it exhibited a monophasic curve with the T_m corresponding to the transition occurring at the highest temperature for the other variants. We proposed that the A99V higher saturation could be related to a stronger bond with PLP, which probably stabilized the less stable intermedia showing a monophasic curve.

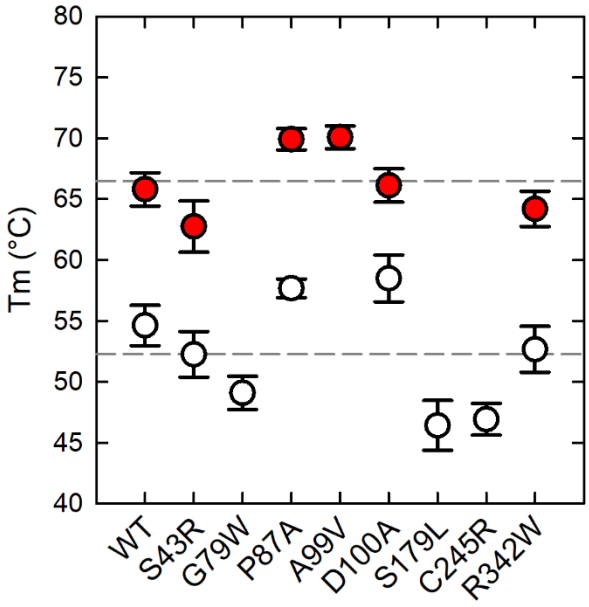

Figure 40. Estimation of the melting temperatures of PSAT variants considering two steps or a single step unfolding transition depending on the shape of the unfolding traces.

2.3.7 Dimer stability

PSAT is a dimeric enzyme composed of two monomers; each monomer contributes to the active sites at their interface. Thus, the dimeric configuration is fundamental for correct active site formation and functional activity (Murtas et al., 2020). As we observed in our enzymatic assay experiments, some PSAT variants were inactive or showed reduced activity compared to WT PSAT. We have hypothesized that the lack of activity could depend on the reduced dimer stability. Therefore, we assessed the oligomerization state for the variants S43R, G79W, S179L, C245R and R342W, which exhibited a deficit in activity through the size exclusion chromatography. In the SEC experiment (Figure 41), the chromatography column is packed with porous beads, and pore sizes are used to separate the proteins based on their dimension (Sakashita et al., 2018).

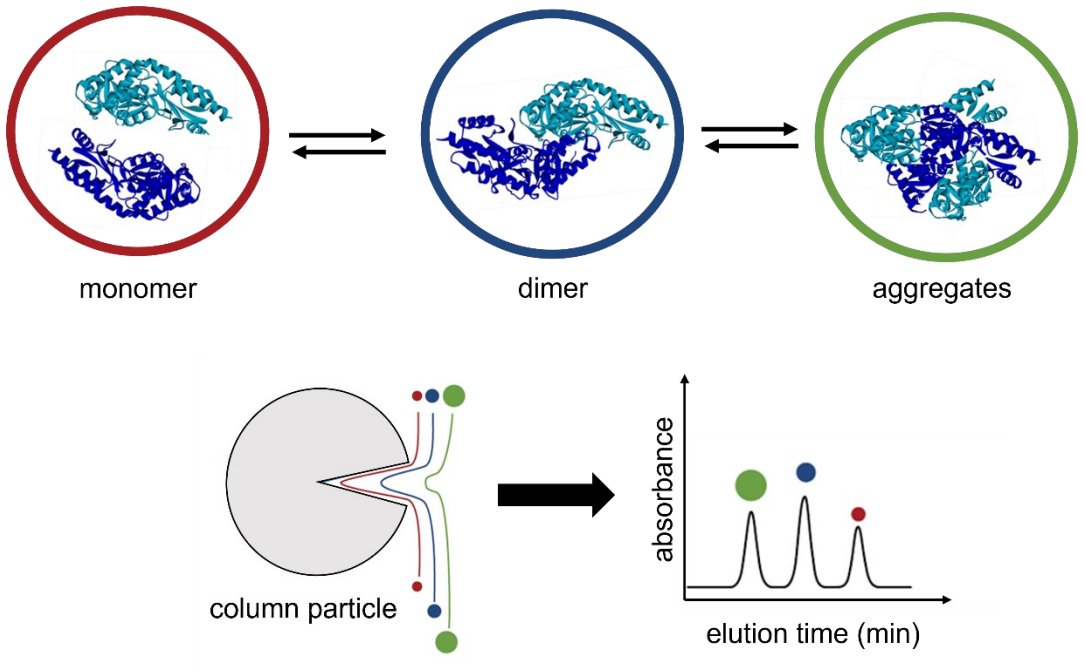

Figure 41. Schematic representation of size exclusion operation.

First, we tested WT PSAT for setting the experimental conditions. To avoid non-size interactions between protein and column beads that could alter the elution based on protein dimension (Lambrecht et al., 2015), we used a 50 mM phosphate running buffer rich in sodium chloride (300 mM) at pH 7. Then, to verify that WT PSAT eluted according to size and to calculate the MW, we performed a calibration curve using the standard proteins: myoglobin (17 kDa), ovalbumin (44 kDa), Immunoglobin G (150 kDa), Immunoglobin A (300 kDa), and bovine thyroglobulin (670 kDa). In particular, the MWs of ovalbumin and IgG perfectly cover the range of WT PSAT oligomerization state: monomer (42.85 kDa), dimer (85.70 kDa), and possible aggregates state (> 85.70 kDa). The WT PSAT was loaded at 23 µM, resulting in an elution concentration of around 2.3 µM. We observed that the peak was well-defined, sharp and base-to-base, indicating that the protein was stable in the chromatographic conditions and that the injection concentration was adequate for the analytical purpose (Figure 42). The retention time was 8.18 minutes; based on the calibration curve, it corresponded to the MW of 76 kDa, resulting consistently in a PSAT dimer (85 kDa). The reduced MW may depend on the protein factor shape; moreover, when the protein has a not a globular shape, the calibration curve based on globular protein standards may be less precise (Some et al., 2019).

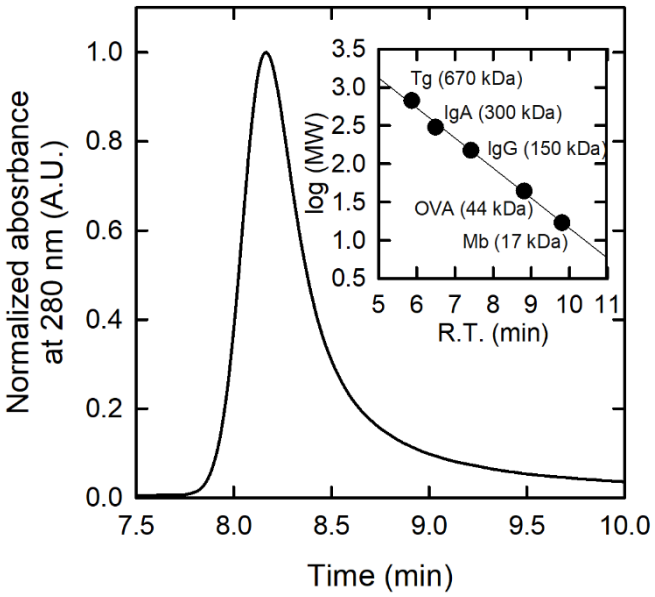

Figure 42. Size exclusion chromatography of 23 µM WT PSAT in 50 mM sodium phosphate buffer and 300 mM NaCl, pH 7. In the inset, the calibration curve. Column: BioSep-2000, flow rate 1 mL/min. The data was normalized for the maximum absorption at 280 nm.

After testing the characteristic of WT PSAT elution and its size compared to the theoretical MW, we evaluated different concentrations in injection of WT PSAT to exclude that, in our condition, the protein showed a concentration-dependent monomerization or aggregation. This step is important for choosing the best analytical protein concentration for studying pathological variants and excluding the abnormal behaviour of variants due to experimental conditions instead of caused by the aminoacid substitutions. Therefore, the experiment was repeated at a higher concentration of 200 µM and a lower loading concentration of 5 µM and 1 µM in the same condition described above (Figure 43). The WT PSAT exhibited at all concentrations peaks well-defined with an average retention time of 8.20, corresponding to a mean MW of 75 kDa. These results confirmed the dimer stability of

WT PSAT under our experimental conditions, excluding the formation of monomers or aggregate ad high MW due to intrinsic experimental setup.

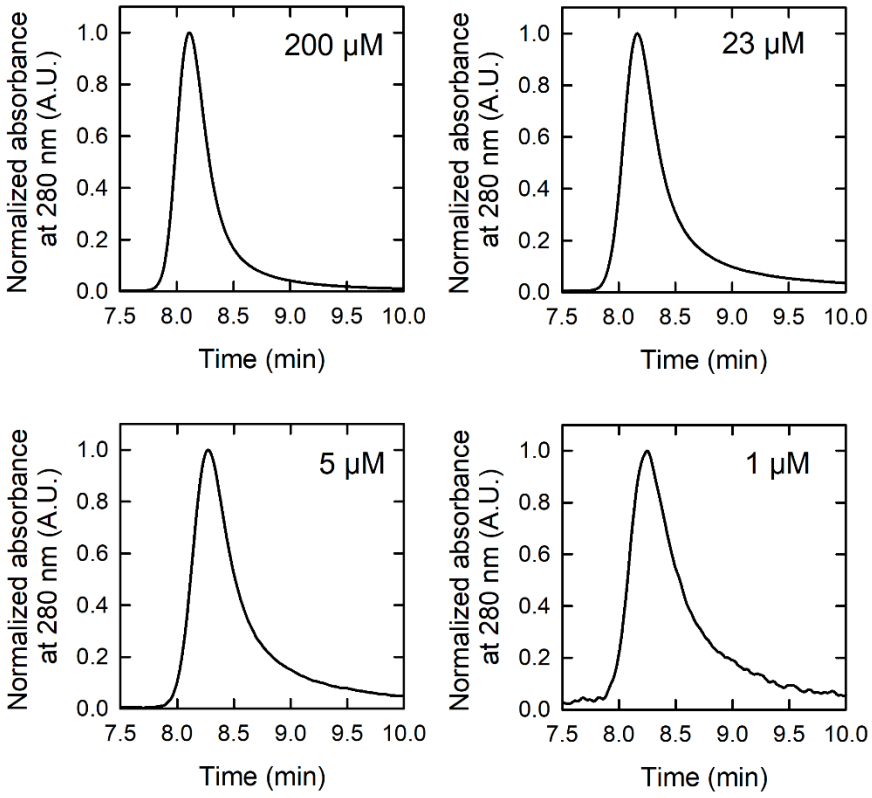

Figure 43. Size exclusion chromatography of WT PSAT. The protein concentration was in the range of 200 µM-1 µM. Column: BioSep-2000, mobile phase: 50 mM sodium phosphate (pH 7) and 300 mM NaCl, flow rate 1 mL/min. All data were normalized for the maximum absorption at 280 nm.

Since WT PSAT showed a dimeric state at all concentrations of protein injection, we decided to test the PSAT variants at the intermedia concentration of 23 µM in order to be more sensitive to possible variations in molecular weight due to the instability of the dimer. The variants S43R, G79W, S179L, C245R and R342W, which exhibited a lack of activity in the enzymatic assay, and that we assumed could monomerize, were analyzed. For this experimental pattern, the variants P87A, A99V and D100A, which

showed the same activity as WT, were temporarily excluded. All variants analyzed exhibited peaks sharp with a shape profile analogous to the WT PSAT (Figure 44), suggesting that the proteins were stable and eluted without column unspecific interaction. We observed that all proteins showed an elution time similar to WT PSAT and, consequently, a similar MW around 76 kDa, suggesting that they all retain a dimeric structure. Therefore, for the variants S43R, G79W, S179L and C245R and R342W, we excluded the dimer stability as a mechanism of pathology and as a cause to reduced enzymatic activity. Other analyses for the variants P87A, A99V and D100A are ongoing.

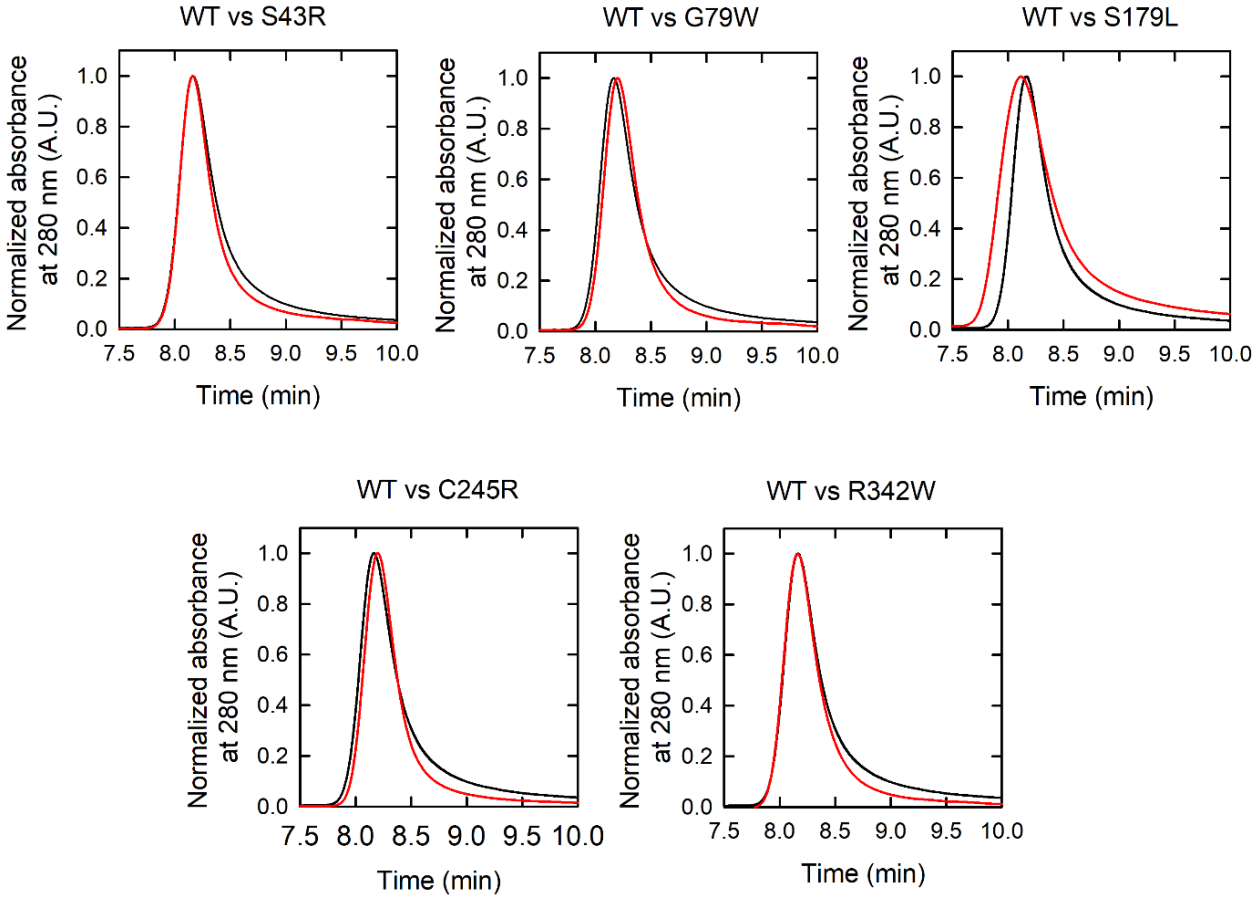

Figure 44. Size exclusion chromatography of WT PSAT (black line) and PSAT variants (red line) in 50 mM sodium phosphate buffer and 300 mM NaCl, pH 7. The protein concentration was 23 μM. Column: BioSep-2000, flow rate 1 mL/min. All data were normalized for the maximum absorption at 280 nm, to facilitate the visual comparison.

2.3.8 Aggregation

The incorrect folding and aggregation of proteins are recognized as characteristic of many human diseases (Nelson et al., 2019). After analysing the changes in the secondary structure, we evaluated the possibility of an increasing tendency to aggregation due to structural perturbations produced by substitutions, as a pathological mechanism for PSAT variants, through dynamic light scattering (DLS) experiments. In the dynamic light scattering technique, a monochromatic beam of light

is sent to the sample, which scatters the light in different directions based on the dimension of the particles. The DLS instrument records how intense scattered light is at a fixed angle. This information can be correlated to the particle's hydrodynamic diameter (d_h) that scatters the light. Through a math algorithm, the hydrodynamic diameter is converted to MW, and we obtain information about the size of the protein and the presence of aggregates. To set the methodology, we performed the experiments on WT PSAT at different concentrations: 50 µM, 25 µM and 12.4 µM, in 50 mM sodium phosphate buffer and 300 mM NaCl pH 7, at 25 °C. No difference was observed between conditions (data not shown). Therefore, we proceeded with 23 µM, the same concentration used in size exclusion experiments for dimer stability evaluation. The conversion from hydrodynamic diameter to MW was calculated by Malvern Zetasizer Software. In literature reported that the DLS experiments on polymerized hemoglobins demonstrated an almost perfect correlation between d_h and MWs (Faggiano et al., 2010). Therefore, to verify the correlation between hydrodynamic diameter and MW in our experimental conditions, we conducted DLS experiments for WT PSAT and standard proteins (Figure 45). We used myoglobin (14 kDa) to test the sensibility at low MW and conalbumin (76 kDa) since it had an MW similar to PSAT dimer (85 kDa) as standard. We observed that myoglobin, ovalbumin and WT PSAT showed a d_h of 3.20, 7.02 and 7.45, respectively, corresponding to 10.1 kDa, 63.5 kDa and 72.8 kDa. The values obtained through algorithm conversion were compatible with the theoretical proteins MWs, demonstrating that under our experimental conditions, DLS technique was sensible to protein size analysis.

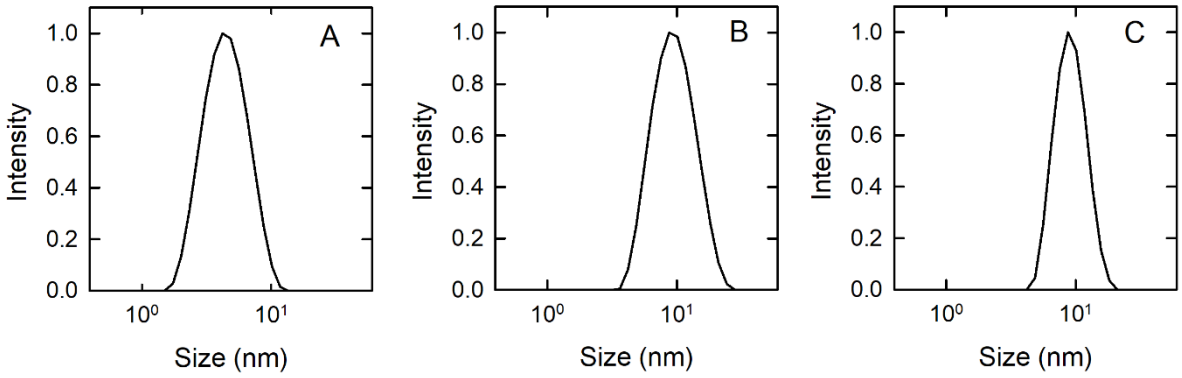

Figure 45. DLS intensity particle size distribution of myoglobin (A), conalbumin (B) and WT PSAT (C), in a buffer containing 50 mM NaH_2PO_4, 300 mM NaCl pH 7. The protein concentration was 23 µM.

After verifying the experimental method, we carried out the DLS experiments for all PSAT variants in the condition described above. Therefore, for all PSAT variants, the intensity particle size distribution was recorded immediately (time 0) after sample preparation (Figure 46). All variants showed a population with an average hydrodynamic diameter of around 7.45 nm, corresponding to the MW of around 73.75 kDa. These MWs, although slightly variable among variants, were all compatible with the PSAT dimers, which have an estimated MW of 86.70 kDa (Table 7). Instead, the minority population of the total signal intensity for all variants, except D100A, was represented in the range of 15-34% with a higher hydrodynamic diameter ranging from 0.4 to 1 µm, corresponding to aggregates of around 0.5x103 - 80x103 copies of PSAT dimers. The variants G79W, S179L and R342W showed a higher percentage of aggregates than 21.35% of WT and other variants, 29.7%, 27.65% and 34.25%, respectively, suggesting a tendency to aggregation. It should be emphasized that the D100A variant exhibited the highest percentage of aggregation of 73.55%, with a d_h of

258.4 nm corresponding to around 3500 dimers, probably due to the exposition of hydrophobic residue toward the bulk solution.

	Est. Mw (kDa±S.E.M.)
WT	73±1
S43R	76±4
G79W	63±0
P87A	78±5
A99V	76±2
D100A	66±1
S179L	97±0
245R	62±5
R342W	72±1

Table 7. DLS PSATs estimate MWs, the conversion of d_h and MW was calculated with Malvern Zetasizer Software.

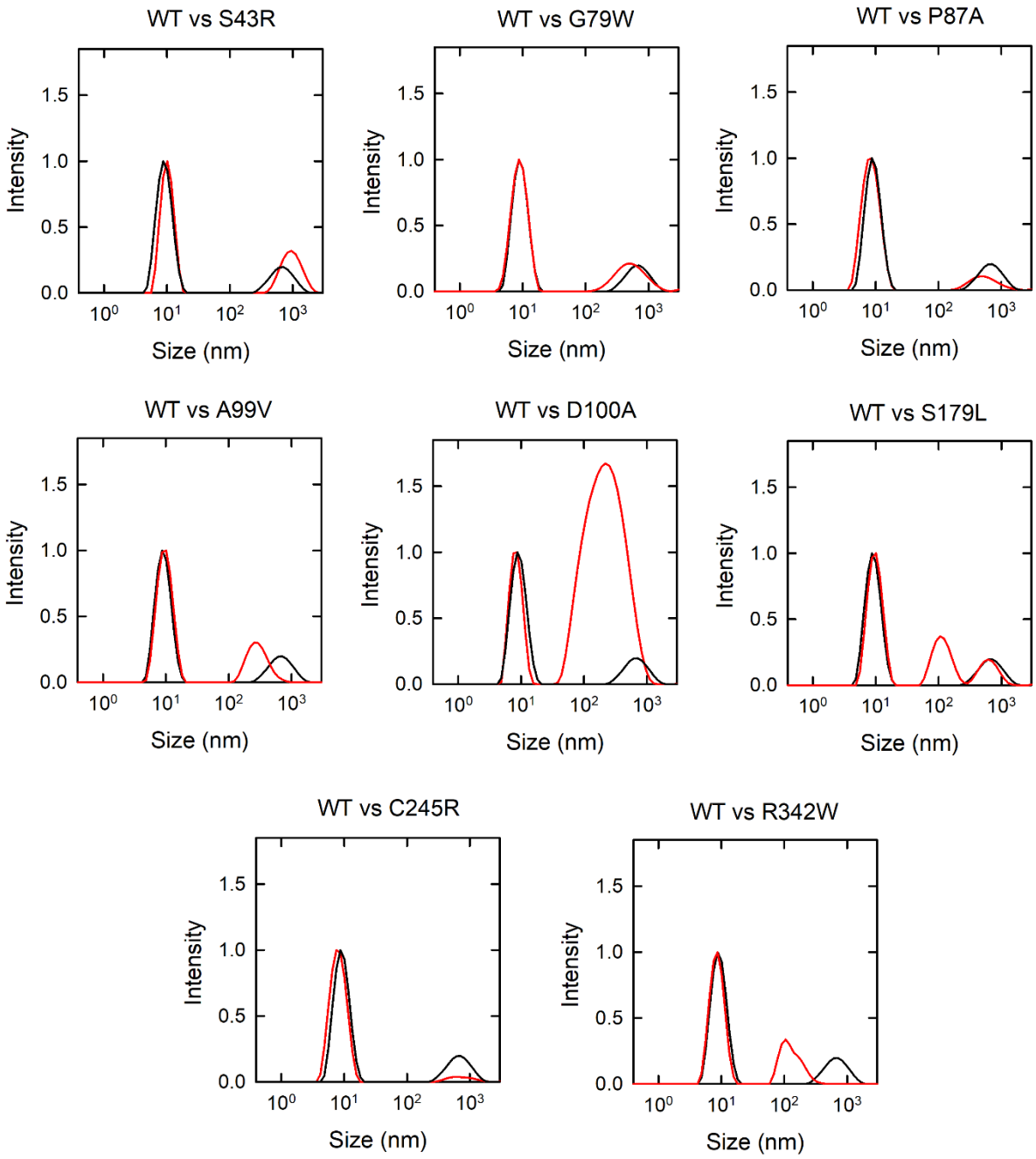

Figure 46. DLS intensity particle size distribution of WT PSAT (black line) compared to PSAT variants (red line) in a buffer containing 50 mM NaH_2PO_4, 300 mM NaCl pH 7. The protein concentration was 23 µM. Data were normalized to the peak intensity of the particle corresponding to dimeric PSAT.

Given the high tendency to aggregation for the same variants, we assessed the time-dependent aggregation phenomena. Therefore, we recorded the intensity particle size distribution after 1 hour (Figure 47). For WT and all variants, no major changes were observed for the population with a hydrodynamic diameter of 7.45 nm. The aggregate percentages at high MWs, although slightly variable among variants, were unchanged, with the only exception of S179L. Indeed, this variant exhibited a tendency to aggregate over time in accordance with its perturbed secondary structure observed in circular dichroism and the lower expression yields. The compared value of aggregation for each variant at time 0 and after 1 h are shown in Table 8.

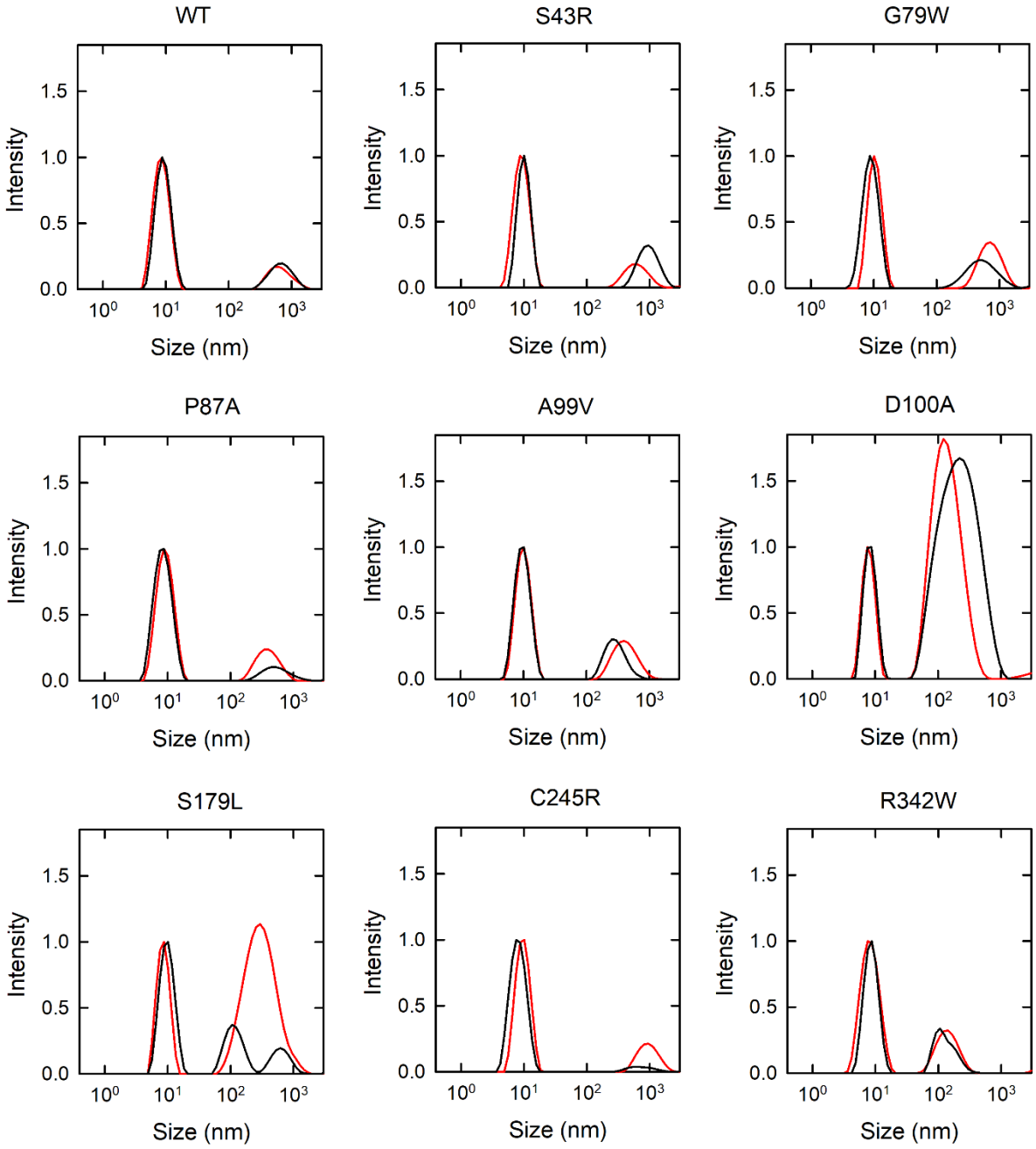

Figure 47. DLS intensity particle size distribution of WT and PSAT variants at time 0 (black line) compared to the same sample analyzed after 1 hour (red line) in a buffer containing 50 mM NaH_2PO_4, 300 mM NaCl pH 7. The protein concentration was 23 μM. Data were normalized to the peak intensity of the particle corresponding to dimeric PSAT.

	Aggregation (% signal intensity)	
	t_0	1 h
WT	21.35	24.75
S43R	24.75	26.30
G79W	29.70	41.45
P87A	19.20	22.90
A99V	19.45	23.95
D100A	73.55	77.80
S179L	27.65	69.59
C245R	15.40	25.95
R342W	34.25	36.85

Table 8. Comparison of aggregates PSATs signal intensity percentage at 0 minutes and after 1 h.

2.4 Conclusions

The essential role played by L-serine as a precursor of phospholipids and neurotransmitters is attested by the occurrence of serine deficiency syndrome caused by mutations in the genes that code for the enzymes of the phosphorylated pathway. The PSAT pathogenetic variants were selected based on NLS2 and PSTD case literature. We expressed and purified the PSAT variants: S43R, G79W, A99V, D100A, S179L, C245R, and R342W. Most of these variants exhibit properties that might be responsible for the pathologies they were associated with. For comparison, the non-pathogenic Uniprot-reported P87A natural variant was also investigated, with no significant differences with respect to WT PSAT in terms of stability, aggregation, PLP saturation and enzyme activity and secondary structure. The G79W and S179L are located in the PLP binding domain. The variants result in being poorly bound to PLP and are virtually inactive. Both PLP saturation levels and activity do not change in the presence of high PLP concentrations in the solution mix. Both variants showed a monophasic unfolding curve with a melting temperature of about 15 degrees below WT PSAT. In addition, S179L showed a change in secondary structure, with a higher B-sheet percentage, compared to WT. It also exhibited a tendency to aggregate on time, showing a great and clear pathogenic mechanism in accordance with the NLS2 association reported in the literature (Acuna-Hidalgo et al., 2014). The R342W variant results in PLP saturated as WT PSAT but inactive. It showed an unfolding biphasic curve with a melting temperature similar to WT PSAT for both PLP and PMP bound forms. R342 residue is localized in the C-terminal domain and is adjacent to the substrate's binding site, forming an ionic bond with its carboxylate group. Probably the pathogenic mechanism is related to the impossibility of the bulky and non-charged

tryptophane to form the necessary molecular link for the transamination reaction. The C245R variant shows a low level of PLP saturation. The activity is around 10% WT PSAT, and it does not change in the presence of higher PLP concentration, suggesting that variants it is at the maximum saturation and that the pathogenetic mechanism is related to the low PLP affinity. It also shows an increase in beta sheet percentage in secondary structure for both PLP and PMP forms. However, the thermal stability and tendency to aggregation are similar to WT PSAT. The S43R variant was predicted to be unstable. However, it is present in dimeric form. In addition, it has an activity of around 80% WT and a similar PLP saturation, thermal stability, secondary structure, and tendency to aggregation. Residue S43 is located at the active site, in proximity (5.8 Å) to the phosphate group of the PSAT substrate. Probably, the pathogenic mechanism is related to the bulkier substituent Arg that interacts with substrate binding. The pathogenic mechanism of D100A and A99V was still unclear. The variants have an activity like WT PSAT and bound PLP and have the same secondary structure as WT PSAT. The D100A has a high tendency to aggregate, probably due to the amino acid substitution being more prone to solvent accessibility. At the same time, the A99V shows a monophasic curve with a temperature of melting around 70 °C, higher than WT, suggesting a more strongly bound PLP. Although some pathogenetic mechanisms are not yet perfectly clear, with this research work, we have helped to better clarify the key role of the enzyme phosphoserine aminotransferase within the biosynthesis of L-serine, confirming the association between mutations in the *PSAT1* gene and serine deficiency disorders, such as PSATD and NLS2.

Chapter 3. Interaction of human serine racemase and glyceraldehyde 3-phosphate dehydrogenase

3.1 Introduction

Protein-protein interactions (PPi) are fundamental for many biological reactions and signalling pathways. Thanks to their functional and regulatory role, the PPi could potentially be exploited as drug targets (Rabbani et al., 2018).

The enzyme serine racemase (SR) exhibits a complex conformational space (Raboni et al., 2019) that can be modulated by protein interactors, particularly by proteins associated with AMPA and NMDA receptors. For example, it is known that PICK1 and GRIP bind SR through the PDZ domain (Baumgart et al., 2007; Jiraskova-Vanickova et al., 2011). Also, there is evidence that Golga-3 and DISC1 maintain SR intracellular concentration constant by controlling its ubiquitination (Wolosker et al., 1999; Canu et al., 2014).

Suzuki et al., 2015 reported murine GAPDH as a protein interactor of murine SR, resulting in its inhibition. Therefore, they envisaged a possible biochemical link between glycolysis and D-serine metabolism through pull-down and immunohistochemistry experiments. In addition, the author explained that adenosine triphosphate (ATP) and glyceraldehyde-3-phosphate (G3P), the substrate of glyceraldehyde-3-phosphate dehydrogenase, were crucial to SR-GAPDH interaction.

To evaluate if the human orthologues of SR and GAPDH form a complex, we expressed and purified the human enzymes. To explore the formation of a stable hSR-hGAPDH complex, we designed a size exclusion chromatography (SEC) experiment. This technique, also known as gel filtration chromatography, allows the separation of proteins according to their molecular weight, thanks to a molecular sieve mechanism. Indeed, the chromatography column is packed with porous beads. Compared to smaller proteins, the complex with large dimensions cannot enter the pore beads and

elutes before in the chromatographic period. In contrast, the single proteins elute with a longer retention time. We also performed a cross-linking experiment to explore the formation of an unstable hSR-hGAPDH complex. Cross-linking is the process of chemically joining two or more molecules through covalent bonds. A cross-linking reagent (or cross-linker) is a molecule containing two or more reactive ends that can chemically bond to specific functional groups (primary amines, sulfhydryls, etc.) on proteins. The protein-protein interaction may be visible on SDS-PAGE. Since hSR and hGAPDH subunits have nearly identical MW, we expressed and purified hSR fused with thioredoxin (hSR-TRX) to distinguish them on the gel.

In this research work, we explored the interaction of the human orthologue of SR and GAPDH to understand better and clarify the regulation of D-serine metabolism in the human brain.

Part of this work was published in:

Michielon A. et al. "Human serine racemase is inhibited by glyceraldehyde 3-phosphate, but not by glyceraldehyde 3-phosphate dehydrogenase." Biochimica et Biophysica Acta (BBA)-Proteins and Proteomics 1869.1 (2021): 140544.

Candidate's contribution:

I expressed and purified the protein human serine racemase. Prof. Stefano Bruno provided the protein human glyceraldehyde 3-phosphate dehydrogenase. I designed and performed the size exclusion chromatography experiments on FPLC. Moreover, I developed and carried out the cross-linking experiments with the collaboration of Prof. Serena Faggiano (University of Parma).

3.2 Materials and Methods

3.2.1 Materials

All reagents were high-quality chemicals purchased from Sigma Aldrich (St. Louis, MO, USA), except for Tris (2-carboxyethyl) phosphine (TCEP), which was purchased from Apollo Scientific (Denton, Manchester, UK).

3.2.2 Protein expression

- **Human serine racemase**

Human serine racemase was expressed in recombinant form as a fusion protein with a six-histidine tag encoded in the expression vector pET28a (EMD Millipore, Darmstadt, Germany). The sequence of the expressed protein is shown in Figure 48.

```
        10         20         30         40         50         60
MGSSHHHHHH SSGLVPRGSH MCAQYCISFA DVEKAHINIR DSIHLTPVLT SSILNQLTGR

        70         80         90        100        110        120
NLFFKCELFQ KTGSFKIRGA LNAVRSLVPD ALERKPKAVV THSSGNHGQA LTYAAKLEGI

       130        140        150        160        170        180
PAYIVVPQTA PDCKKLAIQA YGASIVYCEP SDESRENVAK RVTEETEGIM VHPNQEPAVI

       190        200        210        220        230        240
AGQGTIALEV LNQVPLVDAL VVPVGGGGML AGIAITVKAL KPSVKVYAAE PSNADDCYQS

       250        260        270        280        290        300
KLKGKLMPNL YPPETIADGV KSSIGLNTWP IIRDLVDDIF TVTEDEIKCA TQLVWERMKL

       310        320        330        340        350        360
LIEPTAGVGV AAVLSQHFQT VSPEVKNICI VLSGGNVDLT SSITWVKQAE RPASYQSVSV
```

Figure 48. FASTA sequence of recombinant hSR. The number of amino acids is 360, molecular weight is 38.7 kDa, and theoretical pI is 6.67. Analysis carried out via online software: *https://web.expasy.org/compute_pi/*.

The plasmid was transformed into E. *coli* BL21 Codon Plus (DE3) -RIL (Agilent Technologies, Santa Clara, CA, USA) cells containing the plasmid encoding the chaperonins GroEL and GroES (Chaperone Plasmid set, Takara®). The plasmids pET28a and TAKARA bear resistance to kanamycin and chloramphenicol, respectively. The transformed cells were grown at a temperature of 37 °C in Luria Bertani (LB) medium (tryptone 10 g/L, NaCl 10 g/L and yeast extract 5 g/L), with kanamycin (50 µg/ml) and chloramphenicol (50 µg/ml). Bacterial growth was followed by measuring optical density (OD) at 600 nm. When cells reached about 0.5 OD, arabinose (0.3 mg/ml) was added to induce the production of GroEL/GroES. Also, benzyl alcohol (1 ml/L) was added since it was reported that it increased the expression of molecular chaperones in response to a stress condition (De Marco et al., 2005; Duan et al., 2019). The cultures were transferred at a temperature of 20 °C; after 20 minutes, Isopropyl-β-D-1-thiogalactopyranoside (IPTG) was added at the final concentration of 0.05 mM to induce the expression of human serine racemase. Bacterial growth continued at 20 °C for the next 16 hours. Subsequently, the cells were collected by centrifugation at 4500 g for 15 minutes at 4 °C. Finally, three washes in phosphate buffer and NaCl (PBS) were carried out, and the pellets were frozen at -80 ºC.

- **Human serine racemase-thioredoxin**

The hSR-TRX construct was subcloned into a pET21b-derived expression vector. Between TRX and hSR was inserted a proteolysis site for the TEV protease (EC 3.4.22.44, Tobacco Etch Virus nuclear-inclusion-a endopeptidase) to remove during the purification step the histidine tag. The fusion protein was expressed in *E. coli* BL21 (DE3)-RIL cells (Agilent Technologies, Santa Clara, CA, USA). The expression of

human serine racemase with bacterial thioredoxin and the six-histidine tag was described in detail by Bruno et al., 2017.

- **Human glyceraldehyde 3-phosphate dehydrogenase**

The expression of human glyceraldehyde 3-phosphate dehydrogenase as a recombinant protein was reported by Bruno et al., 2016.

3.2.3 Protein purification

- **Human serine racemase**

Cell frozen at -80 °C were resuspended in 50 mL lysis buffer (50 mM Na_2HPO_4, 150 mM NaCl, 5 mM TCEP, 50 µM PLP, 4 °C) containing protease inhibitors (0.2 mM phenylmethylsulfonyl fluoride at pH 8.0 (PMSF), 0.2 mM benzamidine and 1.5 µM pepstatin A) added. The suspension was left for 45 minutes in agitation at 4 °C in the presence of lysozyme (1 mg/mL) to promote the rupture of the cell wall. Subsequently, cell lysis was performed by sonication with a "macro tip" probe. The sonication phase consisted of 5 cycles lasting 20 seconds. Next, a 50-minute centrifugation step was carried out at 4 °C at a speed of 16000 g to separate the soluble and insoluble components. The supernatant was incubated with 4 mL of TALON® resin (Clontech, Mountain View, CA, USA) for 1 hour at 4 °C. Subsequently, the resin was washed with 120 mL of washing buffer (50 mM Na_2HPO_4, 300 mM NaCl, pH 8), and then the protein was recovered by suspending the resin in an elution buffer (50 mM Na_2HPO_4, 150 mM NaCl, 250 mM imidazole, pH 8). Next, we proceed with a desalting step and buffer exchange in 50 mM triethanolamine (TEA) at pH 8, the HiTrap™ Desalting column (GE Healthcare Life Science, Little Chalfont, United Kingdom). Finally, hSR was

concentrated in Amicon® (Merck/Millipore, Burlington, MA, USA). The protein obtained was aliquoted and stored at -80 °C. Purity was analyzed by SDS-PAGE electrophoresis and densitometric analysis carried out by ChemiDoc Image System™ (Bio-Rad, Hercules, CA, USA).

- **Human serine racemase-thioredoxin**

The purification of hSR-TRX followed the same protocol as the hSR, except for the phase of TEV removal. After the incubation with 4 mL of TALON® resin (Clontech, Mountain View, CA, USA) for 1 hour at 4 °C, the protein was incubated with his-tagged TEV protease (60 µg per mg of protein) for 3 h at 4 °C to remove the his-tagged thioredoxin fragment. Then, the protein was dialyzed to remove the imidazole and further incubated with the TALON resin to remove the uncleaved protein and His-tagged TEV protease, to complete the purification procedure. The purification of human serine racemase with thioredoxin was reported in detail by Bruno et al., 2017.

- **Human glyceraldehyde 3-phosphate dehydrogenase**

Human glyceraldehyde 3-phosphate dehydrogenase was purified as previously described by Bruno et al., 2016.

3.2.4 Size exclusion chromatography

The system AKTA pure FPLC (GE Healthcare Life Science, Little Chalfont, United Kingdom) coupled with a UV detector was employed for the size exclusion chromatography experiments for hSR and hGAPDH. Chromatographic separation was achieved on a Superdex Increase 200 (300 mm x 3.2 mm) column (GE Healthcare Life

Science, Little Chalfont, United Kingdom), pre-packed with agarose beads of 8.6 µm for high flow rates and pH stability. The column separation range molecular weights were between 10 and 600 kDa. The pumps were set on isocratic elution mode. The column was pre-equilibrated for 1 hour at the flow rate of 1 mL/min with a solution containing 25 mM TRIS and 150 mM NaCl pH 8. The manual injection volume was 100 µL at the protein concentration of 16 µM for hSR and 84 µM hGAPDH. The proteins were incubated in different combinations for 30 minutes a 4 °C in 200 mM TEA, 150 mM NaCl, 5 mM DTT, 6 mM ATP and 10 mM $MgCl_2$. Detection was performed by the Uv-vis detector of the FPLC system at 280 nm wavelength for hSR, hGAPDH and standard proteins and 240 nm for the mixer hSR-hGAPDH and hSR-GAPDH with 5 mM D-G3P. The total chromatographic run period was 20 minutes at a flow rate of 1 mL/min. The procedures of column equilibration and experiments were carried out at room temperature. The column was calibrated with different molecular weight standards, including lysozyme (14.4 kDa), trypsinogen (24 kDa), ovalbumin (45 kDa), bovine serum albumin (66 kDa), ferritin (440 kDa) and bovine thyroglobulin (670 kDa).

3.2.5 Cross-linking

For cross-linking experiments, we used the cross-linker glutaraldehyde. The samples were dialyzed in the 20 mM HEPES buffer at pH 7.5 to remove the amino groups contained in the TEA buffer (the hSR storage buffer) that would react with glutaraldehyde. The cross-linker was diluted from 2% to 0.5% stock in 20 mM HEPES. The experiments were conducted at room temperature, and the proteins were incubated with 0.1 glutaraldehyde for 10 minutes. The protein concentration in the reaction mix was 15 µM for hSR-TRX and 30 µM for GAPDH.

The reaction was stopped using 1 M Tris HCl pH 8. Then we performed SDS-PAGE experiments. We used the gel of 10% acrylamide, which was run for 45 minutes at 200 V at room temperature. The gel was stained in Coomassie blue for 50 minutes and then bleached for 5 hours. The densitometric analysis was performed by ChemiDoc Image System™ (Bio-Rad, Hercules, CA, USA).

3.3 Results and discussion

3.3.1 Size exclusion chromatography

We carried out gel filtration experiments to evaluate whether hSR directly interacts with hGAPDH, as reported for the murine orthologue (Suzuki et al., 2015). In SEC experiments, the protein MWs were related to the chromatographic elution period. Large proteins elute before smaller proteins because they were excluded by the size pore beads of the column.

Since Suzuki et al., 2015 showed that, in pull-down experiments, ATP augmented the SR-GAPDH interaction in a dose-dependent manner ranging from 2 to 10 mM, we decided to evaluate the hypothetical hSR-hGAPDH interaction in the presence of 6 mM ATP in the incubation mix. In addition, the authors hypothesized that GAPDH needed a conformational change to interact with SR and reported that G3P increased the SR-GAPDH interaction in a dose-dependent manner ranging from 0.5 to 1 mM. In the literature, there was evidence that G3P modulated GAPDH conformation (Mozzarelli et al., 1982; Bruno et al., 2014). Therefore, we decided to test the possible hSR-hGAPDH complex formation with 6 mM ATP both in the presence and absence of a large excess of 5 mM G3P.

To evaluate whether hSR directly interacts with hGAPDH, we used hSR as a spectroscopic reporter. The chromatographic course was followed by absorbance at 420 nm (around the absorption maximum of hSR-PLP internal aldimine) to check the elution peak of hSR and avoid ATP or hGAPDH absorption interference. In this way, it was possible to use a concentration of hGAPDH 5-fold higher than hSR. All experiments were performed in a solution of 200 mM TEA, 150 mM NaCl, 5 mM DTT, and 10 mM $MgCl_2$. To evaluate the MWs of our protein of interest, we created a

calibration curve using a standard protein range of 14-670 kDa. We used lysozyme, trypsinogen, ovalbumin, bovine serum albumin, ferritin, and bovine thyroglobulin. In particular, the bovine serum albumin (66 kDa) was near the theoretical hSR dimer MWs (74 kDa). After the calibration, we carried out the hSR at the concentration of 18 μM to evaluate the elution characteristic. We observed that the peak was sharp and well-defined, indicating that the protein concentration in injection was correct for the analytic purpose and that the proteins were stable in the chromatographic conditions (Figure 49-A). Then we tested 18 μM hSR in the presence of 84 μM hGAPDH and 6 mM ATP (Figure 49-B), and finally, we assessed 18 μM hSR with 84 μM hGAPDH, 6 mM ATP and in the presence of 5 mM D-G3P (Figure 49-C).

Based on the calibration curve, we estimated for hSR alone an MW of 59.2 kDa, for the condition hSR with hGAPDH and ATP an MW of 51.2 kDa and the hSR with hGAPDH, ATP and G3P in solution mix an MW of 43.4 kDa. These values were lower than the theoretical MW of the hSR dimer of 74 kDa, probably due to differences in protein shape. However, we excluded the hSR-hGAPDH complex formation, which had a theoretical MW of 22 kDa in 1 a 1 stoichiometry.

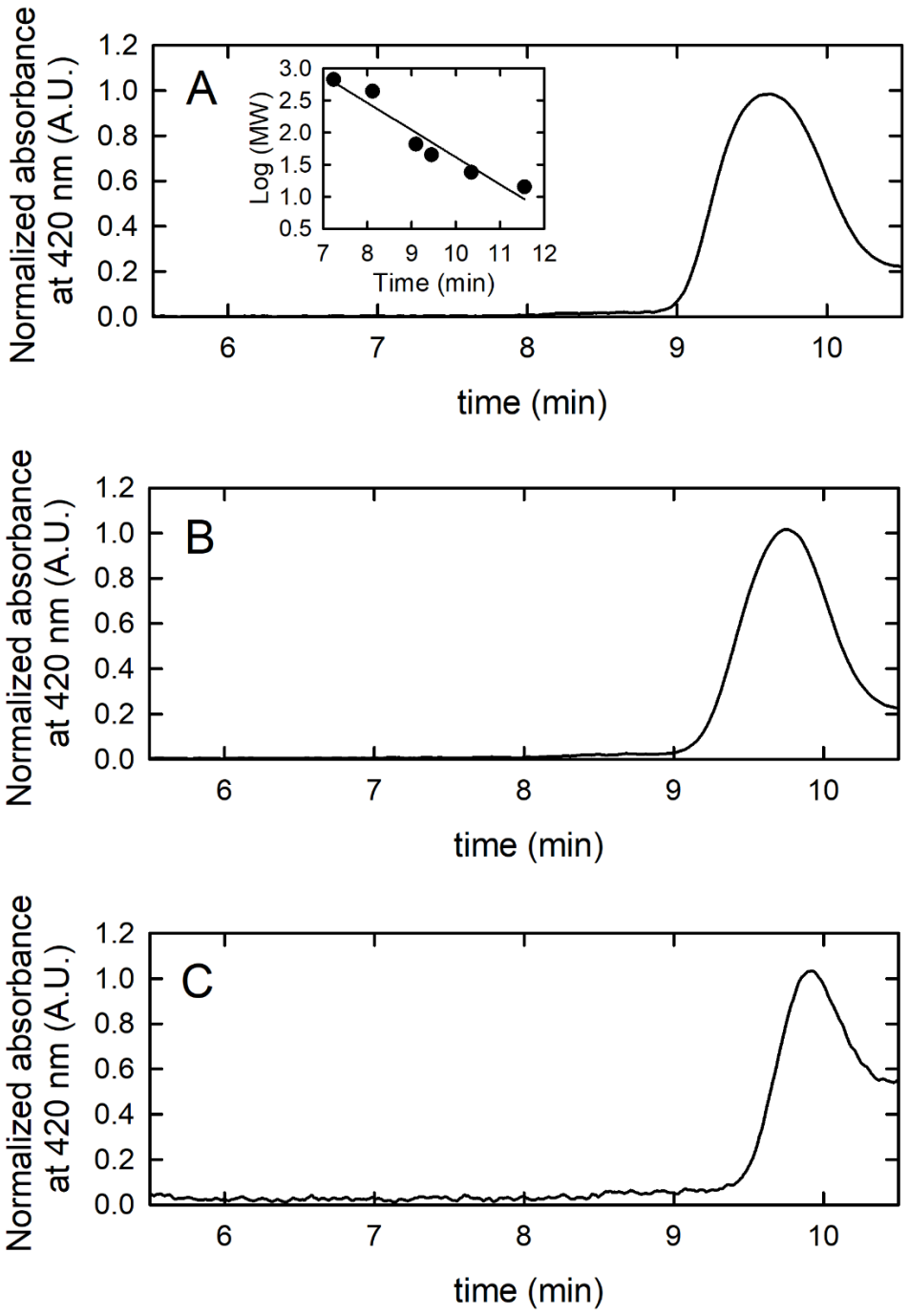

Figure 49. Size exclusion chromatography experiments in a solution of 200 mM TEA, 150 mM NaCl, 5 mM DTT, and 10 mM $MgCl_2$. **A)** 18 µM hSR + 6 mM ATP. In the inset is reported the calibration curve. **B)** 18 µM hSR + 84 µM hGAPDH + 6 mM ATP. **C)** 18 µM hSR + 84 µM hGAPDH + 6 mM ATP + 5 mM D-G3P. The chromatographic courses were shown from 5 to 15 minutes to demonstrate the absence of peaks at higher MWs than hSR. All absorbances were normalized for the maximum absorption value at 420 nm to facilitate the visual comparison.

3.3.2 Cross-linking experiment

We performed a cross-linking experiment to rule out the possibility of an unstable complex between hSR and hGAPDH, not visible under size exclusion chromatography conditions. The glutaraldehyde is able to form covalent binds, in this way it is possible to fix the interactions of hSR and hGAPDH. Indeed, they are present as dimers and tetramers, respectively, and the formation of oligomers of higher MW is visible on the SDS-PAGE. Since hSR and hGAPDH subunits have nearly identical MW, we expressed and purified hSR fused with thioredoxin (hSR-TRX) to distinguish them on gel (Table 9). Thioredoxin is a small protein composed of 105 amino acids with a molecular weight of 12.5 kDa.

	Length (Number of amino acid)	**MW (kDa)**
hSR	360	38.7
hSR-TRX	465	51.2

Table 9. Compare hSR and hSR with thioredoxin.

Several concentrations of glutaraldehyde were tested: 0.1%, 0.5% and 1%. The 0.1% had the best protein cross-linking ratio and visual quality of the electrophoretic mobility. In the cross-linking experiments, the concentration of ATP was decreased at 2 mM, compared to the 6 mM in the gel filtration experiment, due to the possibility of the ATP amino group interacting with the cross-linker. Anyway, Suzuki et al., 2015 reported that 2 mM ATP was already sufficient for the formation of complex SR-GAPDH.

We first tested the proteins without glutaraldehyde to set the methodology and evaluate the electrophoretic mobility in the presence of ATP and G3P. So, we conducted two experiments in parallel in the absence and presence of ATP and G3P.

For both gels, we prepared the samples: hSR-TRX alone, hGAPDH alone and the mix of hSR-TRX+hGAPDH. We observed that, as expected, all proteins migrate according to their MWs: around 51 kDa for hSR-TRX and 38 kDa for hGAPDH. The same MWs were present in the lanes with hSR-TRX+hGAPDH. It was confirmed that there were no electrophoretic mobility differences in the presence of ATP and G3P (Figure 50). Since the amount of protein loaded into the well was very high (around 5 µg), we saw the presence of contaminants. However, the purity estimated after purification was around 98% for hGAPDH and 94% for hSR-TRX.

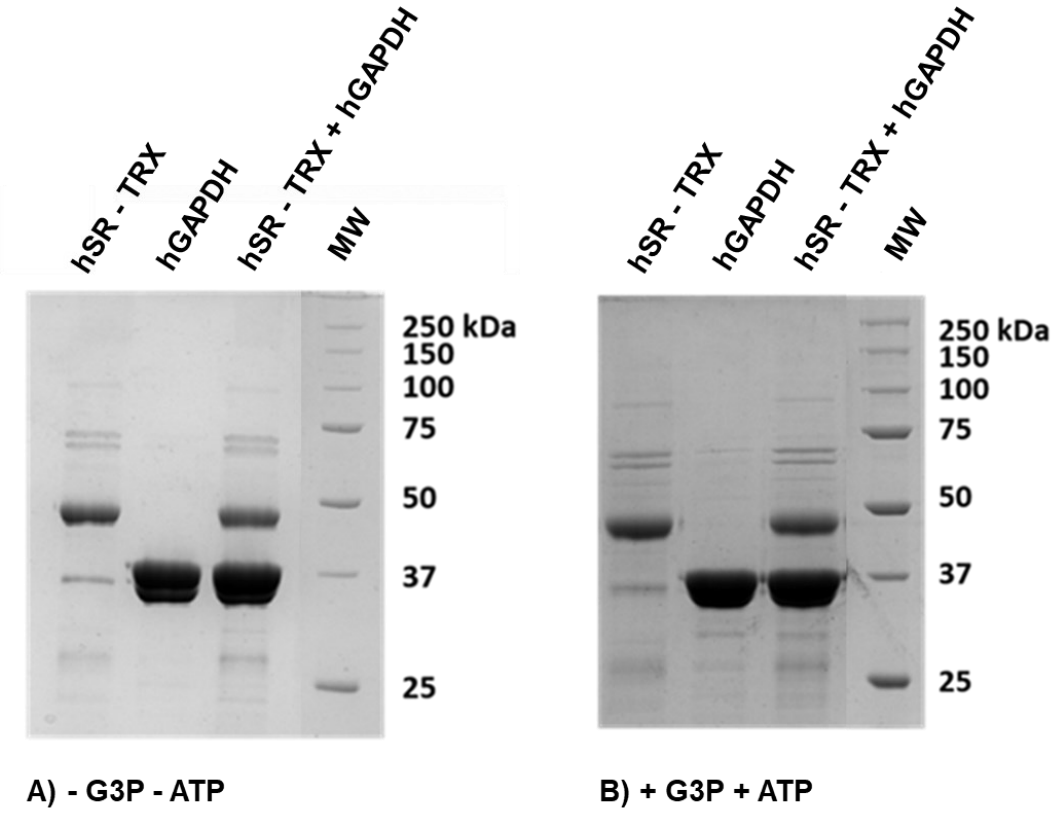

Figure 50. SDS-PAGE of 15 μM hSR and 30 μM hGAPDH in the absence **(A)** and presence **(B)** of 2 mM ATP and 5 mM D-G3P.

After testing the protein without a cross-linker, we reproduced the same experiments in parallel with or without ATP and G3P in the presence of 0.1% glutaraldehyde. We prepared the sample with 10 minutes of incubation: hSR-TRX+glutaraldehyde, hGAPDH+glutaraldehyde and the mix of hSR-TRX+hGAPDH+glutaraldehyde. The lane patterns were the same compared to the conditions' presence and absence of ATP and G3P. In detail, we observed that hSR-TRX with glutaraldehyde formed aggregates at high MWs, higher than the theoretical dimer of 100 kDa, showing that the cross-linking reaction took place. Instead, hGAPDH maintained a faint band at the MW of monomer 38 kDa. In addition, a band appeared

at 75 kDa, probably a dimeric form of hGAPDH, and we observed aggregates at high MW in the well. However, in the conditions with two mixed proteins, we did not see a band corresponding to the sum of hSR-TRX and hGAPDH monomers of 90 kDa. The band related to the MW of the complex was not present either in the condition with ATP+G3P or without (Figure 51). So, we ruled out that hSR formed a complex with hGAPDH. As confirmation of the technique's validity, cross-linking was recently used on human serine racemases to demonstrate the interaction with the PDZ domain (Giaccari et al., 2022).

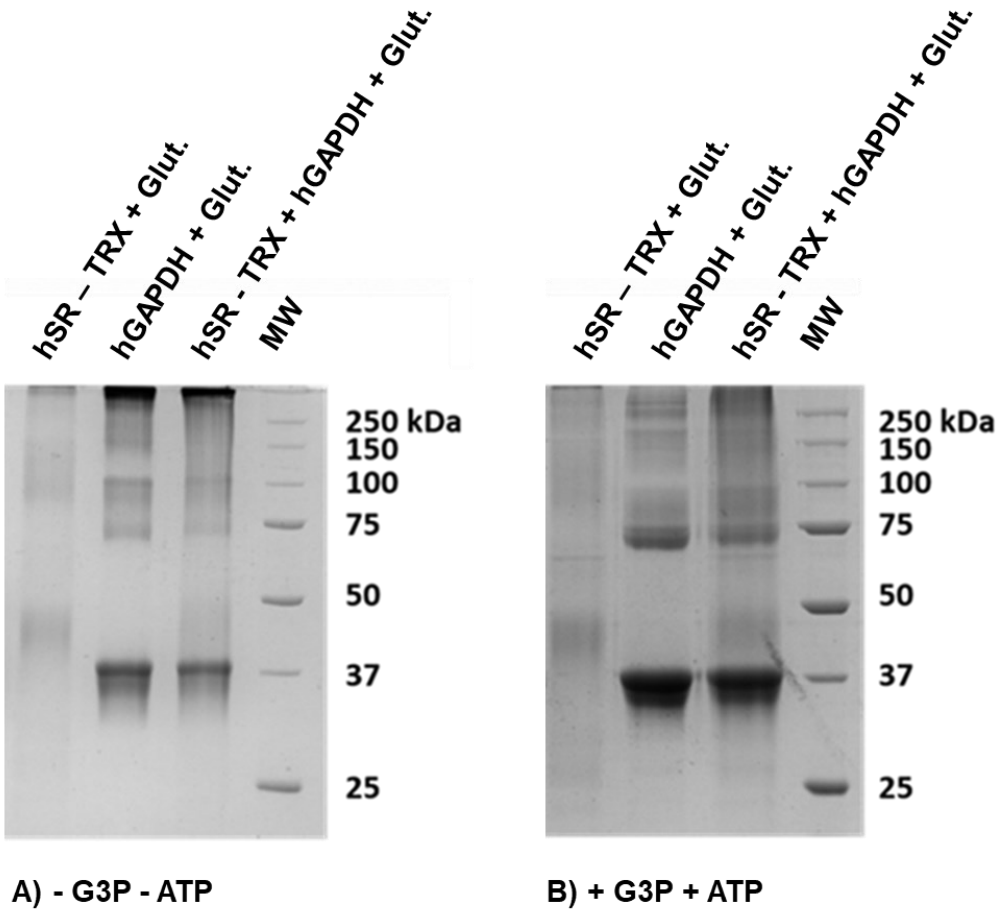

Figure 51. SDS-PAGE with the crosslinker 0.1% glutaraldehyde of 15 μM hSR and 30 μM hGAPDH in the absence **(A)** and presence **(B)** of 2 mM ATP and 5 mM D-G3P.

3.4 Conclusions

Human serine racemase has a wide, still unclear interactome. Exploring its interaction with other proteins is important to better understand the regulation of D-serine production in the human brain and, consequently, to clarify the pathogenic mechanism in D-serine diseases such as Parkinson's and Alzheimer's diseases. In the case of our research, studying the interaction between hGAPDH was also crucial to better explain the contribution to the glycolytic flux at the human serine biosynthesis. Suzuki et al., 2015 reported that the murine SR interact directly with murine GAPDH. In addition, through pull-down and immunohistochemistry experiments, the authors explained that ATP increased the interaction in a dose-dependent manner. The substrate of GAPDH, G3P, also contributed to the stabilization of mSR-mGAPDH interaction. However, we explained that human orthologues undergo a different regulation than murine. Indeed, the techniques of gel filtration chromatography and cross-linking on the human purified enzymes performed in the presence of the same ATP concentration used by Suzuki demonstrated that hSR did not interact with hGAPDH either in the presence of G3P or in its absence.

Chapter 4. Inhibition of human serine racemase by glyceraldehyde-3-phosphate

4.1 Introduction

Human serine racemase is a PLP-dependent enzyme. It catalyzes D-serine formation from L-serine and eliminates both enantiomers to pyruvate and ammonia (Graham et al., 2019)

Small ligands, halides and proteins finely tune the enzyme; the extensive hSR regulation is crucial for maintaining tight control of D-serine homeostasis in the human brain (Campanini et al., 2013; Raboni et al., 2019). Indeed, an alteration of D-serine levels in the central nervous system has been linked to neuropathologies such as Alzheimer's disease, Parkinson's disease, and schizophrenia (Coyle et al., 2018).

Suzuki et al., 2015 reported a regulation mechanism in which the interaction of murine glyceraldehyde-3-phosphate dehydrogenase in the presence of its substrate glyceraldehyde-3-phosphate (G3P) inhibited murine serine racemase. However, in Chapter 3, we demonstrated that the two human orthologues did not form a protein-protein complex either in the presence of G3P or in the absence.

Given the importance of serine metabolism in the human brain, we deemed it necessary to explore better the possibility of hSR inhibition by the G3P. Therefore, in this research work, we explored in detail many possible inhibition mechanisms of G3P exploiting the spectroscopic properties of serine cofactor racemase, PLP. We also performed the activity assays to evaluate the inhibition on time and for both G3P enantiomers.

Part of this work was published in:

Michielon A. et al., "Human serine racemase is inhibited by glyceraldehyde 3-phosphate, but not by glyceraldehyde 3-phosphate dehydrogenase." Biochimica et Biophysica Acta (BBA)-Proteins and Proteomics 1869.1 (2021): 140544.

Candidate's contribution:

I expressed and purified human serine racemase. I designed and performed all activity assays and spectra absorbance experiments.

4.2 Materials and Methods

4.2.1 Materials

Tris (2-carboxyethyl) phosphine (TCEP), which was purchased from Apollo Scientific (Denton, Manchester, UK). All other chemicals and reagents were purchased from Sigma - Aldrich (St. Louis, MO, USA) and were of the highest grade commercially available unless otherwise stated. Materials were used as received.

4.2.2 Protein expression and purification

Recombinant hSR was expressed as a hexa-His tagged fusion protein encoded in a pET28a-derived plasmid (Dixon et al., 2006) and transformed in *Escherichia Coli* BL21 CodonPlus (DE3)-RIL cells (Merck-Millipore, Darmstadt, Germany), previously transformed with plasmids encoding GroEL and GroES chaperonins. The procedure was described in detail by Marchetti et al., 2013 and Canosa et al., 2018.

4.2.3 Preparation of experimental buffer

The pH of commercial L-G3P and D- G3P (Sigma – Aldrich, St. Louis, MO, USA) were measured by a pH paper testing and verified the pH at 37 °C in the 1 mL volume in the absence and presence of 5 mM D-G3P at different concentrations of hSR storage buffer (TEA solution) with a pH meter:

A) 50 mM TEA, pH 8.00

B) 150 mM TEA, pH 8.00

C) 200 mM TEA, pH 8.00

To obtain the complete experimental solution were added to 150 mM NaCl, 2 mM ATP, 2 mM $MgCl_2$, 50 µM PLP and 5 mM DTT. To avoid a pH change in the experimental solution, the compounds ATP and PLP were corrected during solubilization to obtain a pH of around 6.50-7.00. The ATP was prepared in a 250 mM stock in H_20 and adjusted pH with 2 M HCl to attain a pH of around 6.5. The PLP was solubilized in H_20 at a concentration of 25 mM stock and adjusted pH with 2 M NaOH to obtain a solution at pH 7. The final buffer solution was 200 mM TEA, 150 mM NaCl, 2 mM ATP, 2 mM $MgCl_2$, 50 µM PLP and 5 mM DTT, pH 8.00 at 37 °C.

4.2.4 Absorption spectra

Protein UV-visible absorption spectra were acquired using a CARY4000 UV-Vis spectrophotometer (Agilent Technologies, Santa Clara, CA, USA) with a temperature-controlled cell-holder Hellma™. Far UV Quartz Cuvettes with 1 cm pathlength were used for all experiments. All spectra were recorded in the 600-240 nm range and corrected for buffer contribution. All experiments were performed, unless otherwise indicated, in a solution containing 200 mM TEA, 150 mM NaCl, 2 mM ATP, 2 mM $MgCl_2$ and 5 mM DTT, at pH 8.0. The compound D-G3P, when present, was added at the 5 mM final concentration and incubated on the reaction mixture for 30 minutes unless otherwise indicated. The compound PLP was added at 50 µM and incubated for 10 minutes. A control condition was prepared for all absorption experiments in the presence of D-G3P and PLP.

4.2.5 Preparation of hSR apo form

To obtain the apo form of hSR, the protein was incubated with 10 mM of L-serine (a value close to the K_m) for 1 hour at ambient temperature. Then 500 µL of hSR 50 µM was dialyzed using membrane dialysis with 16 kDa cut-off against 50 mL of a buffer containing 200 mM TEA, pH 8.0, for 3 hours at 4 °C. The dialysis buffer was changed every hour.

4.2.6 Enzymatic assay

The Cary 4000 UV-Vis spectrophotometer (Agilent Technologies, Santa Clara, CA, USA) coupled with a temperature-controlled cell-holder Hellma™ was used to follow the initial velocity of L-serine elimination catalyzed by hSR. It was a coupled assay with lactate dehydrogenase (LDH) that measures the pyruvate that spontaneously forms from α-aminoacrylate (Foltyn et al., 2005; Marchetti et al., 2013). The pyruvate produced by SR reacts with a molecule of NADH, producing NAD^+ and lactate. The NADH has a characteristic absorption peak at 340 nm, whereas its oxidized shape does not absorb at this wavelength. So, it was possible to monitor the kinetic following the NADH disappearance at 340 nm (Eisenthal and Danson 1993). The final volume of assay solution was 150 µL in a quartz cuvette with 1 cm of path length. When the experiment started, a trace of 1-2 minutes was acquired in the presence of protein and NADH. The eventual slope of this trace reflected the contribution of NADH oxidation. After three minutes, the L-serine was added and started the reaction. The signal was collected for a total of 15 minutes. The slope was read before the 4 minutes. The value was calculated on a 1-minute track. The slope

(ΔOD / min) was divided for the NADH molar coefficient (6200 M^{-1} cm^{-1}). All data were acquired in triplicate.

- **Evaluation of G3P inhibition**

The activity of 0.44 μM hSR was incubated for 5 minutes at 37 °C in the presence of 10 mM D-G3P in a solution containing 200 mM TEA, 150 mM NaCl, 2 mM ATP, 2 mM $MgCl_2$, 50 μM PLP and 5 mM DTT at pH 8.0. A control condition was prepared with the same incubation time. The 320 μM NADH, 66 U/mL LDH, and 500 mM L-serine were added to start the reaction.

- **Time dependent L-G3P and D-G3P inhibition**

To evaluate the time-dependent G3P inhibition, we tested the activity of hSR in the presence of 5 mM D-G3P or 5 mM L-G3P. We prepared a solution containing 200 mM TEA, 150 mM NaCl, 2 mM ATP, 2 mM $MgCl_2$, 50 μM PLP and 5 mM DTT at pH 8.0. Then we added 0.88 μM hSR and divided the solution into two samples. In one sample, we added 5 mM D-G3P or L-G3P; in the other, we added the same volume of H_20. Both samples were incubated in a thermostatic bath at 37 °C for up to 120 min. For each time point: 0, 10, 30, 60, 90, and 120 minutes we added 320 μM NADH, 66 U/mL LDH, and 10 mM L-serine to trigger the reaction.

- **Michaelis-Menten parameters for L-serine in the presence of D-G3P**

To estimate the Michaelis-Menten parameters for L-serine, we incubated 0.44 μM hSR in the presence of 5 mM D-G3P for 60 minutes at 37 °C. Then 320 μM NADH, 66 U/mL LDH, and L-serine were added to trigger the reaction. The L-serine concentrations

were: 0, 5, 10, 50, 200, and 500 µM. The same experimental setup was used to obtain the k_M parameters of hSR without G3P. The experimental data were fitted with the equation:

$$V_0 = (V_{max} [S]) / (K_m + [S])$$

V_0 is the initial rate, $[S]$ is the concentrations of the substrate (L-serine) in the assay, V_{max} is the maximal velocities in µM/s divided by the enzyme concentrations (in µM), and K_m is the Michaelis-Menten constant.

- **Enzymatic assay in the presence of D-G3P, malonate, glycine and ATP**

For testing the effect of hSR ligands on G3P-induced inhibition, 0.88 µM hSR was incubated for 60 min at 37 °C in a buffer containing 200 mM TEA, 150 mM NaCl, 2 mM ATP, 2 mM $MgCl_2$, 50 µM PLP, 5 mM DTT and 5 mM D-G3P in the presence of either 1 mM malonate, 5 mM glycine, and 2 mM ATP and 10 mM ATP.

- **Enzymatic assay in the presence of D-G3P and different PLP concentration**

To explore if the PLP incrementing hSR activity, the protein at 0.88 µM concentration was incubated for 60 minutes with D-G3P at 5 mM concentration in the absence and presence of 250 µM PLP in a solution containing 200 mM TEA, 150 mM NaCl, 5 mM DTT, 2 mM ATP and 2 mM $MgCl_2$. The control condition was prepared to incubate the protein without G3P.

4.3 Results and discussion

4.3.1 Evaluation of D-G3P inhibition

Although hSR did not form a complex with hGAPDH (as explained in chapter 3), we proposed the hypothesis that the hSR might be inhibited by the hGAPDH substrate, G3P. To teste the G3P inhibition, a concentration of 10 mM D-G3P, the natural substrate of GAPDH, was incubated with hSR for 5 minutes in a solution containing 200 mM TEA, 150 mM NaCl, 2 mM ATP, 2 mM $MgCl_2$, 50 µM PLP, 5 mM DTT. A control condition was incubated in the absence of D-G3P. We observed that in the presence of D-G3P, the hSR activity was reduced to less than a third compared to the control (Figure 52).

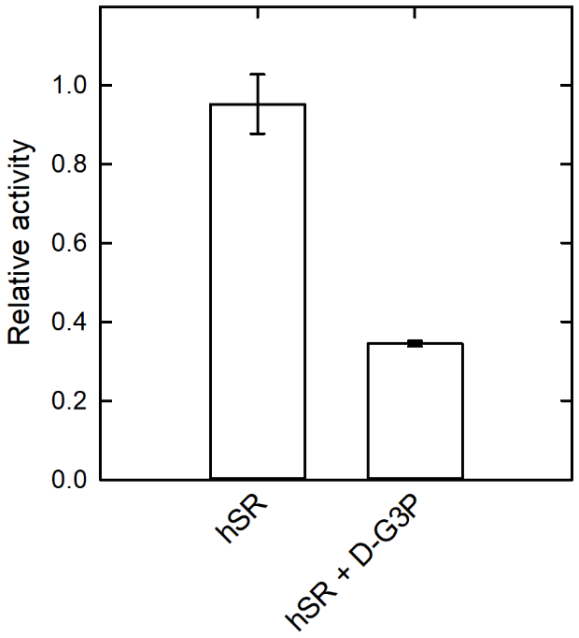

Figure 52. Relative activity of 0.44 µM hSR in the presence of 10 mM D-G3P in a solution of 200 mM TEA, 150 mM NaCl, 2 mM ATP, 2 mM $MgCl_2$, 50 µM PLP, 5 mM DTT, pH 8.00 at 37 °C.

We also tested the dependence of hSR inhibition in the presence of D-G3P at the range between 1-10 mM after 5 minutes of incubations (data not shown), and we chose the intermediate concentration of 5 mM D-G3P for the next experiments. In addition, to exclude the possibility of experimental activity inhibition due to pH and not the G3P, we controlled the final pH of the hSR in the presence of 5 mM G3P in the solution assay (200 mM TEA, 150 mM NaCl, 2 mM ATP, 2 mM $MgCl_2$, 50 µM PLP, 5 mM DTT, pH 8.00), confirming that the solution pH remained unchanged.

4.3.2 L-G3P and D-G3P time-dependent inhibition

After observing hSR inhibition in the presence of D-G3P, we wondered if inhibition depended on a specific interaction between the enantiomer D and serine racemase. Therefore, to better understand the hSR inhibition by the G3P, we also tested the enantiomer L-G3P. For both enantiomers, we investigated the behaviour over time to evaluate if the enantiomers had the same inhibition rate on hSR activity. We tested both compounds at a concentration of 5 mM in a solution of 200 mM TEA, 150 mM NaCl, 2 mM ATP, 2 mM $MgCl_2$, 50 µM PLP and 5 mM DTT, pH 8.00. The reaction was followed for 120 minutes. In these conditions, both compounds showed time-dependent inhibition of hSR. After 10 minutes, the inhibitions were around 35% and after 60 minutes reached 50% of the total (Figure 53). There was no significant inhibition difference between the two enantiomers over time. In the next experiments, we used the natural enantiomer D-G3P.

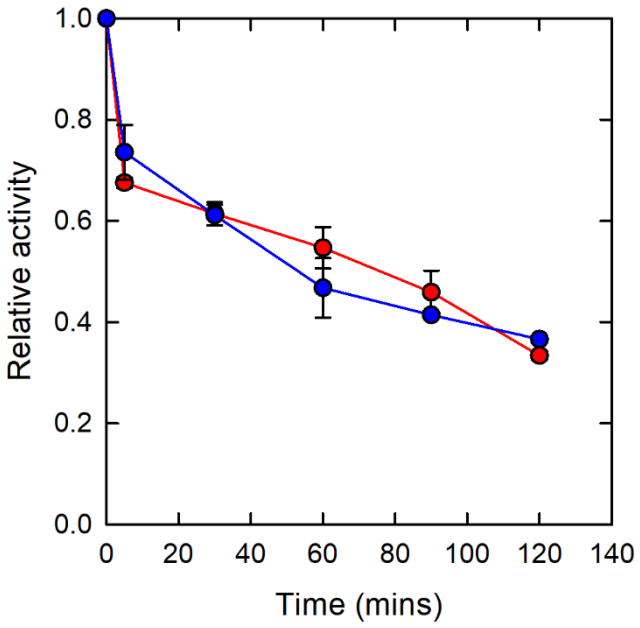

Figure 53. Comparison between the relative activity of 0.88 μM hSR in the presence of D-G3P (red circles) and 5 mM L-G3P (blue circles) in the solution of 200 mM TEA 150 mM NaCl, 2 mM ATP, 2 mM $MgCl_2$, 50 μM PLP, 5 mM DTT, 320 μM NADH, 66 U/mL LDH, and 10 mM L-serine at pH 8.00, 37 °C.

For the purpose of better understanding the inhibition mechanism, we estimated the Michaelis-Menten parameters for the L-serine β-elimination reaction after a 60-minute incubation with 5 mM D-G3P when the inhibition arrived at a *plateau*. Relative to the enzyme without D-G3P, K_m increased about twice, from 15.0 ± 1.7 to 28.6 ± 6.2 mM. Moreover, V_{max} diminished by around 30%, representing a likely indication of a mixed inhibition mechanism (Figure 54). It is known that hSR has considerable conformational plasticity (Raboni et al., 2019), and these data suggest that G3P may be able to stabilize an enzymatic conformation with reduced activity.

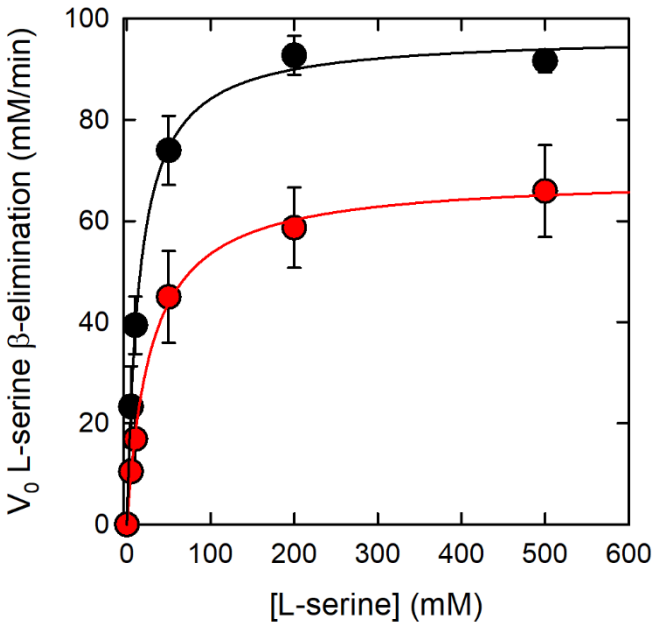

Figure 54. Dependence of the β-elimination activity of 0.44 μM hSR on L-serine concentration upon incubation for 60 minutes at 37 °C in the absence (black circles) and presence of 5 mM D-G3P (red circles). The solution contains 200 mM TEA 150 mM NaCl, 2 mM ATP, 2 mM $MgCl_2$, 50 μM PLP, 5 mM DTT, 320 μM NADH, 66 U/mL LDH at pH 8.00, 37 °C. The solid lines fit the experimental points to the Michaelis-Menten equation.

.

4.3.3 G3P and PLP competition

To explore the inhibition mechanism, we compared the G3P and PLP structures. The PLP is the cofactor of hSR. In the absence of substrate L-serine, the aldehyde group of PLP is covalently bound to the amino group of Lys56 present in the active site of the enzyme, constituting one internal aldimine (De Miranda et al., 2000, Foltyn et al. 2005). Since G3P and PLP showed a nearly perfect overlapping of carbonyl and phosphate groups (Figure 55), we hypothesized that they could compete to form the internal aldimine. Lumeng et al., 1978, reported an analogous inhibitory mechanism

for other PLP-dependent enzymes in which the presence of acetaldehyde promotes the release of the PLP from the active site.

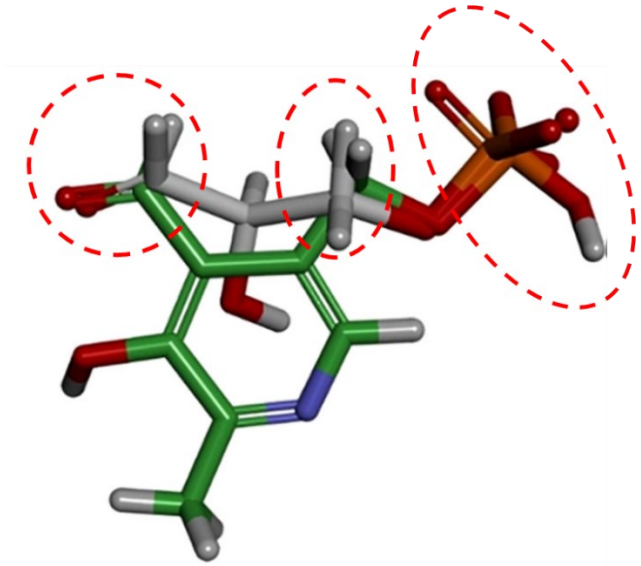

Figure 55. Overlay of pyridoxal phosphate and D-G3P. The similarity points were circled in red.

To observe the possible competition of G3P and PLP, we collected the spectra of hSR in the region of PLP absorption (300-500 nm). The intermediates of PLP (internal and external aldimine) show different spectroscopic properties depending on their surroundings. Indeed, when the PLP is bound to the Lys56, it has a maximum absorption at 412 nm, while the free PLP (external aldimine) absorbs at 390 nm. Thanks to the different wavelength absorption, it was possible to understand if PLP formed the internal aldimine in solution in the presence of G3P. We acquired the spectra of hSR before and after incubation of 5 mM D-G3P for 30 minutes (Figure 56). However, no significant spectral alteration was observed in the area around 412 nm. In addition, in the region at 390 nm, no band formed over time. This result shows that

the enzyme does not release PLP following incubation with D-G3P, excluding this inhibition mechanism.

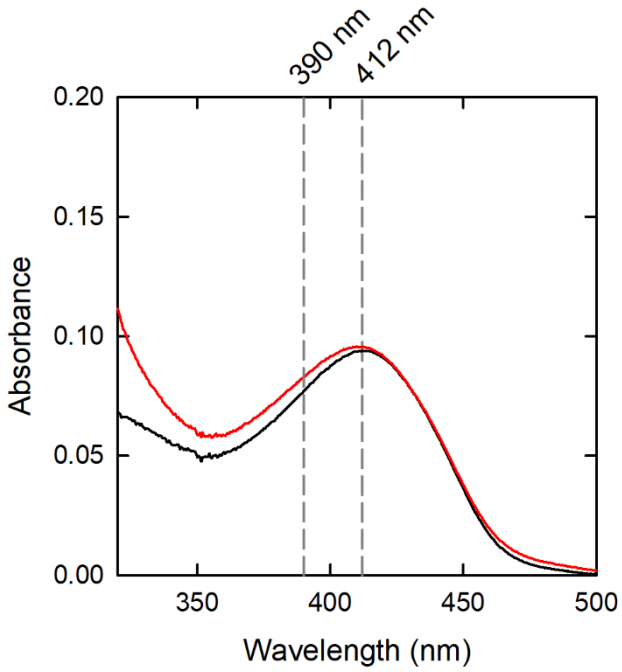

Figure 56. Absorption spectra of 17 µM hSR in a solution containing 200 mM TEA, 150 mM NaCl, 5 mM DTT, 2 mM ATP and 2 mM $MgCl_2$ before (black line) and after (red line) incubation with 5 mM D-G3P for 30 min.

To rule out definitely the PLP and G3P competition for internal aldimine, it was necessary to test G3P in the presence of high levels of PLP conditions. However, in the absorption experiment described above, it was not possible to test higher concentrations of PLP due to the PLP contribution absorption. Therefore, we evaluated the possible competition for the internal aldimine formation, between G3P and PLP, by activity assay, in which the PLP absorption was not a limit. So, we tested the hSR activity in the absence and the presence of 250 µM PLP (Figure 57). Both conditions were incubated with 5 mM D-G3P for 30 minutes. A control condition without D-G3P was prepared and incubated. According to what we have seen in absorption, no recovery of enzymatic activity is observed in the presence of high concentrations of

PLP. The rate of G3P inhibition was the same for both conditions with and without PLP, indicating that G3P inhibition was not dependent on the presence of PLP in the solution incubation.

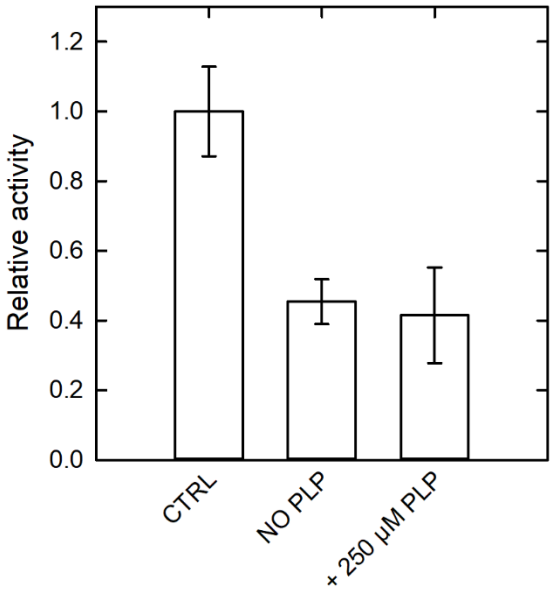

Figure 57. Relative activity of 0.88 µM hSR after incubation for 60 minutes with 5 mM D-G3P in the absence (NO PLP) and presence of 250 µM PLP in a solution containing 200 mM TEA, 150 mM NaCl, 5 mM DTT, 2 mM ATP and 2 mM $MgCl_2$. The CTRL bar is the activity of hSR in the absence of G3P.

4.3.4 Evaluation of G3P inhibition

Serine racemase is a PLP-dependent enzyme, it was purified in the presence of PLP, and the final protein is in the catalytic intermedia form, with Lys56 bound PLP. Therefore, to assess the G3P inhibition mechanism in detail, we prepared an hSR enzyme without bound PLP to avoid bias. To bring out the PLP, we incubated hSR at 37 °C with its substrate L-serine in 200 mM TEA, 150 mM NaCl, 5 mM DTT, 2 mM ATP and 2 mM $MgCl_2$ at pH 8, and we followed the reaction over time. In the presence of substrate took place the L-serine β-elimination reaction and hSR produced pyruvate

ad ammonia (De Miranda et al. 2002). In the absorption spectra (Figure 58), we observed a progressive release of PLP by decreasing the band ad 412 nm. After 30 minutes, the internal aldimine absorption was at a minimum. Also, an increase at the peak at 320 nm was present due to the pyruvate formation in the solution.

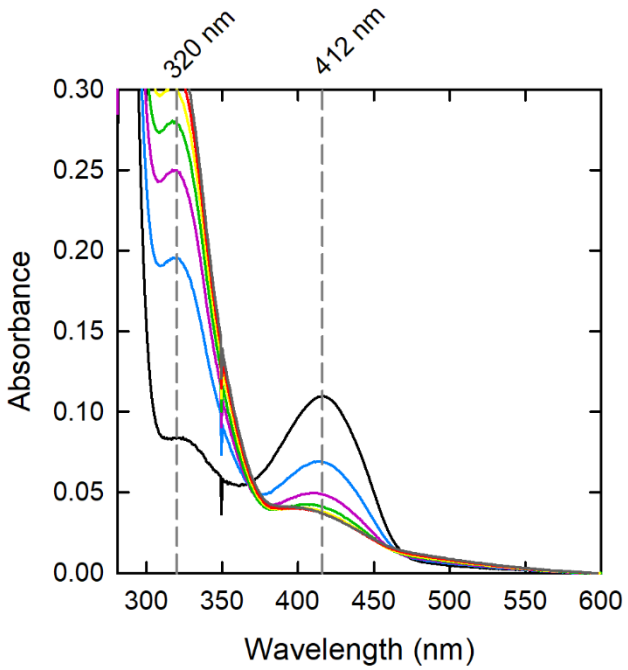

Figure 58. Absorption spectra of 17 µM hSR (black line), in 200 mM TEA, 150 mM NaCl, 5 mM DTT, 2 mM ATP and 2 mM $MgCl_2$, at 37 °C. Spectra upon the addition of 10 mM L-serine: after 5 minutes (in blue), 10 minutes (magenta), 15 minutes (green), 20 minutes (yellow), 25 minutes (red) and 30 minutes (grey).

Subsequently, at the complete release of PLP, we divided the solution into two parts. One part was incubated with 5 mM D-G3P for 30 minutes, and the other no. Then, after 10 minutes, at both conditions was added 50 µM PLP. The absorption spectra were acquired. For both conditions in the presence (Figure 59-A) and the absence (Figure 59-B) of G3P, the band at 412 nm was recovered. This indicated that

the PLP added to the solution, despite G3P presence previously incubated, formed the internal aldimine. Suggesting that G3P did not tightly bind the Lys56 and did not compete with PLP.

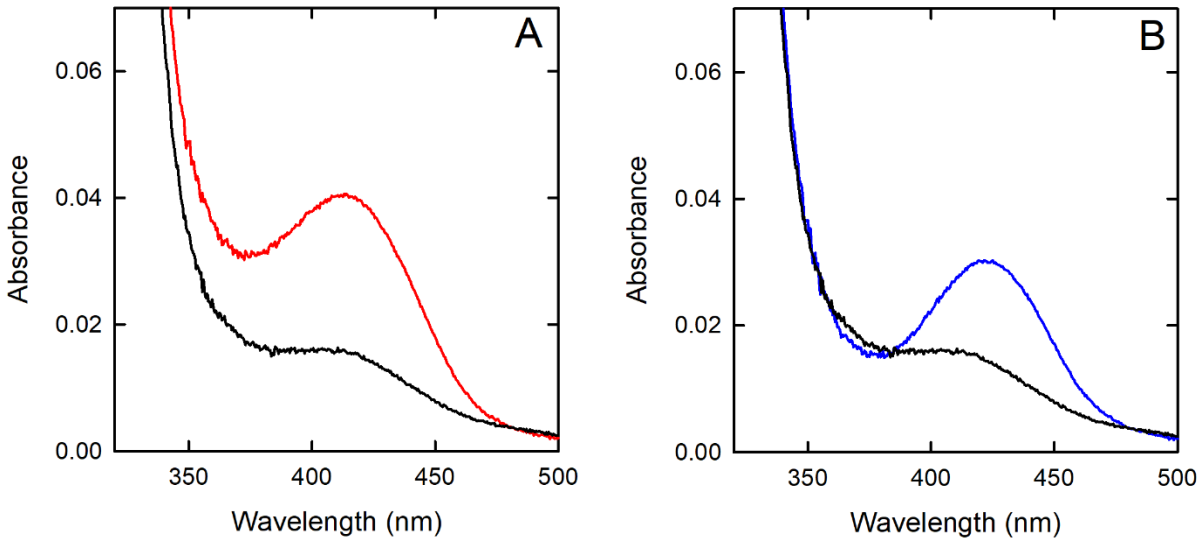

Figure 59. Absorption spectra of hSR previously stripped of PLP in the presence of L-serine (black line) and then incubated with 50 μM PLP in the presence **(A)** and absence **(B)** of 5 mM D-G3P.

4.3.5 G3P inhibition in the presence of malonate and glycine

Malonate and glycine are the active-site ligands of hSR. In the crystal structure, it was reported that malonate induced a conformational change in which the small domain shifts of 20 ° on the large domain. This rotation leads to the closing of the active site (Yamauchi et al., 2009; Smith et al., 2010). To understand if the G3P inhibition mechanism can be related to the active site accessibility, we evaluated the hSR activity in the presence of the active-site ligands. We incubated hSR for 60 minutes with glycine or malonate in the presence and absence of 5 mM D-G3P (Figure 60). We observed that when glycine or malonate was present in the incubation mix, the

inhibition rate of G3P was decreased. Indeed, the relative activity for glycine was 0.6 and for malonate was 0.7, both higher than the hSR control (mean around 0.4). According to this result, it is plausible that G3P partially compete with the orthostatic ligands to bind the active site. Moreover, it could be possible that G3P bind an allosteric site connected to the conformational change produced by the active-site ligands.

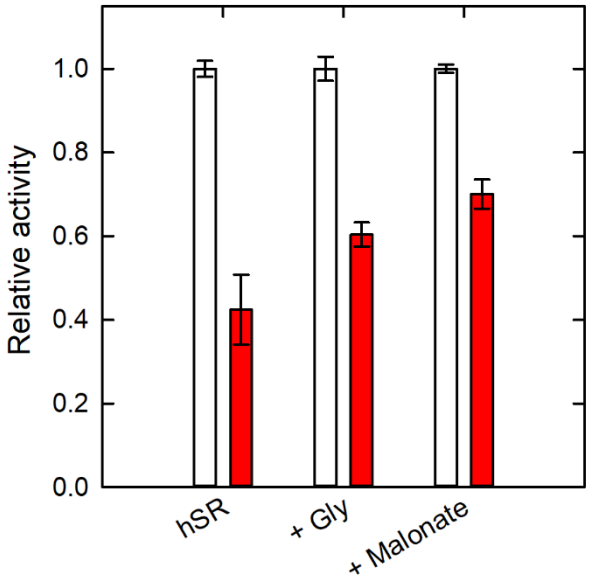

Figure 60. Relative activity of 0.88 µM hSR with 1 mM malonate and 5 mM glycine. The white bars are the conditions without G3P. In the red bars, the presence of 5 mM D-G3P.

4.3.6 G3P inhibition in the presence of ATP

The nucleotide ATP is an allosteric effector of hSR. It binds at the interface of the protein domains, where several positively charged residues link its phosphate moieties (Goto et al., 2009). Since G3P and ATP have in common a phosphate group, we explored the possibility of G3P binding at the ATP site. We tested the G3P inhibition in the presence of 2 mM ATP and 10 mM ATP after 60 minutes of incubation (Figure 61). A control condition without ATP in the incubation mixer was also prepared. We

observed an increase in relative activity in both conditions where ATP was present compared to the control without ATP. In particular, in the presence of a 10 mM concentration of ATP, the hSR activity was highest. This suggests that the presence of ATP hindered the G3P inhibition, and we proposed that G3P compete with ATP for the binding. It was known that in the presence of ATP, hSR assumed a conformation like the open state, but the active site is more closed (Marchetti et al., 2013). Moreover, Goto et al., 2009 showed in a crystal structure that, when ATP binds at the interface of the two protein domains, they change the orientation increasing the width of the groove formed by the two monomers. According to this evidence, we also proposed that ATP promoted an enzymatic conformation most unfavourable to G3P binding.

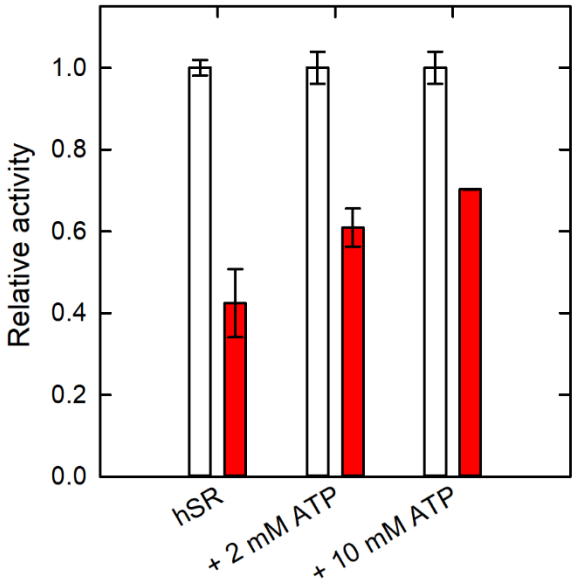

Figure 61. Relative activity of 0.88 µM hSR with 2 mM and 10 mM ATP. The white bars are the conditions without G3P. In the red bars, the presence of 5 mM D-G3P.

4.4 Conclusions

To investigate the connection between biochemical glycolytic flux and D-serine metabolism, we have investigated the relationship between human SR and GAPDH. We observed a direct partial inhibition, at non-physiological concentrations, by the GAPDH substrate G3P for both enantiomers. Thanks to the absorption experiment on *olo* and *apo* hSR form, we excluded that G3P competed with PLP to form the internal aldimine. However, we were not able to establish the inhibition mechanism unequivocally. We proposed the possibility that G3P competed for ATP binding site or that it was susceptible to protein conformational change induced by active-site ligands such as malonate and glycine. In any case, we helped better explain the complex and delicate regulation of hSR in D-serine homeostasis and, thus, human glutamatergic communication.

References

Abdelfattah, F., Kariminejad, A., Kahlert, A. K., Morrison, P. J., Gumus, E., Mathews, K. D., ... & Schanze, D. (2020). Expanding the genotypic and phenotypic spectrum of severe serine biosynthesis disorders. Human mutation, 41(9), 1615-1628.

Acuna-Hidalgo, R., Schanze, D., Kariminejad, A., Nordgren, A., Kariminejad, M. H., Conner, P., ... & Zenker, M. (2014). Neu-Laxova syndrome is a heterogeneous metabolic disorder caused by defects in enzymes of the L-serine biosynthesis pathway. The American Journal of Human Genetics, 95(3), 285-293.

Adzhubei, I. A., Schmidt, S., Peshkin, L., Ramensky, V. E., Gerasimova, A., Bork, P., ... & Sunyaev, S. R. (2010). A method and server for predicting damaging missense mutations. Nature methods, 7(4), 248-249.

Amelio, I., Cutruzzolá, F., Antonov, A., Agostini, M., & Melino, G. (2014). Serine and glycine metabolism in cancer. Trends in biochemical sciences, 39(4), 191-198.

Baek, J. Y., JUN, D. Y., Taub, D., & Kim, Y. H. (2003). Characterization of human phosphoserine aminotransferase involved in the phosphorylated pathway of L-serine biosynthesis. Biochemical Journal, 373(1), 191-200.

Balu, D. T., Li, Y., Puhl, M. D., Benneyworth, M. A., Basu, A. C., Takagi, S., ... & Coyle, J. T. (2013). Multiple risk pathways for schizophrenia converge in serine racemase knockout mice, a mouse model of NMDA receptor hypofunction. Proceedings of the National Academy of Sciences, 110(26), E2400-E2409.

Basurko, M. J., Marche, M., Darriet, M., & Cassaigne, A. (1999). Phosphoserine aminotransferase, the second step-catalyzing enzyme for serine biosynthesis. IUBMB life, 48(5), 525-529.

Battula, P., Dubnovitsky, A. P., & Papageorgiou, A. C. (2013). Structural basis of L-phosphoserine binding to Bacillus alcalophilus phosphoserine aminotransferase. Acta Crystallographica Section D: Biological Crystallography, 69(5), 804-811.

Baumgart, F., Mancheno, J. M., & Rodríguez-Crespo, I. (2007). Insights into the activation of brain serine racemase by the multi-PDZ domain glutamate receptor interacting protein, divalent cations and ATP. The FEBS Journal, 274(17), 4561-4571.

Baumgartner, M., Radziwill, G., Lorger, M., Weiss, A., & Moelling, K. (2008). c-Src-mediated epithelial cell migration and invasion regulated by PDZ binding site. Molecular and cellular biology, 28(2), 642-655.

Benke, P. J., Hidalgo, R. J., Braffman, B. H., Jans, J., Gassen, K. L. V., Sunbul, R., & El-Hattab, A. W. (2017). Infantile serine biosynthesis defect due to phosphoglycerate dehydrogenase deficiency: Variability in phenotype and treatment response, novel mutations, and diagnostic challenges. Journal of child neurology, 32(6), 543-549.

Bennett, M. (2009). Positive and negative symptoms in schizophrenia: the NMDA receptor hypofunction hypothesis, neuregulin/ErbB4 and synapse regression. Australian & New Zealand Journal of Psychiatry, 43(8), 711-721.

Bourque, D. K., Cloutier, M., Kernohan, K. D., Bareke, E., Grynspan, D., Michaud, J., ... & Boycott, K. M. (2019). Neu–Laxova syndrome presenting prenatally with increased nuchal translucency and cystic hygroma: The utility of exome sequencing in deciphering the diagnosis. American Journal of Medical Genetics Part A, 179(5), 813-816.

Brassier, A., Valayannopoulos, V., Bahi-Buisson, N., Wiame, E., Hubert, L., Boddaert, N., ... & De Lonlay, P. (2016). Two new cases of serine deficiency disorders treated with l-serine. european journal of paediatric neurology, 20(1), 53-60.

Bruno, S., Margiotta, M., Marchesani, F., Paredi, G., Orlandi, V., Faggiano, S., ... & Mozzarelli, A. (2017). Magnesium and calcium ions differentially affect human serine racemase activity and modulate its quaternary equilibrium toward a tetrameric form. Biochimica et Biophysica Acta (BBA)-Proteins and Proteomics, 1865(4), 381-387.

Bruno, S., Margiotta, M., Pinto, A., Cullia, G., Conti, P., De Micheli, C., & Mozzarelli, A. (2016). Selectivity of 3-bromo-isoxazoline inhibitors between human and Plasmodium falciparum glyceraldehyde-3-phosphate dehydrogenases. Bioorganic & Medicinal Chemistry, 24(12), 2654-2659.

Bruno, S., Pinto, A., Paredi, G., Tamborini, L., De Micheli, C., La Pietra, V., ... & Mozzarelli, A. (2014). Discovery of covalent inhibitors of glyceraldehyde-3-phosphate dehydrogenase, a target for the treatment of malaria. Journal of Medicinal Chemistry, 57(17), 7465-7471.

Campanini, B., Spyrakis, F., Peracchi, A., & Mozzarelli, A. (2013). Serine racemase: a key player in neuron activity and in neuropathologies. Frontiers in Bioscience-Landmark, 18(3), 1112-1128.

Canosa, A. V., Faggiano, S., Marchetti, M., Armao, S., Bettati, S., Bruno, S., ... & Mozzarelli, A. (2018). Glutamine 89 is a key residue in the allosteric modulation of human serine racemase activity by ATP. Scientific reports, 8(1), 1-13.

Canu, N., Ciotti, M. T., & Pollegioni, L. (2014). Serine racemase: a key player in apoptosis and necrosis. Frontiers in synaptic neuroscience, 6, 9.

Cappello, A., Mancini, M., Madonna, S., Rinaldo, S., Paone, A., Scarponi, C., ... & Candi, E. (2022). Extracellular serine empowers epidermal proliferation and psoriasis-like symptoms. Science Advances, 8(50), eabm7902.

Cavole, T. R., Perrone, E., Lucena de Castro, F. S., Alvarez Perez, A. B., Waitzberg, A. F. L., & Cernach, M. C. (2020). Clinical, molecular, and pathological findings in a

Neu–Laxova syndrome stillborn: A Brazilian case report. American Journal of Medical Genetics Part A, 182(6), 1473-1476.

Chen, S., Xu, D., Fan, L., Fang, Z., Wang, X., & Li, M. (2022). Roles of N-Methyl-D-Aspartate receptors (NMDARs) in epilepsy. Frontiers in Molecular Neuroscience, 14, 797253.

Chen, Z., Yuan, Z., Yang, S., Zhu, Y., Xue, M., Zhang, J., & Leng, L. (2023). Brain energy metabolism: astrocytes in neurodegenerative diseases. CNS Neuroscience & Therapeutics, 29(1), 24-36.

Clayton, P. T. (2006). B6-responsive disorders: a model of vitamin dependency. Journal of inherited metabolic disease, 29(2), 317-326.

Conti, P., Tamborini, L., Pinto, A., Blondel, A., Minoprio, P., Mozzarelli, A., & De Micheli, C. (2011). Drug discovery targeting amino acid racemases. Chemical reviews, 111(11), 6919-6946.

Cook, S. P., Galve-Roperh, I., del Pozo, A. M., & Rodríguez-Crespo, I. (2002). Direct calcium binding results in activation of brain serine racemase. Journal of Biological Chemistry, 277(31), 27782-27792.

Coto-Puckett, W. L., Gilbert-Barness, E., Steelman, C. K., Stuart, T., Robinson, H. B., & Shehata, B. M. (2010). A spectrum of phenotypical expression of Neu-Laxova syndrome: three case reports and a review of the literature. Fetal and Pediatric Pathology, 29(2), 108-119.

Coulibaly, F., Lassalle, E., Baker, H. M., & Baker, E. N. (2012). Structure of phosphoserine aminotransferase from Mycobacterium tuberculosis. Acta Crystallographica Section D: Biological Crystallography, 68(5), 553-563.

Coyle, J. T., & Balu, D. T. (2018). The role of serine racemase in the pathophysiology of brain disorders. Advances in pharmacology, 82, 35-56.

Dai, X., Zhou, E., Yang, W., Zhang, X., Zhang, W., & Rao, Y. (2019). D-Serine made by serine racemase in Drosophila intestine plays a physiological role in sleep. Nature communications, 10(1), 1-11.

De Koning, T. J. (2006). Treatment with amino acids in serine deficiency disorders. Journal of inherited metabolic disease, 29(2-3), 347-351.

De Marco, A., Vigh, L., Diamant, S., & Goloubinoff, P. (2005). Native folding of aggregation-prone recombinant proteins in Escherichia coli by osmolytes, plasmid-or benzyl alcohol–overexpressed molecular chaperones. Cell stress & chaperones, 10(4), 329-339.

De Miranda, J., Santoro, A., Engelender, S., & Wolosker, H. (2000). Human serine racemase: moleular cloning, genomic organization and functional analysis. Gene, 256(1-2), 183-188.

Debs, S., Ferreira, C. R., Groden, C., Kim, H. J., King, K. A., King, M. C., ... & Soldatos, A. (2021). Adult diagnosis of congenital serine biosynthesis defect: A treatable cause of progressive neuropathy. American Journal of Medical Genetics Part A, 185(7), 2102-2107.

Dietzen, D. J. (2018). Amino acids, peptides, and proteins. In Principles and Applications of Molecular Diagnostics (pp. 345-380). Elsevier.

Dixon, S. M., Li, P., Liu, R., Wolosker, H., Lam, K. S., Kurth, M. J., & Toney, M. D. (2006). Slow-binding human serine racemase inhibitors from high-throughput screening of combinatorial libraries. Journal of medicinal chemistry, 49(8), 2388-2397.

Donini, S., Ferrari, M., Fedeli, C., Faini, M., Lamberto, I., Marletta, A. S., ... & Peracchi, A. (2009). Recombinant production of eight human cytosolic aminotransferases and assessment of their potential involvement in glyoxylate metabolism. Biochemical Journal, 422(2), 265-272.

D'Souza, A., Nozohouri, S., Bleier, B. S., & Amiji, M. M. (2023). CNS delivery of nucleic acid therapeutics: beyond the blood–brain barrier and towards specific cellular targeting. Pharmaceutical Research, 40(1), 77-105.

Duan, X., Zhang, X., Shen, Z., Su, E., Zhao, L., & Pei, J. (2019). Efficient production of aggregation prone 4-α-glucanotransferase by combined use of molecular chaperones and chemical chaperones in Escherichia coli. Journal of biotechnology, 292, 68-75.

Dumin, E., Bendikov, I., Foltyn, V. N., Misumi, Y., Ikehara, Y., Kartvelishvily, E., & Wolosker, H. (2006). Modulation of D-serine levels via ubiquitin-dependent proteasomal degradation of serine racemase. Journal of Biological Chemistry, 281(29), 20291-20302.

Duncan, K., Lewendon, A., & Coggins, J. R. (1984). The purification of 5-enolpyruvylshikimate 3-phosphate synthase from an overproducing strain of Escherichia coli. FEBS letters, 165(1), 121-127.

El-Hattab, A. W. (2016). Serine biosynthesis and transport defects. Molecular genetics and metabolism, 118(3), 153-159.

Eliot, A. C., & Kirsch, J. F. (2004). Pyridoxal phosphate enzymes: mechanistic, structural, and evolutionary considerations. Annual review of biochemistry, 73, 383.

Faggiano, S., Ronda, L., Bruno, S., Jankevics, H., & Mozzarelli, A. (2010). Polymerized and polyethylene glycol-conjugated hemoglobins: a globin-based calibration curve for dynamic light scattering analysis. Analytical biochemistry, 401(2), 266-270.

Fauziah Ma'ruf, I., Sasaki, Y., Kerbs, A., Nießer, J., Sato, Y., Taniguchi, H., ... & Honda, K. (2021). Heterologous gene expression and characterization of two serine hydroxymethyltransferases from Thermoplasma acidophilum. Extremophiles, 25(4), 393-402.

Florio, R., di Salvo, M. L., Vivoli, M., & Contestabile, R. (2011). Serine hydroxymethyltransferase: a model enzyme for mechanistic, structural, and evolutionary studies. Biochimica et Biophysica Acta (BBA)-Proteins and Proteomics, 1814(11), 1489-1496.

Foltyn, V. N., Bendikov, I., De Miranda, J., Panizzutti, R., Dumin, E., Shleper, M., ... & Wolosker, H. (2005). Serine racemase modulates intracellular D-serine levels through an α, β-elimination activity. Journal of Biological Chemistry, 280(3), 1754-1763.

Foltyn, V. N., Zehl, M., Dikopoltsev, E., Jensen, O. N., & Wolosker, H. (2010). Phosphorylation of mouse serine racemase regulates D-serine synthesis. FEBS letters, 584(13), 2937-2941.

Footitt, E. J., Heales, S. J., Mills, P. B., Allen, G. F., Oppenheim, M., & Clayton, P. T. (2011). Pyridoxal 5'-phosphate in cerebrospinal fluid; factors affecting concentration. Journal of inherited metabolic disease, 34(2), 529-538.

Friederichs, J., Rosenberg, R., Mages, J., Janssen, K. P., Maeckl, C., Nekarda, H., ... & Siewert, J. R. (2005). Gene expression profiles of different clinical stages of colorectal carcinoma: toward a molecular genetic understanding of tumor progression. International journal of colorectal disease, 20(5), 391-402.

Fujii, K., Maeda, K., Hikida, T., Mustafa, A. K., Balkissoon, R., Xia, J., ... & Sawa, A. (2006). Serine racemase binds to PICK1: potential relevance to schizophrenia. Molecular psychiatry, 11(2), 150-157.

Fukui, T., & Soda, K. (Eds.). (2008). Molecular aspects of enzyme catalysis. John Wiley & Sons.

Furuya, S. (2008). An essential role for de novo biosynthesis of L-serine in CNS development. Asia Pacific journal of clinical nutrition, 17.

Furuya, S., Tabata, T., Mitoma, J., Yamada, K., Yamasaki, M., Makino, A., ... & Hirabayashi, Y. (2000). L-serine and glycine serve as major astroglia-derived trophic factors for cerebellar Purkinje neurons. Proceedings of the National Academy of Sciences, 97(21), 11528-11533.

Giaccari, R., Marchesani, F., Compari, C., Fisicaro, E., Mozzarelli, A., Campanini, B., ... & Faggiano, S. (2022). Human serine racemase weakly binds the third PDZ domain of PSD-95. International journal of molecular sciences, 23(9), 4959.

Goto, M., Yamauchi, T., Kamiya, N., Miyahara, I., Yoshimura, T., Mihara, H., ... & Esaki, N. (2009). Crystal structure of a homolog of mammalian serine racemase from Schizosaccharomyces pombe. Journal of Biological Chemistry, 284(38), 25944-25952.

Graham, D. L., Beio, M. L., Nelson, D. L., & Berkowitz, D. B. (2019). Human serine racemase: Key residues/active site motifs and their relation to enzyme function. Frontiers in molecular biosciences, 6, 8.

Hart, C. E., Race, V., Achouri, Y., Wiame, E., Sharrard, M., Olpin, S. E., ... & Van Schaftingen, E. (2007). Phosphoserine aminotransferase deficiency: a novel disorder of the serine biosynthesis pathway. The American Journal of Human Genetics, 80(5), 931-937.

Herbig, K., Chiang, E. P., Lee, L. R., Hills, J., Shane, B., & Stover, P. J. (2002). Cytoplasmic serine hydroxymethyltransferase mediates competition between folate-

dependent deoxyribonucleotide andS-adenosylmethionine biosyntheses. Journal of Biological Chemistry, 277(41), 38381-38389.

Hester, G., Stark, W., Moser, M., Kallen, J., Marković-Housley, Z., & Jansonius, J. N. (1999). Crystal structure of phosphoserine aminotransferase from Escherichia coli at 2.3 Å resolution: comparison of the unligated enzyme and a complex with α-methyl-L-glutamate. Journal of molecular biology, 286(3), 829-850.

Hirabayashi, Y., & Furuya, S. (2008). Roles of l-serine and sphingolipid synthesis in brain development and neuronal survival. Progress in lipid research, 47(3), 188-203.

Holeček, M. (2022). Serine metabolism in health and disease and as a conditionally essential amino acid. Nutrients, 14(9), 1987.

Holm, L. J., & Buschard, K. (2019). L-serine: a neglected amino acid with a potential therapeutic role in diabetes. Apmis, 127(10), 655-659.

Inoue, R., Hashimoto, K., Harai, T., & Mori, H. (2008). NMDA-and β-amyloid1–42-induced neurotoxicity is attenuated in serine racemase knock-out mice. Journal of Neuroscience, 28(53), 14486-14491.

Ito, T., Matsuoka, M., Goto, M., Watanabe, S., Mizobuchi, T., Matsushita, K., ... & Yoshimura, T. (2020). Mechanism of eukaryotic serine racemase-catalyzed serine dehydration. Biochimica et Biophysica Acta (BBA)-Proteins and Proteomics, 1868(9), 140460.

Ito, T., Murase, H., Maekawa, M., Goto, M., Hayashi, S., Saito, H., ... & Yoshimura, T. (2012). Metal ion dependency of serine racemase from Dictyostelium discoideum. Amino Acids, 43(4), 1567-1576.

Jaeken, J., Detheux, M., Van Maldergem, L., Foulon, M., Carchon, H., & Van Schaftingen, E. (1996). 3-Phosphoglycerate dehydrogenase deficiency: an inborn error of serine biosynthesis. Archives of Disease in Childhood, 74(6), 542-545.

Jaeken, J., Martens, K., François, I., Eyskens, F., Lecointre, C., Derua, R., ... & Matthijs, G. (2006). Deletion of PREPL, a gene encoding a putative serine oligopeptidase, in patients with hypotonia-cystinuria syndrome. The American Journal of Human Genetics, 78(1), 38-51.

Jiraskova-Vanickova, J., Ettrich, R., Vorlova, B., E Hoffman, H., Lepsik, M., Jansa, P., & Konvalinka, J. (2011). Inhibition of human serine racemase, an emerging target for medicinal chemistry. Current drug targets, 12(7), 1037-1055.

John, R. A. (1995). Pyridoxal phosphate-dependent enzymes. Biochimica Et Biophysica Acta (BBA)-Protein Structure and Molecular Enzymology, 1248(2), 81-96.

Kapil, S., & Sharma,V. (2020). Serine racemases from prokaryotes to eukaryotes: an overview on its role and existence. Plant Cell Biotechnology and Molecular Biology, 17-28.

Kelly, S. M., Jess, T. J., & Price, N. C. (2005). How to study proteins by circular dichroism. Biochimica et Biophysica Acta (BBA)-Proteins and Proteomics, 1751(2), 119-139.

Kent, C. (1995). Eukaryotic phospholipid biosynthesis. Annual review of biochemistry, 64(1), 315-343.

Kim, E., & Sheng, M. (2004). PDZ domain proteins of synapses. Nature Reviews Neuroscience, 5(10), 771-781.

Koulouris, C. R., Bax, B. D., Atack, J. R., & Roe, S. M. (2020). Conformational flexibility within the small domain of human serine racemase. Acta Crystallographica Section F: Structural Biology Communications, 76(2), 65-73.

Labrie, V., Fukumura, R., Rastogi, A., Fick, L. J., Wang, W., Boutros, P. C., ... & Roder, J. C. (2009). Serine racemase is associated with schizophrenia susceptibility in humans and in a mouse model. Human molecular genetics, 18(17), 3227-3243.

Lambrecht, M. A., Rombouts, I., Van Kelst, L., & Delcour, J. A. (2015). Impact of extraction and elution media on non-size effects in size exclusion chromatography of proteins. Journal of Chromatography A, 1415, 100-107.

Lewendon, A. (1984). Studies on the 5-enolpyruvylshikimate 3-phosphate synthase of Escherichia coli. University of Glasgow (United Kingdom).

Liang, J., Han, Q., Tan, Y., Ding, H., & Li, J. (2019). Current advances on structure-function relationships of pyridoxal 5′-phosphate-dependent enzymes. Frontiers in Molecular Biosciences, 6, 4.

Lu, C. H., Chang, H. T., Hsu, L. F., Lee, M. H., Cheng, J., Wu, D. C., & Lin, W. Y. (2023). In Silico and In Vitro Screening of Serine Racemase Agonist and In Vivo Efficacy on Alzheimer's Disease Drosophila melanogaster. Pharmaceuticals, 16(2), 280.

Lueck, J. D., & Fromm, H. J. (1973). Analysis of exchange rates for the Ping Pong Bi Bi mechanism and the concept of substrate synergism. FEBS letters, 32(1), 184-186.

Lumeng, L. (1978). The role of acetaldehyde in mediating the deleterious effect of ethanol on pyridoxal 5′-phosphate metabolism. The Journal of clinical investigation, 62(2), 286-293.

Ma, T. M., Abazyan, S., Abazyan, B., Nomura, J., Yang, C., Seshadri, S., ... & Pletnikov, M. V. (2013). Pathogenic disruption of DISC1-serine racemase binding elicits schizophrenia-like behavior via D-serine depletion. Molecular psychiatry, 18(5), 557-567.

Manning, M. A., Cunniff, C. M., Colby, C. E., El-Sayed, Y. Y., & Hoyme, H. E. (2004). Neu–Laxova syndrome: Detailed prenatal diagnostic and post-mortem findings and literature review. American Journal of Medical Genetics Part A, 125(3), 240-249.

Marchetti, M., Bruno, S., Campanini, B., Peracchi, A., Mai, N., & Mozzarelli, A. (2013). ATP binding to human serine racemase is cooperative and modulated by glycine. The FEBS Journal, 280(22), 5853-5863.

Martens, J. W., Nimmrich, I., Koenig, T., Look, M. P., Harbeck, N., Model, F., ... & Foekens, J. A. (2005). Association of DNA methylation of phosphoserine aminotransferase with response to endocrine therapy in patients with recurrent breast cancer. Cancer research, 65(10), 4101-4117.

Martineau, M., Galli, T., Baux, G., & Mothet, J. P. (2008). Confocal imaging and tracking of the exocytotic routes for D-serine-mediated gliotransmission. Glia, 56(12), 1271-1284.

Matthews, P. M., Pinggera, A., Kampjut, D., & Greger, I. H. (2021). Biology of AMPA receptor interacting proteins-From biogenesis to synaptic plasticity. Neuropharmacology, 197, 108709.

Mattos, E. P., Silva, A. A. D., Magalhaes, J. A. A., Leite, J. C. L., Leistner-Segal, S., Gus-Kessler, R., ... & Sanseverino, M. T. V. (2015). Identification of a premature stop codon mutation in the PHGDH gene in severe Neu-Laxova syndrome—evidence for phenotypic variability. American Journal of Medical Genetics Part A, 167(6), 1323-1329.

McCluskey, G., Donaghy, C., Morrison, K. E., McConville, J., Duddy, W., & Duguez, S. (2022). The Role of Sphingomyelin and Ceramide in Motor Neuron Diseases. Journal of personalized medicine, 12(9), 1418.

Miles, A. J., Janes, R. W., & Wallace, B. A. (2021). Tools and methods for circular dichroism spectroscopy of proteins: A tutorial review. Chemical Society Reviews, 50(15), 8400-8413.

Moat, S., Carling, R., Nix, A., Henderson, M., Briddon, A., Prunty, H., ... & de Koning, T. (2010). Multicentre age-related reference intervals for cerebrospinal fluid serine concentrations: Implications for the diagnosis and follow-up of serine biosynthesis disorders. Molecular genetics and metabolism, 101(2-3), 149-152.

Mozzarelli, A., Berni, R., Rossi, G. L., Vas, M., Bartha, F., & Keleti, T. (1982). Protein isomerization in the NAD+-dependent activation of beta-(2-furyl) acryloyl-glyceraldehyde-3-phosphate dehydrogenase in the crystal. Journal of Biological Chemistry, 257(12), 6739-6744.

Murtas, G., Marcone, G. L., Sacchi, S., & Pollegioni, L. (2020). L-serine synthesis via the phosphorylated pathway in humans. Cellular and Molecular Life Sciences, 77(24), 5131-5148.

Neame, S., Safory, H., Radzishevsky, I., Touitou, A., Marchesani, F., Marchetti, M., ... & Wolosker, H. (2019). The NMDA receptor activation by d-serine and glycine is controlled by an astrocytic Phgdh-dependent serine shuttle. Proceedings of the National Academy of Sciences, 116(41), 20736-20742.

Neu, R. L., Kajii, T., Gardner, L. I., Nagyfy, S. F., & King, S. (1971). A lethal syndrome of microcephaly with multiple congenital anomalies in three siblings. Pediatrics, 47(3), 610-612.

Nguyen, D. Q., Park, H., Park, Y. S., Kwak, K., Kim, T., Lee, J. H., ... & Kang, L. W. (2022). Conformational change of organic cofactor PLP is essential for catalysis in PLP-dependent enzymes. BMB reports, 55(9), 439-446.

Ni, C., Cheng, R. H., Zhang, J., Liang, J. Y., Wei, R. Q., Li, M., & Yao, Z. R. (2019). Novel and recurrent PHGDH and PSAT1 mutations in Chinese patients with Neu-Laxova syndrome. European Journal of Dermatology, 29(6), 641-646.

Ni, X., & Mori, H. (2022). Complex Processes Underlying the Dynamic Changes of D-serine Levels in AD Brains. Current Alzheimer Research, 19(7), 485-493.

Ojala, P., Sundström, J., Grönroos, J. M., Virtanen, E., Talvinen, K., & Nevalainen, T. J. (2002). mRNA differential display of gene expression in colonic carcinoma. Electrophoresis, 23(11), 1667-1676.

Percudani, R., & Peracchi, A. (2009). The B6 database: a tool for the description and classification of vitamin B6-dependent enzymatic activities and of the corresponding protein families. BMC bioinformatics, 10(1), 1-8.

Pollegioni, L., Piubelli, L., Sacchi, S., Pilone, M. S., & Molla, G. (2007). Physiological functions of D-amino acid oxidases: from yeast to humans. Cellular and molecular life sciences, 64(11), 1373-1394.

Possemato, R., Marks, K. M., Shaul, Y. D., Pacold, M. E., Kim, D., Birsoy, K., ... & Sabatini, D. M. (2011). Functional genomics reveal that the serine synthesis pathway is essential in breast cancer. Nature, 476(7360), 346-350.

Rabbani, G., Baig, M. H., Ahmad, K., & Choi, I. (2018). Protein-protein interactions and their role in various diseases and their prediction techniques. Current Protein and Peptide Science, 19(10), 948-957.

Raboni, S., Marchetti, M., Faggiano, S., Campanini, B., Bruno, S., Marchesani, F., ... & Mozzarelli, A. (2019). The energy landscape of human serine racemase. Frontiers in Molecular Biosciences, 5, 112.

Ramos de Dios, S. M., Hass, J. L., Graham, D. L., Kumar, N., Antony, A. E., Morton, M. D., & Berkowitz, D. B. (2023). Information-Rich, Dual-Function 13C/2H-Isotopic Crosstalk NMR Assay for Human Serine Racemase (hSR) Provides a PLP-Enzyme "Partitioning Fingerprint" and Reveals Disparate Chemotypes for hSR Inhibition. Journal of the American Chemical Society, 145(5), 3158-3174.

Reva, B., Antipin, Y., & Sander, C. (2011). Predicting the functional impact of protein mutations: application to cancer genomics. Nucleic acids research, 39(17), e118-e118.

Sakashita, G., Kiyoi, H., Naoe, T., & Urano, T. (2018). Analysis of the oligomeric states of nucleophosmin using size exclusion chromatography. Scientific reports, 8(1), 1-12.

Sasabe, J., Chiba, T., Yamada, M., Okamoto, K., Nishimoto, I., Matsuoka, M., & Aiso, S. (2007). d-Serine is a key determinant of glutamate toxicity in amyotrophic lateral sclerosis. The EMBO journal, 26(18), 4149-4159.

Saxena, V. K., Vedamurthy, G. V., & Singh, R. (2022). A novel concept of Pyridoxal 5'-phosphate permeability in E. coli for modulating the heterologous expression of PLP dependent proteins. Process Biochemistry, 113, 37-46.

Sekula, B., Ruszkowski, M., & Dauter, Z. (2018). Structural analysis of phosphoserine aminotransferase (Isoform 1) from Arabidopsis thaliana–the enzyme involved in the phosphorylated pathway of serine biosynthesis. Frontiers in plant science, 9, 876.

Shaheen, R., Rahbeeni, Z., Alhashem, A., Faqeih, E., Zhao, Q., Xiong, Y., ... & Alkuraya, F. S. (2014). Neu-Laxova syndrome, an inborn error of serine metabolism, is caused by mutations in PHGDH. The American Journal of Human Genetics, 94(6), 898-904.

Singh, R. K., Kumar, D., & Gourinath, S. (2021). Phosphoserine Aminotransferase has Conserved Active Site from Microbes to Higher Eukaryotes with Minor Deviations. Protein and Peptide Letters, 28(9), 996-1008.

Singh, R. K., Tomar, P., Dharavath, S., Kumar, S., & Gourinath, S. (2019). N-terminal residues are crucial for quaternary structure and active site conformation for the phosphoserine aminotransferase from enteric human parasite E. histolytica. International journal of biological macromolecules, 132, 1012-1023.

Sirr, A., Lo, R. S., Cromie, G. A., Scott, A. C., Ashmead, J., Heyesus, M., & Dudley, A. M. (2020). A yeast-based complementation assay elucidates the functional impact of 200 missense variants in human PSAT1. Journal of inherited metabolic disease, 43(4), 758-769.

Smith, M. A., Mack, V., Ebneth, A., Moraes, I., Felicetti, B., Wood, M., ... & Barker, J. (2010). The structure of mammalian serine racemase: evidence for conformational changes upon inhibitor binding. Journal of Biological Chemistry, 285(17), 12873-12881.

Some, D., Amartely, H., Tsadok, A., & Lebendiker, M. (2019). Characterization of proteins by size-exclusion chromatography coupled to multi-angle light scattering (SEC-MALS). JoVE (Journal of Visualized Experiments), (148), e59615.

Stevens, A. O., Kazan, I. C., Ozkan, B., & He, Y. (2022). Investigating the allosteric response of the PICK1 PDZ domain to different ligands with all-atom simulations. Protein Science, 31(12), e4474.

Stolz, M., & Doernemann, D. (1995). Kinetic characteristics, substrate specificity and catalytic properties of phosphoserine aminotransferase from the Green Alga Scenedesmus obliquus, Mutant C-2A. Zeitschrift für Naturforschung C, 50(9-10), 630-637.

Suzuki, M., Sasabe, J., Miyoshi, Y., Kuwasako, K., Muto, Y., Hamase, K., ... & Aiso, S. (2015). Glycolytic flux controls D-serine synthesis through glyceraldehyde-3-phosphate dehydrogenase in astrocytes. Proceedings of the National Academy of Sciences, 112(17), E2217-E2224.

Swanson, M. A., Miller, K., Young, S. P., Tong, S., Ghaloul-Gonzalez, L., Neira-Fresneda, J., ... & Van Hove, J. L. (2022). Cerebrospinal fluid amino acids glycine, serine, and threonine in nonketotic hyperglycinemia. Journal of Inherited Metabolic Disease, 45(4), 734-747.

Tabatabaie, L., Klomp, L. W. J., Rubio-Gozalbo, M. E., Spaapen, L. J. M., Haagen, A. A. M., Dorland, L., & De Koning, T. J. (2011). Expanding the clinical spectrum of 3-phosphoglycerate dehydrogenase deficiency. Journal of Inherited Metabolic Disease: Official Journal of the Society for the Study of Inborn Errors of Metabolism, 34(1), 181-184.

Tabatabaie, L., Klomp, L. W., Berger, R., & De Koning, T. J. (2010). L-serine synthesis in the central nervous system: a review on serine deficiency disorders. Molecular genetics and metabolism, 99(3), 256-262.

Takahara, S., Nakagawa, K., Uchiyama, T., Yoshida, T., Matsumoto, K., Kawasumi, Y., ... & Toyooka, N. (2018). Design, synthesis, and evaluation of novel inhibitors for wild-type human serine racemase. Bioorganic & medicinal chemistry letters, 28(3), 441-445.

Timr, S., Madern, D., & Sterpone, F. (2020). Protein thermal stability. Progress in Molecular Biology and Translational Science, 170, 239-272.

Van der Crabben, S. N., Verhoeven-Duif, N. M., Brilstra, E. H., Van Maldergem, L., Coskun, T., Rubio-Gozalbo, E., ... & De Koning, T. J. (2013). An update on serine deficiency disorders. Journal of inherited metabolic disease, 36(4), 613-619.

Van de Gucht, M., Dufait, I., Kerkhove, L., Corbet, C., de Mey, S., Jiang, H., ... & De Ridder, M. (2022). Inhibition of Phosphoglycerate Dehydrogenase Radiosensitizes Human Colorectal Cancer Cells under Hypoxic Conditions. Cancers, 14(20), 5060.

Verleysdonk, S., Martin, H., Willker, W., Leibfritz, D., & Hamprecht, B. (1999). Rapid uptake and degradation of glycine by astroglial cells in culture: synthesis and release of serine and lactate. Glia, 27(3), 239-248.

Vivoli, M., Angelucci, F., Ilari, A., Morea, V., Angelaccio, S., di Salvo, M. L., & Contestabile, R. (2009). Role of a conserved active site cation− π interaction in Escherichia coli serine hydroxymethyltransferase. Biochemistry, 48(50), 12034-12046.

Wang, W., & Barger, S. W. (2012). Cross-linking of serine racemase dimer by reactive oxygen species and reactive nitrogen species. Journal of Neuroscience Research, 90(6), 1218-1229.

Wang, W., Wu, Z., Dai, Z., Yang, Y., Wang, J., & Wu, G. (2013). Glycine metabolism in animals and humans: implications for nutrition and health. Amino acids, 45(3), 463-477.

Wolosker, H. (2011). Serine racemase and the serine shuttle between neurons and astrocytes. Biochimica et Biophysica Acta (BBA)-Proteins and Proteomics, 1814(11), 1558-1566.

Wolosker, H., Balu, D. T., & Coyle, J. T. (2016). The rise and fall of the d-serine-mediated gliotransmission hypothesis. Trends in neurosciences, 39(11), 712-721.

Wolosker, H., Blackshaw, S., & Snyder, S. H. (1999). Serine racemase: a glial enzyme synthesizing D-serine to regulate glutamate-N-methyl-D-aspartate neurotransmission. Proceedings of the National Academy of Sciences, 96(23), 13409-13414.

Wolosker, H., Sheth, K. N., Takahashi, M., Mothet, J. P., Brady Jr, R. O., Ferris, C. D., & Snyder, S. H. (1999). Purification of serine racemase: biosynthesis of the neuromodulator D-serine. Proceedings of the National Academy of Sciences, 96(2), 721-725.

Wu, S., Zhou, J., Zhang, H., & Barger, S. W. (2022). Serine racemase expression differentiates aging from Alzheimer's brain. Current Alzheimer Research, 19(7), 494-502.

Yamasaki, M., Yamada, K., Furuya, S., Mitoma, J., Hirabayashi, Y., & Watanabe, M. (2001). 3-Phosphoglycerate dehydrogenase, a key enzyme for l-serine biosynthesis, is preferentiallyexpressed in the radial glia/astrocyte lineage and olfactory ensheathing glia in the mouse brain. Journal of Neuroscience, 21(19), 7691-7704.

Yamauchi, T., Goto, M., Wu, H. Y., Uo, T., Yoshimura, T., Mihara, H., ... & Esaki, N. (2009). Serine racemase with catalytically active lysinoalanyl residue. Journal of biochemistry, 145(4), 421-424.

Yoshida, K., Furuya, S., Osuka, S., Mitoma, J., Shinoda, Y., Watanabe, M., ... & Hirabayashi, Y. (2004). Targeted disruption of the mouse 3-phosphoglycerate dehydrogenase gene causes severe neurodevelopmental defects and results in embryonic lethality. Journal of Biological Chemistry, 279(5), 3573-3577.

Yoshimura, T. (2022). Molecular basis and functional development of enzymes related to amino acid metabolism. Bioscience, Biotechnology, and Biochemistry, 86(9), 1161-1172.

Yoshimura, T., & Goto, M. (2008). d-Amino acids in the brain: structure and function of pyridoxal phosphate-dependent amino acid racemases. The FEBS journal, 275(14), 3527-3537.

Zeeshan, F., Tabbassum, M., & Kesharwani, P. (2019). Investigation on secondary structure alterations of protein drugs as an indicator of their biological activity upon thermal exposure. The protein journal, 38(5), 551-564.

Zhao, X., Fu, J., Du, J., & Xu, W. (2020). The role of D-3-phosphoglycerate dehydrogenase in cancer. International journal of biological sciences, 16(9), 1495.

Zhu, S., Wang, X., Liu, L., & Ren, G. (2022). Stabilization of Notch1 and β-catenin in response to ER-breast cancer-specific up-regulation of PSAT1 mediates distant metastasis. Translational Oncology, 20, 101399.